DEPLOYABLE ANTENNA KINEMATICS
USING TENSEGRITY STRUCTURE DESIGN

By

BYRON FRANKLIN KNIGHT

A DISSERTATION PRESENTED TO THE GRADUATE SCHOOL
OF THE UNIVERSITY OF FLORIDA IN PARTIAL FULFILLMENT
OF THE REQUIREMENTS FOR THE DEGREE OF
DOCTOR OF PHILOSOPHY

UNIVERSITY OF FLORIDA

2000

For this work I thank Mary, my friend, my partner, and my wife.

ACKNOWLEDGMENTS

TABLE OF CONTENTS

Abstract of Dissertation Presented to the Graduate School
of the University of Florida in Partial Fulfillment of the
Requirements for the Degree of Doctor of Philosophy

DEPLOYABLE ANTENNA KINEMATICS USING
TENSEGRITY STRUCTURE DESIGN

By

Byron Franklin Knight

May 2000

Chairman: Dr. Joseph Duffy
Major Department: Mechanical Engineering

   With vast changes in spacecraft development over the last decade, a new, cheaper

approach was needed for deployable kinematic systems such as parabolic antenna

reflectors. Historically, these mesh-surface reflectors have resembled folded umbrellas,

with incremental redesigns utilized to save packaging size. These systems are typically

over-constrained designs, the assumption being that high reliability necessary for space

operations requires this level of conservatism. But with the rapid commercialization of

space, smaller launch platforms and satellite buses have demanded much higher

efficiency from all space equipment than can be achieved through this incremental

approach.

   This work applies an approach called tensegrity to deployable antenna development.

Kenneth Snelson, a student of R. Buckminster Fuller, invented tensegrity structures in

1948. Such structures use a minimum number of compression members (struts); stability

is maintained using tension members (ties). The novelty introduced in this work is that

the ties are elastic, allowing the ties to extend or contract, and in this way changing the surface of the antenna.

Previously, the University of Florida developed an approach to quantify the stability and motion of parallel manipulators. This approach was applied to deployable, tensegrity, antenna structures. Based on the kinematic analyses for the 3-3 (octahedron) and 4-4 (square anti-prism) structures, the 6-6 (hexagonal anti-prism) analysis was completed which establishes usable structural parameters. The primary objective for this work was to prove the stability of this class of deployable structures, and their potential application to space structures. The secondary objective is to define special motions for tensegrity antennas, to meet the subsystem design requirements, such as addressing multiple antenna-feed locations.

This work combines the historical experiences of the artist (Snelson), the mathematician (Ball), and the space systems engineer (Wertz) to develop a new, practical design approach. This kinematic analysis of tensegrity structures blends these differences to provide the design community with a new approach to lightweight, robust, adaptive structures with the high reliability that space demands. Additionally, by applying Screw Theory, a tensegrity structure antenna can be commanded to move along a screw axis, and therefore meeting the requirement to address multiple feed locations.

CHAPTER 1.
BACKGROUND

Space Antenna Basis

The field of deployable space structures has matured significantly in the past decade. What once was a difficult art form to master has been perfected by numerous companies, including TRW, Hughes, and Harris. The significance of this maturity has been the reliable deployment of various antenna systems for spacecraft similar to NASA's Tracking Data Relay Satellite. In recent years, parabolic, mesh-surface, reflector development has been joined by phased arrays (flat panel structures with electronically steered beams). Both of these designs are critical to commercial and defense space programs.

An era has begun where commercial spacecraft production has greatly exceeded military/civil applications. This new era requires structural systems with the proven reliability and performance of the past and reduced cost.

This dissertation addresses one new approach to deployable antenna design utilizing a kinematic approach known as tensegrity, developed by Kenneth Snelson (student of R. Buckminster Fuller) in 1948 [Connelly and Black, 1998]. The name tensegrity is derived from the words Tensile and Integrity, and was originally developed for architectural sculptures. The advantage of this type of design is that there is a minimum of compression tubes (herein referred to as struts); the stability of the system is created

through the use of tension members (ties). Specifically, this work addresses the new application for self-deploying structures.

<div align="center">Antenna Requirements</div>

James R. Wertz of Microcosm, Inc., a leading spacecraft designer, defines a system's requirements through a process of identifying broad objectives, reasonably achievable goals, and cost constraints [Larson and Wertz, 1992]. Space missions vary greatly, and the requirements, goals, and costs associated with each task also vary greatly, but one constraint is ever present: "space is expensive". The rationale behind this study of new deployable techniques is related to the potential cost savings to be gained.

The mission objective for a large, deployable space antenna is to provide reliable radio frequency (RF) energy reflection to an electronic collector (feed) located at the focus of the parabolic surface. The current state of deployable parabolic space antenna design is based on a segmented construction, much like an umbrella. Radial ribs are connected to a central hub with a mechanical advantaged linear actuator to drive the segments into a locked, over-driven, position. Other approaches have been proposed utilizing hoop tensioners (TRW) and mechanical memory surface materials (Hughes), but as of this publication, these alternative approaches have not flown in space.

To meet this objective, an analysis of mathematics and electrical engineering yields three parameters: defocus, mispointing, and surface roughness. For receiving antennas, defocus is the error in the reflector surface that makes the energy paint an area, rather than converge on the focal point. Mispointing is the misplacement of the converged energy to a position other than the designed focal point. Surface roughness, or the approximation to a theoretical parabolic surface, defines the reflector's ability to reflect

and collect a given band of RF energy. Higher band reflectors require a more accurate surface that better approximates the theoretical parabola. Similarly for transmitting antennas, defocus generates divergent rays of energy (rather than parallel) from the reflector surface; mispointing directs these waves in the wrong direction. Defocus (focal area vice point) and mispointing (focus located in the wrong position) are illustrated in Figure 1-1.
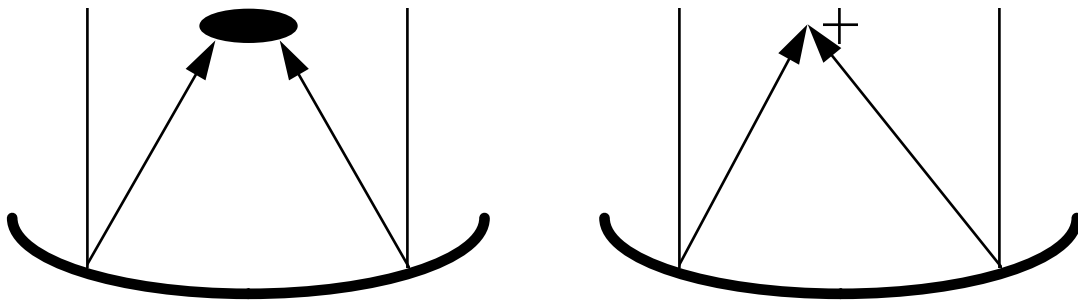
Figure 1-1. Defocus and Mispointing on a Parabolic Antenna

In recent years, numerous Department of Defense organizations have solicited for new approaches to deployable antenna structures. The Air Force Research Laboratories (AFRL) are interested in solutions to aid with their Space Based Laser and Radar programs. Specifically, they have requested new solutions to building precision deployable structures to support the optical and radar payloads.

Improvement Assumptions

The basis for this research is the assumption that the stowed density for deployable antennas can be greatly increased, while maintaining the reliability that the space community has enjoyed in the past. Failure of these structures is unacceptable, but if the

stowed volume is reduced (therefore an increase in density for a given weight), launch services could be applied much more efficiently.

The implementation of multiple vehicle launch platforms (i.e. Iridium built by Motorola) has presented a new case where the launch efficiency is a function of the stowed spacecraft package, and not the weight of the electronic bus. For Extremely High Frequency systems (greater than 20GHz) in low earth orbit (LEO), the antenna aperture need only be a few meters in diameter. But for an L-band, geosyncronous (GEO) satellite (i.e. AceS built by Lockheed Martin), the antenna aperture diameter is 15 meters. And to reach GEO, less weight and payload drag must be achieved to ensure a more efficient ascent into the orbit. Currently, these systems stow within the rocket launchers much like folded inverted umbrellas. This greatly limits the stowage efficiency, greatly increasing the launcher shroud canister height. This research addresses a concept to improve this efficiency.

CHAPTER 2.
INTRODUCTION

Tensegrity Overview

Pugh [1976] simplified Snelson's work in tensegrity structures. He began with a basic description of the attractions and forces in nature that govern everyday life. From there he described the applications in history of tensile and compressive members in buildings and ships to achieve a balance between these forces to achieve the necessary structures for commerce and living. The introduction of Platonic Solids presents the simplicity and art of tensile/compressive structures. The Tetrahedron in Figure 2-1 is a four-vertex, 6-member structure. Framing the interior with a strut (tetrapod) system and connecting the vertices with ties can create the tensegrity. The ties must, of course, always be in tension.
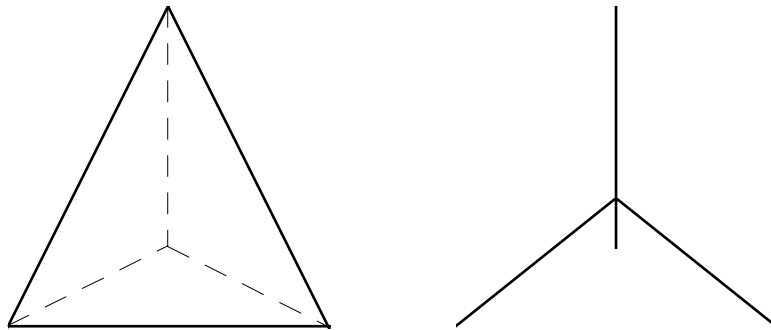
Figure 2-1. A Simple Tetrahedron and Tripod Frame

The Octahedron (6-vertices, 12-members, and 8-faces) is the basis for this research to apply tensegrity to deployable antenna structures. Figure 2-2 presents the simple structure

and tensegrity application (rotated about the center, with alternate struts replaced by ties).

From this simple structure, we have been able to create a class of deployable structures

using platform kinematic geometry. It is apparent that the tensegrity application

resembles a six-leg parallel platform. It is from this mathematics that the new designs are

derived.
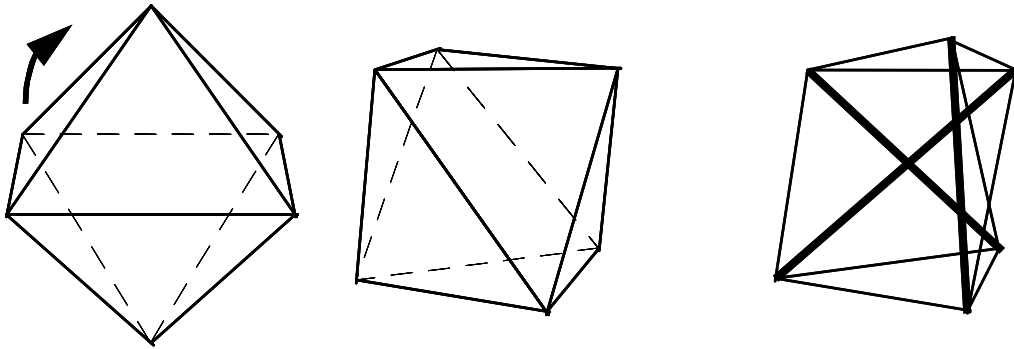
Figure 2-2. The Simple, Rotated, and Tensegrity Structure Octahedron

The work of Architect Peter Pearce [1990] studies the nature of structures and the

discovery of the Platonic Solids. Plato was able to determine the nature of structures, and

the structure of nature (a duality), through observing naturally occurring systems such as

spider webs. Building on this work, Pearce was able to document other natural

phenomena (soap bubbles, Dragonfly wings, and cracked mud) to establish energy

minimization during state change. The assumption here is that nature uses the most

energy-efficient method. From these assumptions and an understanding of stress and

strain in structural members (columns and beams), he was able to present a unique

solution for simple, durable, high strength structures. From these conclusions, he

proposes a family of residential, commercial, and industrial structures that are both esthetically pleasing and functional.

Related Research

The most comprehensive study of the technology needs for future space systems to be published in the last decade was released by the International Technology Research Institute [WTEC, 1998]. This NSF/NASA sponsored research "commissioned a panel of U.S. satellite engineers and scientists to study international satellite R&D projects to evaluate the long-term presence of the United States in this industry." A prior study was undertaken in 1992 to establish that there was significant activity in Europe and Asia that rivaled that of the U.S., and benchmarked this R&D to U.S. capability. The later study added market, regulatory, and policy issues in addition to the technology developments. The conclusion was that while the U.S. holds a commanding lead in the space marketplace, there is continual gaining by both continents. This is evident in space launch, where Ariane Space has nearly achieved the capabilities of Boeing's (Delta) rocket services.

The significance of this study is that U.S. manufacturers are meeting their goals for short-term research (achieving program performance), but have greatly neglected the long-term goals, which has traditionally been funded by the government. The top candidate technologies include structural elements, materials and structures for electronic devices, and large deployable antennas (>25 meters diameter). While there have been 14 meter subsystems developed to meet GEO system requirements during the 1990s, the large deployable requirement has yet to be addressed or developed. This research will address one possible solution to building such a subsystem.

Related Designs

Tetrobots [Hamlin and Sanderson, 1998] have been developed in the last few years as a new approach to modular design. This approach utilizes a system of hardware components, algorithms, and software to build various robotic structures to meet multiple design needs. These structures are similar to tensegrity in that they are based on Platonic Solids (tetrahedral and octahedral modules), but all the connections are made with truss members. Tensegrity utilizes only the necessary struts (compression members) and ties (tensile members) to maintain stability.

Adaptive trusses have been applied to the field of deployable structures, providing the greatest stiffness and strength for a given weight of any articulated structure or mechanism [Tidwell et al. 1990]. The use of the tetrahedron geometry (6-struts and 4-vertices) is the basis for this approach. From that, the authors propose a series of octahedral cells (12-struts and 6-vertices) to build the adaptive structure (Figures 2-3 and 2-4). The conclusion is that from well-defined forward analyses (position, velocity and acceleration), this adaptive truss would be useful for deployed structures to remove position or motion errors caused by manufacturing, temperature change, stress, or external force [Wada et al. 1991].
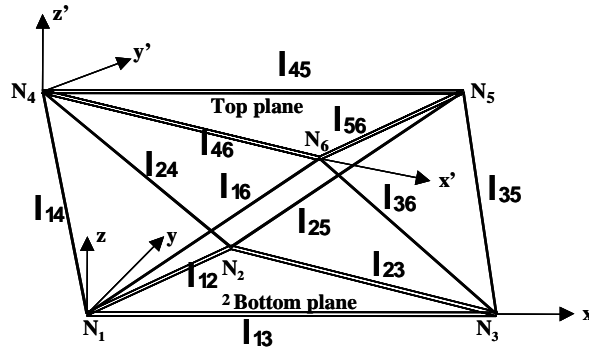
Figure 2-3. Octahedral Truss Notation
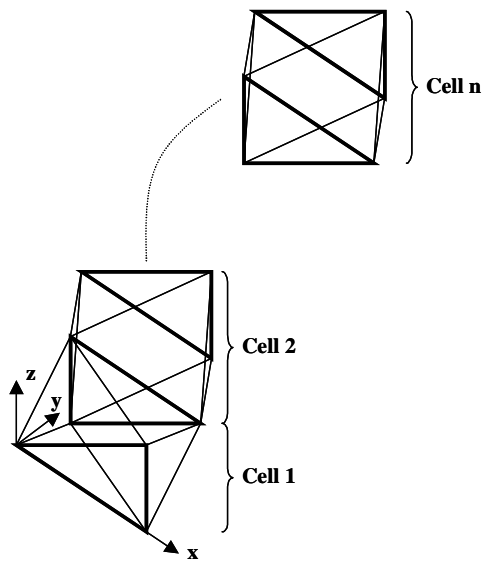
Figure 2-4. Long Chain Octahedron VGT

The most complex issue in developing a reliable deployable structure design is the

packaging of a light weight subsystem in as small a volume as possible, while ensuring

that the deployed structure meets the system requirements and mission performance.

Warnaar developed criteria for deployable-foldable truss structures [Warnaar 1992]. He

addressed the issues of conceptual design, storage space, structural mass, structural integrity, and deployment. This work simplifies the concepts related to a stowed two-dimensional area deploying to a three-dimensional volume. The author also presented a tutorial series [Warnaar and Chew, 1990 (a & b)]. This series of algorithms presents a mathematical representation for the folded (three-dimensional volume in a two-dimensional area) truss. This work aids in determining the various combinations for folded truss design.

NASA Langley Research Center has extensive experience in developing truss structures for space. One application, a 14-meter diameter, three-ring optical truss, was designed for space observation missions (Figure 2-5). A design study was performed [Wu and Lake, 1996] using the Taguchi methods to define key parameters for a Pareto-optimal design: maximum structural frequency, minimum mass, and the maximum frequency to mass ratio. Tetrahedral cells were used for the structure between two precision surfaces. 31 analyses were performed on 19,683 possible designs with an average frequency to mass ratio between 0.11 and 0.13 Hz/kg. This results in an impressive 22 to 26 Hz for a 200-kg structure.

<div align="center">Related Patents</div>

The field of deployable space structures has proven to be both technically challenging and financially lucrative during the last few decades. Such applications as large parabolic antennas require extensive experience and tooling to develop, but this is a key component in the growing personal communications market. The patents on deployable space structures have typically focused on the deployment of general truss network designs,

rather than specific antenna designs. Some of these patents address new approaches that have not been seen in publication.
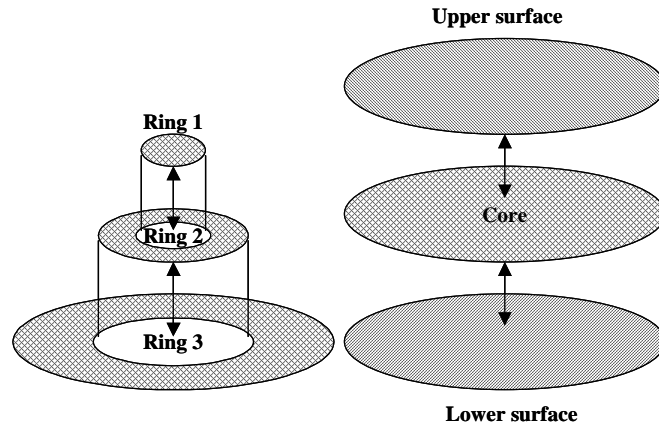
Figure 2-5. Three-ring Tetrahedral Truss Platform

The work of Kaplan and Schultz [1975], and, Waters and Waters [1987] specifically applies strut and tie construction to the problem of deployable antennas, but the majority of patents address trusses and the issues associated with their deployment and minimal stowage volume. Nelson [1983] provides a detailed design for a three-dimensional rectangular volume based on an octahedron. His solution to deployment uses a series of ties within the truss network. Details of the joints and hinges are also included. When networked with other octahedral subsets, a compact stow package could be expanded into a rigid three-dimensional framework.

Other inventors continued work in expandable networks to meet the needs of International Space Station. Natori [1985] used beams and triangular plates to form a tetrahedral unit. These units formed a linear truss; his work included both joint and hinge details and the stowage/deployment kinematics. Kitamura and Yamashiro [1990]

presented a design based on triangular plates, hinged cross members, and ties to build expanding masts from very small packages.

Onoda [1985, 1986, 1987a, 1987b, 1990] patented numerous examples of collapsible/deployable square truss units using struts and ties. Some suggested applications included box section, curved frames for building solar reflectors or antennas. Onoda et al. [1996] published results. Rhodes and Hedgepeth [1986] patented a much more practical design that used no ties, but employed hinges to build a rectangular box from a tube stowage volume.

Krishnapillai [1988] and Skelton [1995] most closely approximate the research presented herein, employing the concepts of radial struts and strut/tie combinations, respectively. The combination of these approaches could provide the necessary design to deploy a small package to a radial backup surface, as with a deployable antenna.

CHAPTER 3.
STUDY REQUIREMENTS

Stability Criterion

The primary assumption for this research is that improved stability will provide a superior deployable structure. Applying a tensegrity approach, the secondary assumption is a resultant lower system development cost. The development of this new approach to antenna systems, assuming these criteria, will provide a usable deployable product with greatly reduced component count, assembly schedule, and final cost, but with equal stability and system characteristics to the currently popular radial rib antenna system. From this assumption, increased stowage density will be realized.

Stowage Approach

Figure 3-1 shows a deployed and stowed antenna package, utilizing a central hub design. Most current deployable antenna designs use this approach. For a single fold system, the height of the stowed package is over one half of the deployed diameter. The approach taken in this research is to employ Tensegrity Structural Design to increase the stowed package density.

Deployment Approach

The deployable approach for this 6-6 system is to manipulate the legs joining the hub to the antenna, to create a tensegrity structure. Onoda suggests a sliding hinge to achieve deployment, but such a package still requires a large height for the stowed structure. This approach does have excellent merit for deployable arrays, as he presents in the paper.
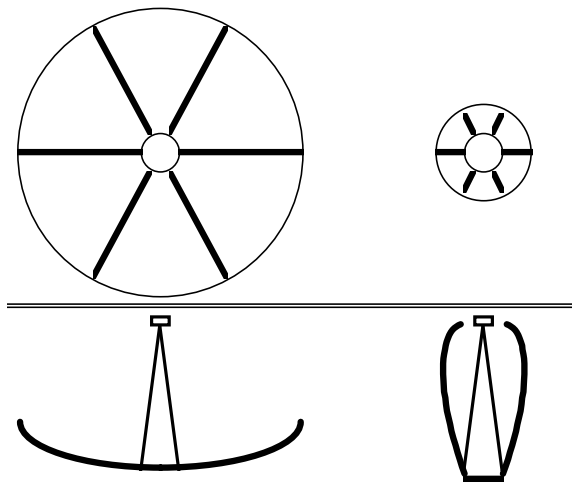
Figure 3-1. Deployed and Stowed Radial Rib Antenna Model

The tensegrity 6-6 antenna structure would utilize a deployment scheme whereby the lowest energy state for the structure is in a tensegrity position. Figure 3-2 shows this position, with the broken lines representing the ties (tension) and the solid lines representing the struts (compression). Clearly, equilibrium of this structure requires that the tie forces sum to match the compression forces at the end of each strut.
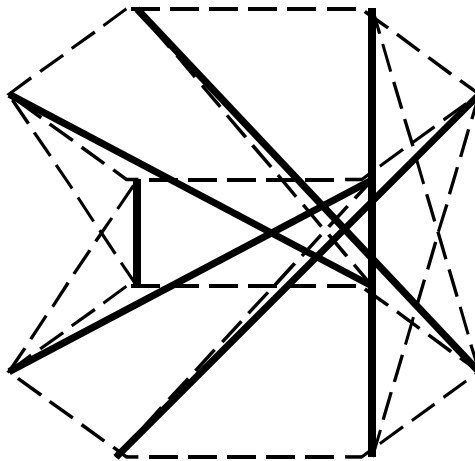
Figure 3-2. 6-6 Tensegrity Platform

Mechanism Issues

Rooney et al. [1999] developed a concept for deploying struts and ties using a "reel"

design, thereby allowing the ties to stow within the struts. This simple, yet durable

approach solves the problem of variable length ties for special antenna designs, such as

those with multiple feed centers (focal points on the parabolic antenna surface). Figure

3-3 shows this concept, using a deployment mechanism for the ties; spherical joints

would be necessary to ensure that there are only translational constraints.

**Elastic Ties Deployed
from the Strut (3 each)**

Strut Tube

**Angle-Unconstrained
Revolute Joint**
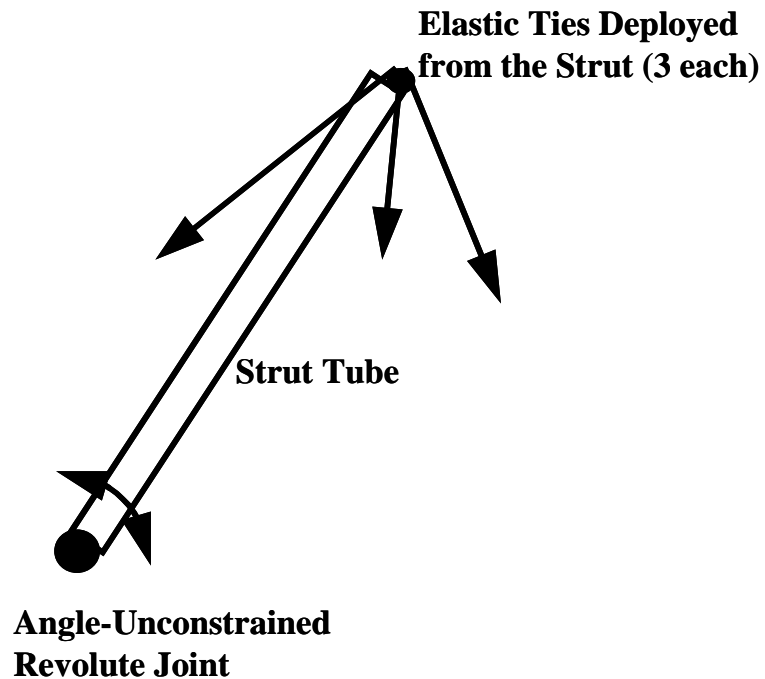
Figure 3-3. The Struts Are Only Constrained in Translation

CHAPTER 4.
BASIC GEOMETRY FOR THE 6-6 TENSEGRITY APPLICATION

The application of tensegrity structures to the field of deployable antenna design is a

significant departure from currently accepted practices. Not only must this new structure

meet the system parameters previously described, but there also must be a process to

validate the performance reliability and repeatability. Figure 4-1 shows the rotation of the

6-6 structures through tensegrity. Tensegrity occurs when all struts are in compression,

and all ties are in tension. When describing a stable structure, the struts cannot be in

tension because they only interface with tensile members (ties).
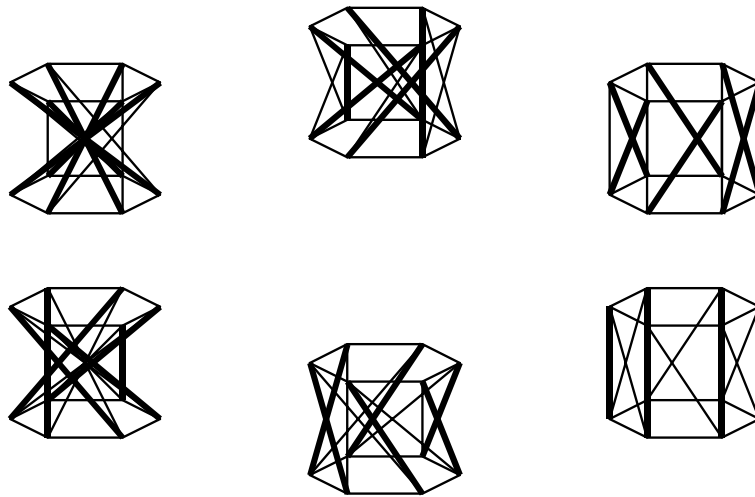
Figure 4-1. A 6-6 Structure Rotated through Tensegrity

As presented in Chapter 1, the accepted subsystem mechanical requirements applied

to deployable parabolic antennas are defocus, mispointing, and surface roughness.

Defocus, or the "cupping" of the structure, must be corrected once the subsystem is deployed to correct any energy spreading which occurs. A correctly shaped parabolic antenna surface may not direct the radio frequency (RF) energy in the correct direction (to the right focal point). This is known as mispointing. Practically, antenna design requires that the theoretical focal "point" be a "plane", due to energy management issues of RF transmitter/receivers. The surface accuracy is a coupled effect, which is influenced by the non-linear stiffness (displacement is not linear with respect to the applied force), structural time constant, and general stability of the backup reflector structure and facing antenna mesh surface. Positioning and control of this mesh surface defines the antenna's "accuracy". Pellegrino (The University of Cambridge) has developed applicable tools for calculating the motions of pre-stressed nodes by actuating flexible ties [You, 1997].

In order to address adequately these three design parameters, the stability of this subsystem must be assured. During his career, Hunt [1990] has addressed line geometry, the linear dependence of lines, the linear complex, and the hyperboloid. All of these studies have direct application in the case of tensegrity structures. This linear dependence relates to the stability of the structure. For this to occur, the two sets of lines on the tensegrity structure, the struts and ties, must lie on co-axial hyperboloids of one sheet. This builds the case to explain how such a structure in tensegrity can be stable yet at a singularity, having instantaneous mobility. To explain this, an introduction into points, planes, lines, and Screw Theory is presented.

<div align="center">Points, Planes, Lines, and Screws</div>

The vector equation for a point can be expressed in terms of the Cartesian coordinates by

$$\vec{r} = x\vec{i} + y\vec{j} + z\vec{k} \tag{4-1}$$

Referencing Hunt [1990], these coordinates can be written $x = \dfrac{X}{W}$, $y = \dfrac{Y}{W}$, $z = \dfrac{Z}{W}$.

This expresses the point in terms of the homogeneous coordinates $(W; X, Y, Z)$. A point is completely specified by the three independent ratios $\dfrac{X}{W}, \dfrac{Y}{W}, \dfrac{Z}{W}$ and therefore there are an ∞^3 points in three space.

Similarly, the equation for a plane can be expressed in the form

$$D + Ax + By + Cz = 0 \tag{4-2}$$

or in terms of the homogeneous point coordinates by

$$Dw + Ax + By + Cz = 0 \tag{4-3}$$

The homogeneous coordinates for a plane are $(D; A, B, C)$ and a plane is completely specified by three independent ratios $\left(\dfrac{A}{D}, \dfrac{B}{D}, \dfrac{C}{D} \right)$. Therefore, there are an ∞^3 planes in three space. It is well known that in three space the plane and the point are dual.

Using Grassmann's [Meserve, 1983] determinant principles the six homogeneous coordinates for a line, which is the join of two points (x_1, y_1, z_1) and (x_2, y_2, z_2), can be obtained by counting the 2x2 determinants of the 2x4 array.

$$\begin{bmatrix} 1 & x_1 & y_1 & z_1 \\ 1 & x_2 & y_2 & z_2 \end{bmatrix} \tag{4-4}$$

$$L = \begin{vmatrix} 1 & x_1 \\ 1 & x_2 \end{vmatrix} \qquad M = \begin{vmatrix} 1 & y_1 \\ 1 & y_2 \end{vmatrix} \qquad N = \begin{vmatrix} 1 & z_1 \\ 1 & z_2 \end{vmatrix}$$

$$P = \begin{vmatrix} y_1 & z_1 \\ y_2 & z_2 \end{vmatrix} \qquad Q = \begin{vmatrix} z_1 & x_1 \\ z_2 & x_2 \end{vmatrix} \qquad R = \begin{vmatrix} x_1 & y_1 \\ x_2 & y_2 \end{vmatrix} \tag{4-5}$$

The six homogeneous coordinates $(L, M, N; P, Q, R)$ or $(\overline{S}; \overline{S}_0)$ are superabundant by 2

since they must satisfy the following relationships.

$$\overline{S} \cdot \overline{S} = L^2 + M^2 + N^2 = d^2 \tag{4-6}$$

where d is the distance between the two points and,

$$\overline{S} \cdot \overline{S}_0 = LP + MQ + NR = 0 \tag{4-7}$$

which is the orthogonality condition. Briefly, as mentioned, the vector equation for a line

is given by $\vec{r} \times \overline{S} = \overline{S}_0$. Clearly, $\overline{S}$ and $\overline{S}_0$ are orthogonal since $\overline{S} \cdot \overline{S}_0 = \overline{S} \cdot \vec{r} \times \overline{S} = 0$. A

line is completely specified by four independent ratios. Therefore, these are an ∞^4 lines

in three space.

Ball [1998, p.48] defines a screw by, *"A screw is a straight line with which a definite*

linear magnitude termed the pitch is associated". For a screw, $\overline{S} \cdot \overline{S}_0 \neq 0$, and the pitch

is defined by $h = \dfrac{LP + MQ + NR}{L^2 + M^2 + N^2}$. It follows that there are an ∞^5 screws in three space.

By applying Ball's Screw Theory, the mathematics are developed to show that this class

of tensegrity structures can follow a screw. This is very applicable in antenna design to

allow a subsystem to direct energy to multiple feed centers.

<div align="center">The Linear Complex</div>

Many models have been developed for the geometry and mobility of octahedral

manipulators. Instant mobility of the deployable, tensegrity, antenna structure is of much

interest within the design community. This instant mobility is caused by the *Linear*

Dependence of Lines. This occurs when the connecting lines of a structure become

linearly dependent. They can belong to (i) a linear complex (∞^3 of lines); (ii) a linear

congruence (∞^2 of lines); or (iii) a ruled surface called a cylindroid (∞^1 of lines). The linear complex has been investigated by, for example, Jessop [1903]. Of interest here is the linear complex described by Hunt [1990], which will be described shortly. Before proceeding, it is useful to note that the resultant of a pair of forces, which lie on a pair of skew lines, lies on the cylindroid. The resultant is a wrench, which is simply a line on the cylindroid with an associated pitch **h**. The resultant is only a pure force when a pair of forces intersects in a finite point or at infinity (i.e. they are parallel).

Hunt [1990] describes a linear complex obtained by considering an infinitesimal twist of a screw with pitch h on the z-axis. For such an infinitesimal twist, a system of ∞^2 coaxial helices of equal pitch is defined. Every point on the body lies on a helix, with the velocity vector tangential to the helix at that point. Such a system of ∞^3 tangents to ∞^2 coaxial helices is called a *helicoidal velocity field*.
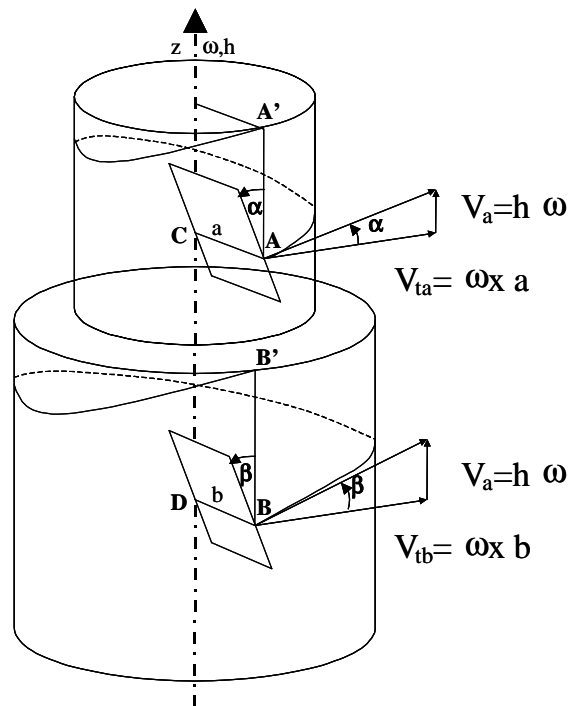
Figure 4-2. Two equal-pitched helices

In Figure 4-2, two helices are defined, one lying on a circular cylinder of radius **a**, and the other on a coaxial circular cylinder of radius **b**. Two points **A** and **B** are taken on the respective radii and both cylinders are on the same z-axis. After one complete revolution, the points have moved to **A'** and **B'**, with **AA'=BB'=2πh**. Both advance along the **z**-axis a distance **hθ** for a rotation **θ**. Now, the instantaneous tangential velocities are $\underline{V}_{ta} = \underline{\omega}$ x $\underline{a}$ and $\underline{V}_{tb} = \underline{\omega}$ x $\underline{b}$. Further, $\underline{V}_a = h\underline{\omega}$ and $\underline{V}_{ta} = \omega$ x $\underline{a}$. The ratio $|\underline{V}_a|/|\underline{V}_{ta}| = h/a = \tan \alpha$, or $h = a \tan \alpha$. Similarly, $h/b = \tan \beta$, or $h = b \tan \beta$.
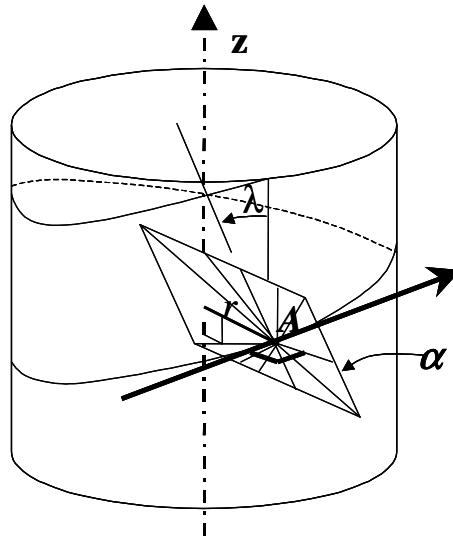
Figure 4-3. A Pencil of Lines in the Polar Plane α Through the Pole **A**

Further, Figure 4-3 (see [Hunt, 1990]) illustrates a pole **A** through which a helix passes together with a polar plane α. The pencil of lines in α which pass through **A** are normal to the helix (i.e. the vector through **A** tangent to the helix). The plane α contains a pencil of lines (∞^1) through the pole **A.** Clearly, as a point **A** moves on the helix, an ∞^2 lines is generated. If we now count ∞^1 concentric helices of pitch **h**, and consider the totality of the ∞^2 lines generated at each polar plane on a single helix, we will generate ∞^3

lines, which comprises the linear complex. All such lines are reciprocal to the screw of pitch **h** on the **z**-axis. The result with respect to anti-prism tensegrity structures will be shown in (4-26) and (4-27) and it is clear by (4-28) that the pitch **h** is given by **–ab/6z**.

The Hyperboloid of One Sheet

Snyder and Sisam [1914] developed the mathematics to describe a hyperbola of rotation, known as the hyperboloid of one sheet (Figure 4-4). The surface is represented by the equation

$$\frac{x^2}{a^2} + \frac{y^2}{b^2} - \frac{z^2}{c^2} = 1 \qquad (4\text{-}8)$$

which is a standard three-dimensional geometry equation. This equation can be factored into the form

$$\left(\frac{x}{a} + \frac{z}{c}\right)\left(\frac{x}{a} - \frac{z}{c}\right) = \left(1 + \frac{y}{b}\right)\left(1 - \frac{y}{b}\right) \qquad (4\text{-}9)$$

and can become an alternate form

$$\frac{\left(\dfrac{x}{a} + \dfrac{z}{c}\right)}{\left(1 + \dfrac{y}{b}\right)} = \frac{\left(1 - \dfrac{y}{b}\right)}{\left(\dfrac{x}{a} - \dfrac{z}{c}\right)} = \rho \qquad (4\text{-}10)$$

Similarly,

$$\frac{\left(\dfrac{x}{a} + \dfrac{z}{c}\right)}{\left(1 - \dfrac{y}{b}\right)} = \frac{\left(1 + \dfrac{y}{b}\right)}{\left(\dfrac{x}{a} - \dfrac{z}{c}\right)} = \eta \qquad (4\text{-}11)$$

The equations can be manipulated to form:

$$\left(\frac{x}{a}+\frac{z}{c}\right)=\rho\left(1+\frac{y}{b}\right) \quad \text{and} \quad \left(1-\frac{y}{b}\right)=\rho\left(\frac{x}{a}-\frac{z}{c}\right) \tag{4-12}$$
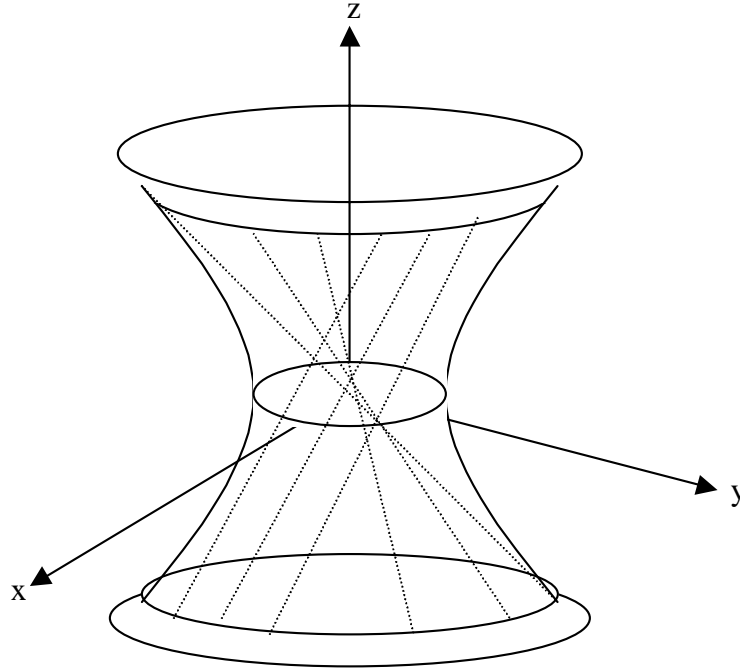
Figure 4-4. A Ruled Hyperboloid of One Sheet

These formulae describe the intersection of two planes, which is a line. Therefore, for every value of ρ there is a pair of plane equations. Every point on the line lies on the surface of the hyperboloid since the line coordinates satisfy 4-10. Similarly, any point on the surface, which is generated by the line equation, also satisfies the equations in 4-12 as they are derived from 4-10. The system of lines, which is described by 4-12, where ρ is a parameter, is called a *regulus* of lines on this hyperboloid. Any individual line of the *regulus* is called a *generator*. A similar set of equations can be created for the value η

$$\left(\frac{x}{a}+\frac{z}{c}\right)=\eta\left(1-\frac{y}{b}\right) \quad \text{and} \quad \left(1+\frac{y}{b}\right)=\eta\left(\frac{x}{a}-\frac{z}{c}\right) \tag{4-13}$$

The lines that correspond to η constitute a second regulus, which is complementary to the original regulus and also lies on the surface of the hyperboloid.

<u>Regulus Plücker Coordinates</u>

Using Plücker Coordinates [Bottema and Roth, 1979], three equations describe a line: S (L, M, N) and S_o (P, Q, R)

$$Ny - Mz = P$$
$$Lz - Nx = Q \qquad (4\text{-}14)$$
$$Mx - Ly = R$$

Expanding 4-12, the equations become

$$\rho\, abc - bcx + \rho\, acy - abz = 0$$
$$\text{and} \qquad (4\text{-}15)$$
$$abc - \rho\, bcx - acy + \rho abz = 0$$

The Plücker axis coordinates for the line in the ρ regulus are obtained by counting the 2x2 determinants of the 2x4 arrays, which are built from these equations.

$$\begin{bmatrix} \rho\, abc & -bc & \rho\, ac & -ab \\ abc & -\rho\, bc & -ac & \rho ab \end{bmatrix} \qquad (4\text{-}16)$$

Therefore,

$$P = ab^2 c^2 \begin{vmatrix} \rho & -1 \\ 1 & -\rho \end{vmatrix} = ab^2 c^2 (1 - \rho^2)$$

$$Q = a^2 bc^2 \begin{vmatrix} \rho & \rho \\ 1 & -1 \end{vmatrix} = -2a^2 bc^2 \rho \qquad (4\text{-}17)$$

$$R = a^2 b^2 c \begin{vmatrix} \rho & -1 \\ 1 & \rho \end{vmatrix} = a^2 b^2 c(1 + \rho^2)$$

and

$$L = a^2bc \begin{vmatrix} \rho & -1 \\ -1 & \rho \end{vmatrix} = -a^2bc(1-\rho^2)$$

$$M = ab^2c \begin{vmatrix} -1 & -1 \\ \rho & -\rho \end{vmatrix} = 2ab^2c\rho \qquad (4\text{-}18)$$

$$N = abc^2 \begin{vmatrix} -1 & \rho \\ -\rho & -1 \end{vmatrix} = abc^2(1+\rho^2)$$

This set of coordinates is homogeneous, and we can divide through by the common factor

abc. Further, we have in ray coordinates:

$$
\begin{aligned}
L &= -a(1-\rho^2) & P &= bc(1-\rho^2) \\
M &= 2b\rho & Q &= -2ac\rho \\
N &= c(1+\rho^2) & R &= ab(1+\rho^2)
\end{aligned}
\qquad (4\text{-}19)
$$

By using the same method for developing the Plücker coordinates and the

homogeneous ray coordinates, the η equations are developed with 4-13.

$$\eta abc - bcx - \eta acy - abz = 0$$
$$\text{and} \qquad\qquad (4\text{-}20)$$
$$abc - \eta bcx + acy + \eta abz = 0$$

and

$$
\begin{bmatrix}
\eta abc & -bc & -\eta ac & -ab \\
abc & -\eta bc & ac & \eta ab
\end{bmatrix}
\qquad (4\text{-}21)
$$

to form the Plücker coordinates

$$P = ab^2c^2 \begin{vmatrix} \eta & -1 \\ 1 & -\eta \end{vmatrix} = ab^2c^2(1-\eta^2)$$

$$Q = a^2bc^2 \begin{vmatrix} \eta & -\eta \\ 1 & 1 \end{vmatrix} = 2a^2bc^2\eta \qquad (4\text{-}22)$$

$$R = a^2b^2c \begin{vmatrix} \eta & -1 \\ 1 & \eta \end{vmatrix} = a^2b^2c(1+\eta^2)$$

and

$$L = a^2 bc \begin{vmatrix} -\eta & -1 \\ 1 & \eta \end{vmatrix} = a^2 bc(1-\eta^2)$$

$$M = ab^2 c \begin{vmatrix} -1 & -1 \\ \eta & -\eta \end{vmatrix} = 2ab^2 c\eta \qquad (4\text{-}23)$$

$$N = abc^2 \begin{vmatrix} -1 & -\eta \\ -\eta & 1 \end{vmatrix} = -abc^2(1+\eta^2)$$

yielding, after dividing by the common factor **abc**, the ray coordinates:

$$L = a\,(1-\eta^2) \qquad P = bc\,(1-\eta^2)$$

$$M = 2b\eta \qquad\qquad Q = 2ac\eta \qquad (4\text{-}24)$$

$$N = -c\,(1+\eta^2) \qquad R = ab\,(1+\eta^2)$$

This series of calculations shows that the lines of the tensegrity structure lie on a hyperboloid of one sheet, either in the "forward" (ρ) or the reverse (η) directions. The next section addresses the linear dependence inherent in the lines of a hyperboloid of one sheet and therefore the effect on the stability of the tensegrity structure.

<div align="center">Singularity Condition of the Octahedron</div>

In Chapter 5, a comparison between a 3-3 parallel platform and the octahedron will be developed. Figure 4-5 is a plan view of the octahedron (3-3 platform) with the upper platform in a central position for which the quality index, $\lambda = \dfrac{|\det J|}{|\det J_m|} = 1$ [Lee et al. 1998]. When the upper platform is rotated through $\pm 90°$ about the normal z-axis the octahedron is in a singularity. Figure 4-6 illustrates the singularity for $\phi = 90°$ when $\lambda = 0$ since $|\det J| = 0$. The rank of J is therefore 5 or less. It is not immediately obvious from the figure why the six connecting legs are in a singularity position.
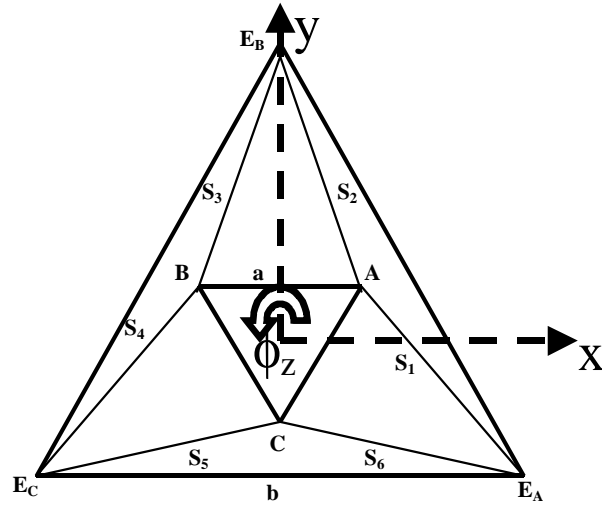
Figure 4-5. Octahedron (3-3) Platform in Central Position
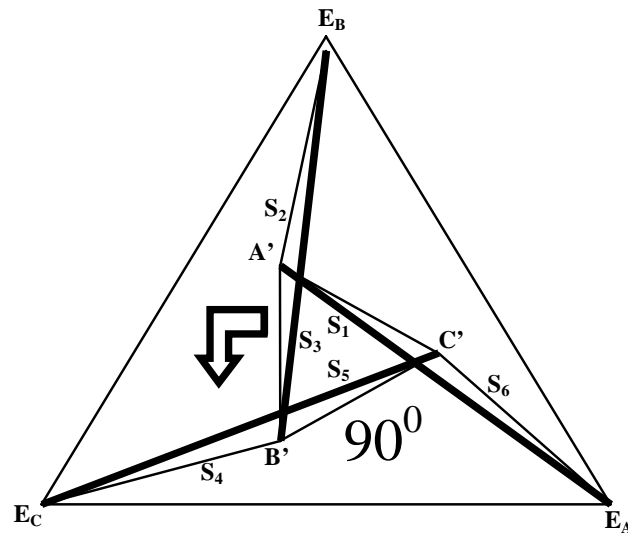
Figure 4-6. Octahedron Rotated 90° into Tensegrity

However, this illustrates a plan view of the octahedron with the moving platform

ABC rotated through $\phi = 90^{\circ}$ to the position $A'B'C'$. As defined by Lee et al. [1998],

the coordinates of $A'B'C'$ are

$$x'_A = r\cos(90° + 30°) \quad y'_A = r\sin(90° + 30°)$$

$$x'_B = r\cos(90° + 30°) \quad y'_B = -r\sin(90° + 30°)$$

$$x'_C = r\sin(90°) \qquad\quad y'_C = r\cos(90°) \tag{4-25}$$

where $r = \dfrac{a}{\sqrt{3}}$

By applying the Grassmann principles presented in (4-4), at $\phi = 90°$, the $\hat{k}$ components

for the six legs are $N_i = z$ and $R_i = \dfrac{1}{6}ab$ where i=1, 2, …6. The Plücker coordinates of

all six legs can be expressed in the form

$$\hat{S}_i^T = \begin{bmatrix} L_i & M_i & z; & P_i & Q_i & \dfrac{ab}{6} \end{bmatrix} \tag{4-26}$$

Therefore, a screw of pitch **h** on the **z**-axis is reciprocal to all six legs and the coordinates

for this screw are

$$\hat{S}^T = \begin{bmatrix} 0, & 0, & 1; & 0 & 0 & h \end{bmatrix} \tag{4-27}$$

For these equations,

$$hz + \dfrac{ab}{6} = 0 \quad \text{or} \quad h = -\dfrac{ab}{6z} \tag{4-28}$$

It follows from the previous section that all six legs lie on a linear complex and that the

platform can move instantaneously on a screw of pitch h. This suggests that the tensegrity

structure is in a singularity and therefore has instantaneous mobility.

<u>Other Forms of Quadric Surfaces</u>

The locus of an equation of the second degree in x, y, and z is called a quadric

surface. The family that includes the hyperboloid of one sheet includes the ellipsoid,

described by the equation:

$$\frac{x^2}{a^2}+\frac{y^2}{b^2}+\frac{z^2}{c^2}=1 \tag{4-29}$$

The surface is symmetrical about the origin because only second powers of the variables (x, y, and z) appear in the equation. Sections of the ellipsoid can be developed, as presented by Snyder and Sisam [1914], including imaginary sections where the coefficients become $\sqrt{-1}$. If the coefficients are a=b>c then the ellipsoid is a surface of revolution about the minor axis. If the coefficients are a>b=c then it is a surface of revolution about the major axis. If a=b=c then the surface is a sphere. If a=b=c=0 the surface is a point.

Although it is not relevant to this tensegrity structure analysis, the hyperboloid of two sheets (Figure 4-7) is described by the equation

$$\frac{x^2}{a^2}-\frac{y^2}{b^2}-\frac{z^2}{c^2}=1 \tag{4-30}$$
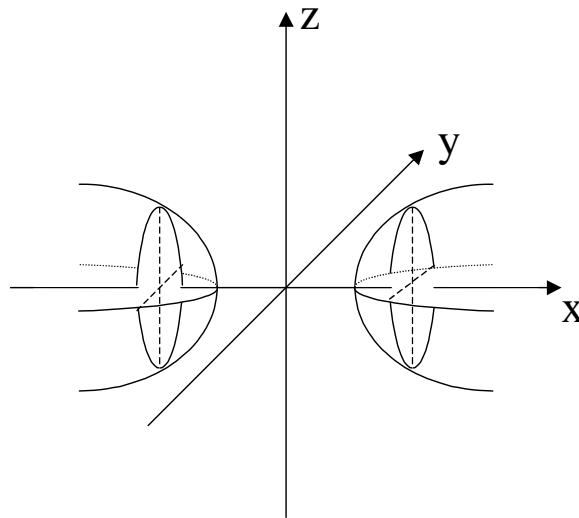
Figure 4-7. Hyperboloid of Two Sheets

Snyder and Sisam [1914] state, "It is symmetric as to each of the coordinate planes, the coordinate axes, and the origin. The plane $z = k$ intersects the surface in the hyperbola."

$$\frac{x^2}{a^2\left(1+\dfrac{k^2}{c^2}\right)} - \frac{y^2}{b^2\left(1+\dfrac{k^2}{c^2}\right)} = 1, z=k \tag{4-31}$$

The traverse axis is $y = 0$, $z = k$, for all values of k. The lengths of the semi-axes are

$a\sqrt{1+\dfrac{k^2}{c^2}}, b\sqrt{1+\dfrac{k^2}{c^2}}$. They are smallest for $k = 0$, namely a and b, and increase

without limit as $|k|$ increases. The hyperbola is not composite for any real value of k.

CHAPTER 5.
PARALLEL PLATFORM RESULTS

3-3 Solution

Previous University of Florida CIMAR research [Lee et al. 1998] on the subject of 3-3 parallel platforms, Figure 5-1 is the basis work for this research. Their study addressed the optimal metrics for a stable parallel platform.

The octahedral manipulator is a "3-3" device that is fully in parallel. It has a linear actuator on each of its six legs. The legs connect an equilateral platform triangle to a similar base triangle in a zigzag pattern between vertices. Our proposed quality index takes a maximum value of 1 at a central symmetrical configuration that is shown to correspond to the maximum value of the determinant of the 6x6 Jacobian matrix of the manipulator. This matrix is none other than that of the normalized line coordinates of the six leg-lines; for its determinant to be a maximum, the platform triangle is found to be half of the size of the base triangle, and the perpendicular distance between the platform and the base is equal to the side of the platform triangle.

The term in-parallel was first coined by Hunt [1990] to classify platform devices where all the connectors (legs) have the same kinematic structure. A common kinematic structure is designated by S-P-S, where S denotes a ball and socket joint, and P denotes a prismatic, or sliding kinematic pair. The terminology 3-3 is introduced to indicate the number of connection points in the base and top platforms. Clearly, for a 3-3 device,

there are 3 connecting points in the base, and in the top platforms as shown in Figure 5-1.

A 6-6 device would have 6 connecting points in the top and base platforms.
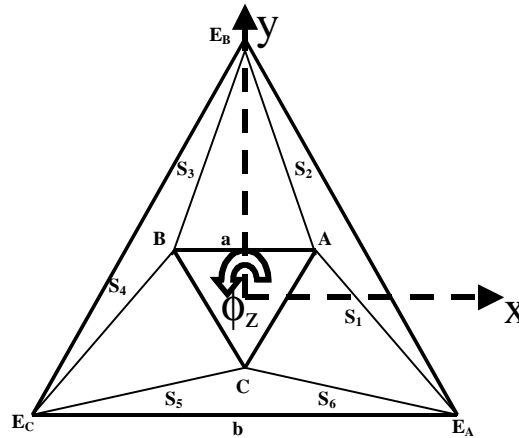
Figure 5-1. 3-3 Parallel Platform (plan view)

The parameter **a** defines the side of the platform (the moving surface); parameter **b** defines the side of the base; and parameter **h** defines the vertical (z-axis) distance between the platform and the base. The assumption that "more stable" is defined as being further away from a singularity. For a singularity, the determinant (**det J**) of the Jacobian matrix (**J**), the columns of which are the Plücker coordinates of the lines connecting the platform and the base, is zero. The most stable position occurs when **det J** is a maximum. These calculations create the "quality index" (λ), which is defined as the ratio of the **J** determinant to the maximum value.

The significance between this 3-3 manipulator research and tensegrity is the assumption that there is a correlation between the stability of a 6-strut platform and a 3-strut, 3-tie tensegrity structure. If true, this would greatly improve the stability prediction possibilities for deployable antennas based on tensegrity. As described in the abstract

paragraph above, the quality index (λ) is the ratio of the determinant of **J** to the

maximum possible value of the determinant of **J**. The dimensionless quality index is

defined by

$$\lambda = \frac{\left|\det J\right|}{\left|\det J\right|_m} \tag{5-1}$$

In later chapters, this same approach applied here for the **J** matrix of the 3-3 platform

will be used for calculating that of the 6-6 tensegrity structure. For the later case the lines

of the connecting points are defined by a 6x12 matrix and will require additional

mathematic manipulation. In this case, a 6x6 matrix defines the lines of the 3-3 platform,

and the determinant is easily calculated. The matrix values are normalized through

dividing by the nominal leg length, to remove any specific design biases.

The centroid of the triangle is considered to be the coordinate (0,0). From that basis,

the coordinates for the upper and lower platforms are

$$A\left(\frac{a}{2} \quad \frac{a}{2\sqrt{3}} \quad 0\right), \; B\left(-\frac{a}{2} \quad \frac{a}{2\sqrt{3}} \quad 0\right), \; C\left(0 \quad -\frac{a}{\sqrt{3}} \quad 0\right) \tag{5-2}$$

$$E_A\left(\frac{b}{2} \quad -\frac{b}{2\sqrt{3}} \quad -h\right), \; E_B\left(0 \quad \frac{b}{\sqrt{3}} \quad -h\right), \; E_C\left(-\frac{b}{2} \quad -\frac{b}{2\sqrt{3}} \quad -h\right) \tag{5-3}$$

The Grassmann method for calculating the Plücker coordinates is now applied to the

3-3 design, as described in Chapter 4. Briefly, the coordinates for a line that joins a pair

of points can easily be obtained by counting the 2x2 determinants of the 2x4 array

describing the connecting lines.

$$\hat{S}_1 \equiv \begin{bmatrix} \dfrac{a-b}{2} & \dfrac{a+b}{2\sqrt{3}} & h; & \dfrac{ah}{2\sqrt{3}} & -\dfrac{ah}{2} & \dfrac{ab}{2\sqrt{3}} \end{bmatrix}$$

$$\hat{S}_2 \equiv \begin{bmatrix} -\dfrac{a}{2} & \dfrac{2b-a}{2\sqrt{3}} & -h; & -\dfrac{ah}{2\sqrt{3}} & \dfrac{ah}{2} & \dfrac{ab}{2\sqrt{3}} \end{bmatrix}$$

$$\hat{S}_3 \equiv \begin{bmatrix} -\dfrac{a}{2} & \dfrac{a-2b}{2\sqrt{3}} & h; & \dfrac{ah}{2\sqrt{3}} & \dfrac{ah}{2} & \dfrac{ab}{2\sqrt{3}} \end{bmatrix}$$

$$\hat{S}_4 \equiv \begin{bmatrix} \dfrac{a-b}{2} & -\dfrac{a+b}{2\sqrt{3}} & -h; & -\dfrac{ah}{2\sqrt{3}} & -\dfrac{ah}{2} & \dfrac{ab}{2\sqrt{3}} \end{bmatrix} \qquad (5\text{-}4)$$

$$\hat{S}_5 \equiv \begin{bmatrix} \dfrac{b}{2} & \dfrac{b-2a}{2\sqrt{3}} & h; & -\dfrac{ah}{\sqrt{3}} & 0 & \dfrac{ab}{2\sqrt{3}} \end{bmatrix}$$

$$\hat{S}_6 \equiv \begin{bmatrix} \dfrac{b}{2} & \dfrac{2a-b}{2\sqrt{3}} & -h; & \dfrac{ah}{\sqrt{3}} & 0 & \dfrac{ab}{2\sqrt{3}} \end{bmatrix}$$

which yields the matrix for this system of

$$\det J = \frac{1}{\ell^6} \begin{vmatrix} \hat{S}_1 & \hat{S}_2 & \hat{S}_3 & \hat{S}_4 & \hat{S}_5 & \hat{S}_6 \end{vmatrix} \qquad (5\text{-}5)$$

The normalization divisor is the same for each leg (they are the same length),

therefore, $\ell = \sqrt{L^2 + M^2 + N^2} = \sqrt{\dfrac{1}{3}\left(a^2 - ab + b^2 + 3h^2\right)}$ and the expansion of the

determinant yields

$$\left| \det J \right| = \frac{3\sqrt{3}a^3b^3h^3}{4\left(\dfrac{a^2 - ab + b^2}{3} + h^2\right)^3} \qquad (5\text{-}6)$$

Dividing above and below by h^3 yields

$$\left| \det J \right| = \frac{3\sqrt{3}a^3b^3}{4\left(\dfrac{a^2 - ab + b^2}{3h} + h\right)^3} \qquad (5\text{-}7)$$

The key to calculating the maximum value for the quality index is to find the maximum

height, **h**. Differentiating the denominator of the determinant with respect to **h**, and

equating to zero to obtain a maximum value for **det J** yields the following expression for h.

$$h = h_m = \sqrt{\frac{1}{3}\left(a^2 - ab + b^2\right)}$$

(5-8)

If we now select values for **a** and **b**, (5-7) yields the value h_m for **det J** to be a maximum.

$$\left|\det J\right|_m = \frac{27a^3 b^3}{32\left(a^2 - ab + b^2\right)^{\frac{3}{2}}}$$

(5-9)

Further, we now determine the ratio $\gamma=b/a$ to yield a maximum absolute value $\left|\det J\right|_m$. Substituting **b= γa** in Equation 5-7 yields

$$\left|\det J\right|_m = \frac{27a^3\gamma^3 a^3}{32\left(a^2 - \gamma a^2 + \gamma^2 a^2\right)^{\frac{3}{2}}} \frac{\frac{1}{\gamma^3 a^3}}{\frac{1}{\gamma^3 a^3}} = \frac{27a^3}{32\left(\frac{1}{\gamma^2} - \frac{1}{\gamma} + 1\right)}$$

(5-10)

To get the absolute maximum value of this determinant, the derivative with respect to **γ** is taken which yields:

$$\frac{1}{\gamma^2}\left(1 - \frac{2}{\gamma}\right) = 0$$
$$\gamma = \frac{b}{a} = 2$$

(5-11)

Substituting this result in (5-8) gives:

$$\frac{h}{a} = 1$$

(5-12)

This work shows some similarity to the values to be derived for the 6-6 platform. The original quality index equation reduces to a function of (platform height) / (platform height at the maximum index).

$$\lambda = \frac{8\left(\dfrac{h}{h_m}\right)^3}{\left\{1+\left(\dfrac{h}{h_m}\right)^2\right\}^3}$$ (5-13)

The resulting quality index plots for this 3-3 structure are found in Figures 5-2 through 5-6. In Figure 5-2, the quality index varies about the geometric center of the structure, with usable working area (index greater than 0.8) within half of the base dimension (b). It is interesting to note that these are not circles, but slightly flattened at the plot's 45° locations.
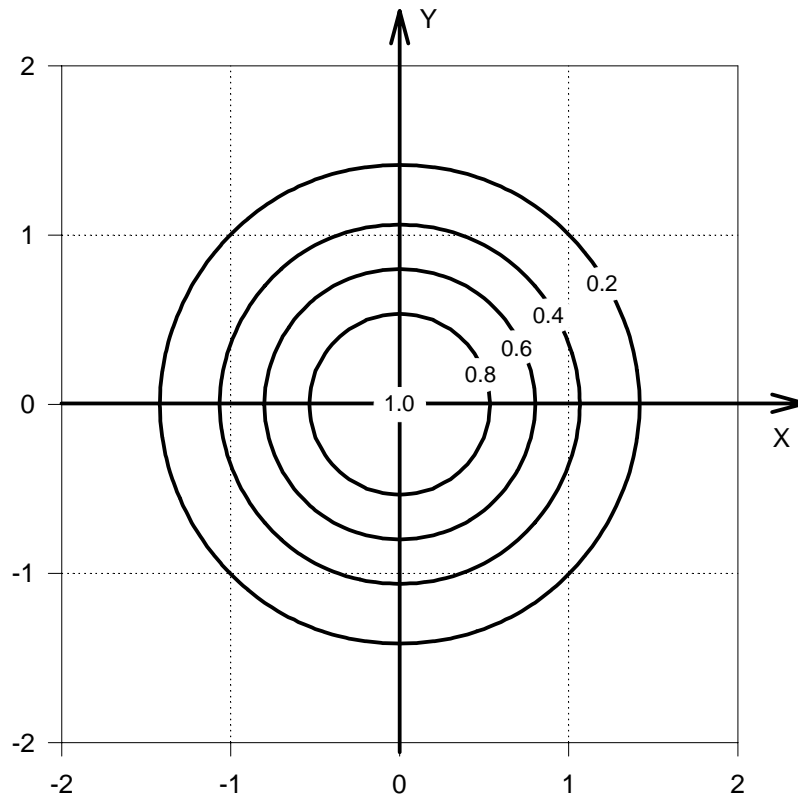
Figure 5-2. Coplanar translation of Platform from Central Location: Contours of Quality Index
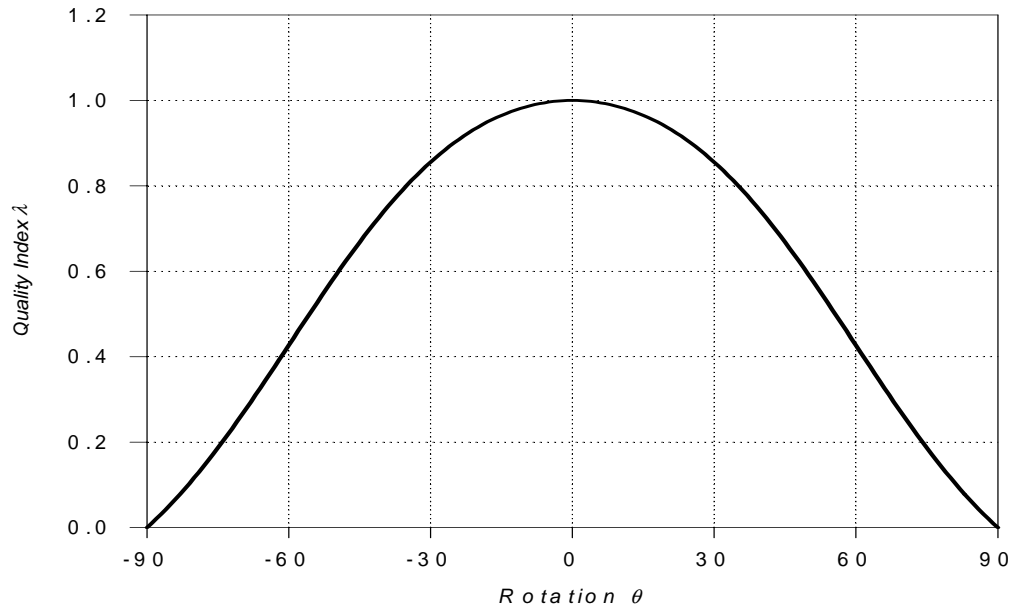
Figure 5-3. Rotation of Platform About Z-axis
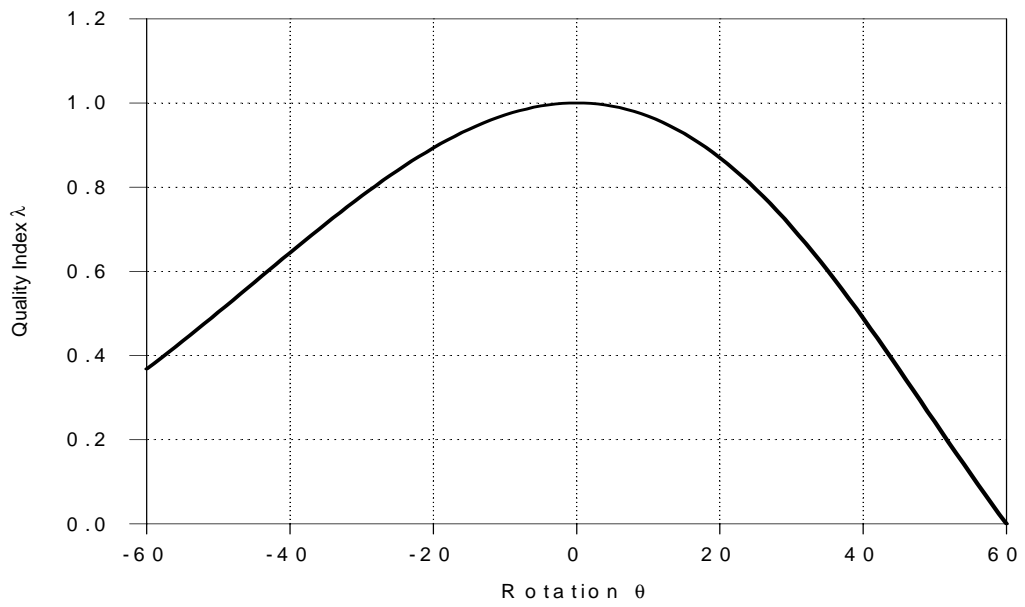
Figure 5-4. Rotation of Platform About X-axis
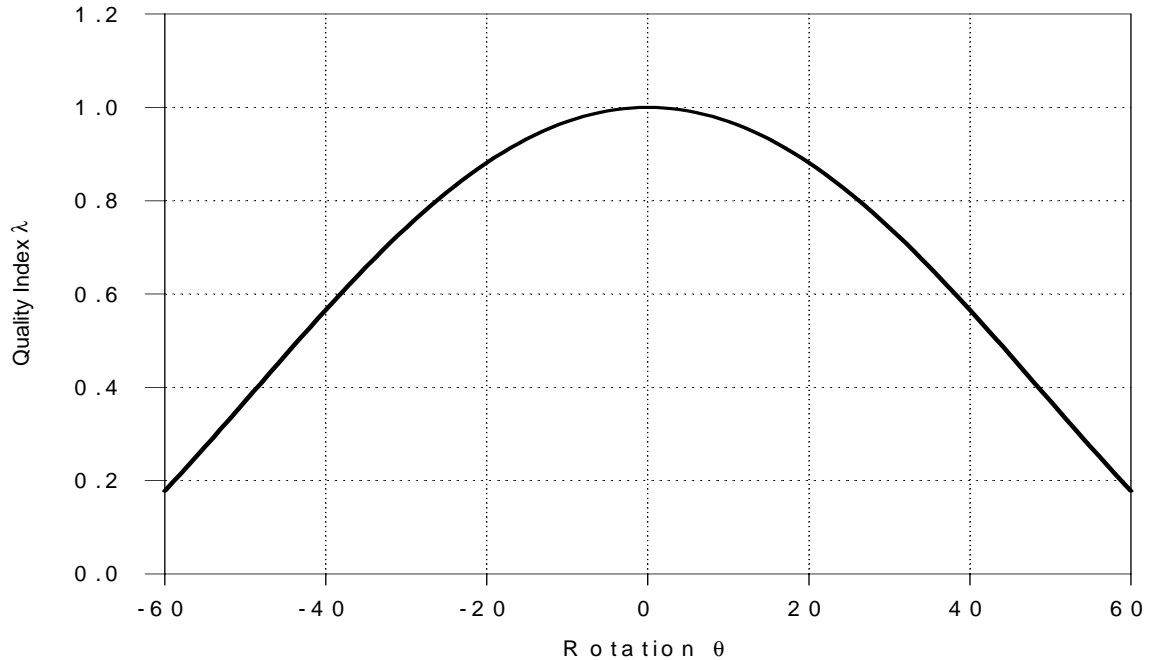
Figure 5-5. Rotation of Platform About Y-axis

As expected, rotations about the z-axis yield values approaching zero, where the singularity occurs. What is unique is that there are workable quality indices when the structure is rotated about the x- and y-axes over 20°. This could be valuable for antenna repointing without using an antenna gimbal.

Figure 5-6 presents the change in quality index due to the height of the platform relative to the maximum value. Obviously, the greatest value (1.0) occurs when these values are equal. From this it is apparent that a working envelope of 40% (+/-20% about the maximum) is achievable. Again, this discovery is helpful in the design on working antenna systems to address multiple feed centers.
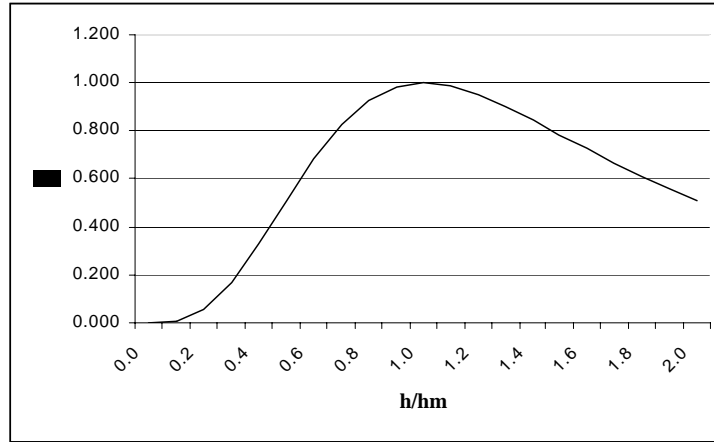
Figure 5-6. Quality Index as a Function of the Height Ratio

4-4 Solution

The 4-4 parallel platform (Figure 5-7) is a square anti-prism. The calculations of the 4-4 quality index are similar to those for the 3-3 platform; however, because the 4-4 line coordinates yield a 6x8 matrix, the determinant cannot be calculated directly and we introduce $\mathbf{JJ^T}$ [Knight, 1998], the product of the matrix and its transpose. As with the 3-3 platform, λ is defined as the ratio of the Jacobian determinant to the maximized $\mathbf{J}$ determinant.
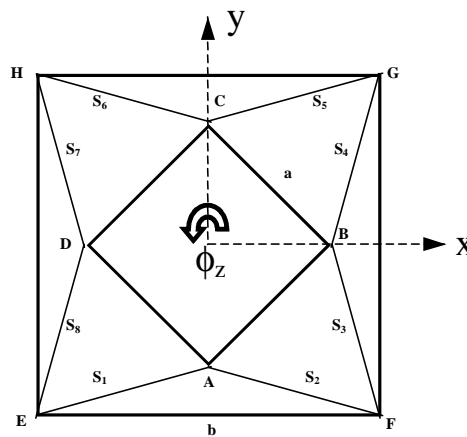
Figure 5-7. The 4-4 Parallel Platform (plan view)

$$\lambda = \sqrt{\dfrac{\det JJ^T}{\det J_m J_m^T}} \qquad (5\text{-}14)$$

From the Cauchy-Binet theorem, it can be shown that $\det J \cdot J^T = \Delta_1^2 + \Delta_2^2 + \ldots + \Delta_n^2$.

Each Δ is the determinant of a 6x6 submatrix of the 6x8 matrix. It is clear that (5-14)

reduces to (5-1) for the 6x6 matrix. This method can be used for any 6xn matrix. As with

the 3-3 platform, the determinant is calculated. As shown in the figure, the value for the

side of the platform (moving plane) is a. Similarly; b is the value for the base side. The

distance between the upper surface and the base surface is h. The definition of the line

coordinate endpoints is

$$A\left(0 \quad -\dfrac{\sqrt{2}a}{2} \quad h\right), \quad B\left(\dfrac{\sqrt{2}a}{2} \quad 0 \quad h\right), \quad C\left(0 \quad \dfrac{\sqrt{2}a}{2} \quad h\right), \quad D\left(-\dfrac{\sqrt{2}a}{2} \quad 0 \quad h\right);$$

$$E\left(-\dfrac{b}{2} \quad -\dfrac{b}{2} \quad 0\right), \quad F\left(\dfrac{b}{2} \quad -\dfrac{b}{2} \quad 0\right), \quad G\left(\dfrac{b}{2} \quad \dfrac{b}{2} \quad 0\right), \quad H\left(-\dfrac{b}{2} \quad \dfrac{b}{2} \quad 0\right) \qquad (5\text{-}15)$$

Therefore, the Jacobian matrix is

$$J = \dfrac{1}{\ell^6}\begin{bmatrix} \dfrac{b}{2} & -\dfrac{b}{2} & \dfrac{\sqrt{2}a-b}{2} & -\dfrac{b}{2} & \dfrac{b}{2} & \dfrac{-\sqrt{2}a+b}{2} & \dfrac{\sqrt{2}a-b}{2} & \dfrac{-\sqrt{2}a+b}{2} \\[2mm] \dfrac{-\sqrt{2}a+b}{2} & \dfrac{-\sqrt{2}a+b}{2} & -\dfrac{b}{2} & \dfrac{\sqrt{2}a-b}{2} & \dfrac{\sqrt{2}a-b}{2} & -\dfrac{b}{2} & \dfrac{b}{2} & \dfrac{b}{2} \\[2mm] h & h & h & h & h & h & h & h \\[2mm] -\dfrac{bh}{2} & -\dfrac{bh}{2} & \dfrac{bh}{2} & \dfrac{bh}{2} & \dfrac{bh}{2} & \dfrac{bh}{2} & -\dfrac{bh}{2} & -\dfrac{bh}{2} \\[2mm] \dfrac{bh}{2} & -\dfrac{bh}{2} & -\dfrac{bh}{2} & -\dfrac{bh}{2} & \dfrac{bh}{2} & \dfrac{bh}{2} & -\dfrac{bh}{2} & -\dfrac{bh}{2} \\[2mm] \dfrac{\sqrt{2}ab}{4} & -\dfrac{\sqrt{2}ab}{4} & -\dfrac{\sqrt{2}ab}{4} & \dfrac{\sqrt{2}ab}{4} & -\dfrac{\sqrt{2}ab}{4} & \dfrac{\sqrt{2}ab}{4} & \dfrac{\sqrt{2}ab}{4} & -\dfrac{\sqrt{2}ab}{4} \end{bmatrix} \qquad (5\text{-}16)$$

It follows that $\sqrt{\det JJ^T}$ is given by

$$\sqrt{\det J \cdot J^T} = \dfrac{32\sqrt{2}a^3 b^3 h^3}{\left(a^2 - \sqrt{2}ab + b^2 + 2h^2\right)^3} \qquad (5\text{-}17)$$

By following the same procedure as used for the 3-3 parallel platform, the key to

calculating the maximum value for the quality index is to find the maximum height, **h**. To

find this expression, the numerator and denominator are both divided by $\mathbf{h^3}$, to ensure that

h is only found in the denominator. Differentiating the denominator with respect to **h**, and

equating this value to zero provides the maximum expression.

$$h = h_m = \sqrt{\frac{1}{2}\left(a^2 - \sqrt{2}ab + b^2\right)} \tag{5-18}$$

Again, as presented in the 3-3 analysis, this maximum value for **h** is included in

(5-17) to provide the maximum determinant.

$$\sqrt{\det J_m J_m^T} = \frac{2a^3 b^3}{\left(a^2 - \sqrt{2}ab + b^2\right)^{\frac{3}{2}}} \tag{5-19}$$

To determine the ratio $\mathbf{\gamma=b/a}$ for the maximum expression for (5-19), $\mathbf{b=\gamma a}$ is substituted.

The numerator and denominator are also both divided by $\mathbf{\gamma^3 a^3}$.

$$\sqrt{\det J_m J_m^T} = \frac{2a^3}{\left(1 - \frac{\sqrt{2}}{\gamma} + \frac{1}{\gamma^2}\right)^{\frac{3}{2}}} \tag{5-20}$$

To get the maximum value of this determinant, the derivative with respect to $\boldsymbol{\gamma}$ is taken.

This yields the ratio between **a**, **b**, and **h**.

$$\gamma = \frac{b}{a} = \sqrt{2} \tag{5-21}$$

CHAPTER 6.
6-6 DESIGN

6-6 Introduction

The 6-6 in-parallel platform (a hexagonal anti-prism) is the basis for this new

deployable antenna design. Using the previously derived mathematics, similar quality

index values are developed. This defines the stability of the structure once it is in an

equilibrium position. As with the 4-4 platform, the Cauchy-Binet theorem is used to

determine the index. Once the mathematics is determined, further attention will be

applied to antenna design.

Sketch

Figure 6-1 presents the 6-6 in-parallel platform. This is a highly redundant parallel

platform with 12 legs for 6 degrees of freedom, but can also be manipulated to define an

antenna subsystem by applying tensegrity structure design. This approach will be

presented in a later chapter.
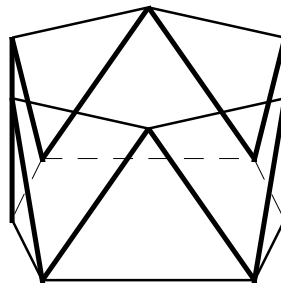
Figure 6-1. A 6-6 Parallel Platform (Hexagonal Anti-Prism)

A plan view of the 6-6 parallel (redundant) platform is shown in Figure 6-2. Double lines depict the base and top platform outlines. Heavy lines depict the connectors. The base coordinates are G_A through G_F; the platform coordinates are A through F. The first segment is S_1 connecting points G_A (base) and A (platform); the last segment is S_{12} connecting points G_A and F. The base coordinates are all fixed and the x-y-z coordinate system is located in the base with the x-y plane in the base plane. Hence, the base coordinates are
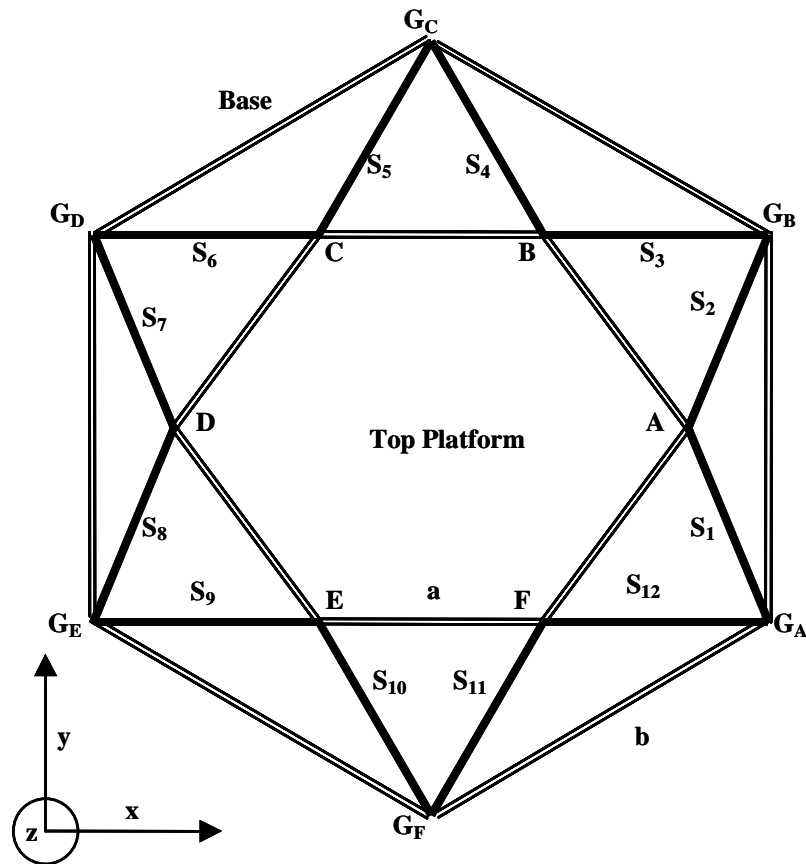
Figure 6-2. A Plan View for the 6-6 Parallel Platform (Hexagonal Anti-Prism)

$$G_A \left[\frac{\sqrt{3b}}{2} \quad -\frac{b}{2} \quad 0 \right] \quad G_B \left[\frac{\sqrt{3b}}{2} \quad \frac{b}{2} \quad 0 \right] \quad G_C \left[0 \quad b \quad 0 \right] \qquad (6\text{-}1)$$

$$G_D\left[-\frac{\sqrt{3b}}{2} \quad \frac{b}{2} \quad 0\right] \quad G_E\left[-\frac{\sqrt{3b}}{2} \quad -\frac{b}{2} \quad 0\right] \quad G_F[0 \quad -b \quad 0] \tag{6-2}$$

The coordinates for the top platform vertices at the central position are (6-3) where h is the height of the top platform above the base.

$$A[a \quad 0 \quad h] \quad B\left[\frac{a}{2} \quad \frac{\sqrt{3a}}{2} \quad h\right] \quad C\left[-\frac{a}{2} \quad \frac{\sqrt{3a}}{2} \quad h\right]$$

$$D[-a \quad 0 \quad h] \quad E\left[-\frac{a}{2} \quad -\frac{\sqrt{3a}}{2} \quad h\right] \quad F\left[\frac{a}{2} \quad -\frac{\sqrt{3a}}{2} \quad h\right] \tag{6-3}$$

Applying Grassmann's method (see Chapter 4) to obtain the line coordinates yields the following 12 arrays.

$$S_1[G_A \quad A]:\begin{bmatrix} 1 & \frac{\sqrt{3b}}{2} & -\frac{b}{2} & 0 \\ 1 & a & 0 & h \end{bmatrix} \quad S_2[G_B \quad A]:\begin{bmatrix} 1 & \frac{\sqrt{3b}}{2} & \frac{b}{2} & 0 \\ 1 & a & 0 & h \end{bmatrix}$$

$$S_3[G_B \quad B]:\begin{bmatrix} 1 & \frac{\sqrt{3b}}{2} & \frac{b}{2} & 0 \\ 1 & \frac{a}{2} & \frac{\sqrt{3a}}{2} & h \end{bmatrix} \quad S_4[G_C \quad B]:\begin{bmatrix} 1 & 0 & b & 0 \\ 1 & \frac{a}{2} & \frac{\sqrt{3a}}{2} & h \end{bmatrix}$$

$$S_5[G_C \quad C]:\begin{bmatrix} 1 & 0 & b & 0 \\ 1 & -\frac{a}{2} & \frac{\sqrt{3a}}{2} & h \end{bmatrix} \quad S_6[G_D \quad C]:\begin{bmatrix} 1 & -\frac{\sqrt{3b}}{2} & \frac{b}{2} & 0 \\ 1 & -\frac{a}{2} & \frac{\sqrt{3a}}{2} & h \end{bmatrix}$$

$$S_7[G_D \quad D]:\begin{bmatrix} 1 & -\frac{\sqrt{3b}}{2} & \frac{b}{2} & 0 \\ 1 & -a & 0 & h \end{bmatrix} \quad S_8[G_E \quad D]:\begin{bmatrix} 1 & -\frac{\sqrt{3b}}{2} & -\frac{b}{2} & 0 \\ 1 & -a & 0 & h \end{bmatrix} \tag{6-4}$$

$$S_9[G_E \quad E]:\begin{bmatrix} 1 & -\frac{\sqrt{3b}}{2} & -\frac{b}{2} & 0 \\ 1 & -\frac{a}{2} & -\frac{\sqrt{3a}}{2} & h \end{bmatrix} \quad S_{10}[G_F \quad E]:\begin{bmatrix} 1 & 0 & -b & 0 \\ 1 & -\frac{a}{2} & -\frac{\sqrt{3a}}{2} & h \end{bmatrix}$$

$$S_{11}[G_F \quad F]:\begin{bmatrix} 1 & 0 & -b & 0 \\ 1 & \frac{a}{2} & -\frac{\sqrt{3a}}{2} & h \end{bmatrix} \quad S_{12}[G_A \quad F]:\begin{bmatrix} 1 & \frac{\sqrt{3b}}{2} & -\frac{b}{2} & 0 \\ 1 & \frac{a}{2} & -\frac{\sqrt{3a}}{2} & h \end{bmatrix}$$

Counting the 2x2 determinants (see Chapter 4) yields the [L, M, N; P, Q, R] line coordinates for each of the twelve legs. The normalized line coordinates were found by dividing the calculated value by the nominal lengths of the legs for the central position.

$$\ell = \frac{1}{2}\sqrt{4\left(a - \frac{\sqrt{3}}{2}b\right)^2 + b^2 + 4h^2}$$
(6-5)

Evaluating the Jacobian

The **J** matrix, comprised of the line coordinates for the twelve legs, is a 6x12 array.

$$\frac{1}{2^{12}\ell^{12}}\begin{bmatrix} 2a-\sqrt{3}b & 2a-\sqrt{3}b & a-\sqrt{3}b & a & -a & -a+\sqrt{3}b \\ b & -b & \sqrt{3}a-b & \sqrt{3}a-2b & \sqrt{3}a-2b & \sqrt{3}a-b \\ 2h & 2h & 2h & 2h & 2h & 2h \\ -bh & bh & bh & 2bh & 2bh & bh \\ -\sqrt{3}bh & -\sqrt{3}bh & -\sqrt{3}bh & 0 & 0 & \sqrt{3}bh \\ ab & -ab & ab & -ab & ab & -ab \end{bmatrix}$$

(6-6)

$$\begin{bmatrix} -2a+\sqrt{3}b & -2a+\sqrt{3}b & -a+\sqrt{3}b & -a & a & a-\sqrt{3}b \\ -b & b & -\sqrt{3}a+b & -\sqrt{3}a+2b & -\sqrt{3}a+2b & -\sqrt{3}a+b \\ 2h & 2h & 2h & 2h & 2h & 2h \\ bh & -bh & -bh & -2bh & 2h & -bh \\ \sqrt{3}bh & \sqrt{3}bh & \sqrt{3}bh & 0 & -2bh & -\sqrt{3}bh \\ ab & -ab & ab & -ab & ab & -ab \end{bmatrix}$$

$\mathbf{J^T}$ is, therefore, the transpose (a 12x6 matrix).

$$\frac{1}{2^{12}\ell^{12}}\begin{bmatrix} 2a-\sqrt{3}b & b & 2h & -bh & -\sqrt{3}bh & ab \\ 2a-\sqrt{3}b & -b & 2h & bh & -\sqrt{3}bh & -ab \\ a-\sqrt{3}b & \sqrt{3}a-b & 2h & bh & -\sqrt{3}bh & ab \\ a & \sqrt{3}a-2b & 2h & 2bh & 0 & -ab \\ -a & \sqrt{3}a-2b & 2h & 2bh & 0 & ab \\ -a+\sqrt{3}b & \sqrt{3}a-b & 2h & bh & \sqrt{3}bh & -ab \\ -2a+\sqrt{3}b & -b & 2h & bh & \sqrt{3}bh & ab \\ -2a+\sqrt{3}b & b & 2h & -bh & \sqrt{3}bh & -ab \\ -a+\sqrt{3}b & -\sqrt{3}a+b & 2h & -bh & \sqrt{3}bh & ab \\ -a & -\sqrt{3}a+2b & 2h & -2bh & 0 & -ab \\ a & -\sqrt{3}a+2b & 2h & -2bh & 0 & ab \\ a-\sqrt{3}b & -\sqrt{3}a+b & 2h & -bh & -\sqrt{3}bh & -ab \end{bmatrix} \qquad (6\text{-}7)$$

Optimization Solution

Lee et al. [1998] developed the optimization method for the 3-3 and 4-4 platforms. The method for calculating the optimization value for the 6-6 J matrix (non-symmetric) is an extension of the 4-4 platform solution. The quality index λ is given by

$$\lambda = \left[\frac{\sqrt{\det \mathbf{JJ^T}}}{\sqrt{\det \mathbf{J_m J_m^T}}}\right] \qquad (6\text{-}8)$$

For this example, $\sqrt{\det \mathbf{JJ^T}}$ is calculated.

$$\sqrt{\det \mathbf{JJ^T}} = 54\frac{a^3 b^3 h^3}{\left(a^2 - \sqrt{3}ab + b^2 + h^2\right)^3} \qquad (6\text{-}9)$$

As with the 4-4 parallel platform calculation, the maximum height (**h**) must be found. To find this expression, the numerator and denominator of (6-9) are both divided by $\mathbf{h^3}$, to ensure that **h** is only found in the denominator. Then, differentiating with respect to **h** and equating to zero provides the maximum expression.

$$h = h_m = \sqrt{a^2 - \sqrt{3}ab + b^2} \tag{6-10}$$

As with the 4-4 analysis, this maximum value for **h** is included in (6-9) to provide the maximum determinant.

$$\sqrt{\det J_m J_m^T} = \frac{54}{8} \frac{a^3 b^3}{\left(a^2 - \sqrt{3}ab + b^2\right)^{\frac{3}{2}}} \tag{6-11}$$

This yields the λ value (quality index) as a function of **a** and **b**.

$$\lambda = \frac{\sqrt{\det JJ^T}}{\sqrt{\det J_m J_m^T}} = \frac{8h^3 \left(a^2 - \sqrt{3}ab + b^2\right)^{\frac{3}{2}}}{\left(a^2 - \sqrt{3}ab + b^2 + h^2\right)^3} \tag{6-12}$$

This index (λ) is a value between zero (0) and one (1), which represents the stability of the structure.

As with the 4-4 structure, the ratio γ=**b/a**, which represents the parameter ratio at the maximum quality index, is determined by substituting for **b**=γ**a**.

$$\sqrt{\det J_m J_m^T} = \frac{54}{8} \frac{a^3 \gamma^3 a^3}{\left(a^2 - \sqrt{3}a\gamma a + (\gamma a)^2\right)^{\frac{3}{2}}} \tag{6-13}$$

Again, the numerator and denominator are both divided by $\mathbf{\gamma^3 a^3}$.

$$\sqrt{\det J_m J_m^T} = \frac{54}{8} \frac{a^3}{\left(\dfrac{1}{\gamma^2} - \dfrac{\sqrt{3}}{\gamma} + 1\right)^{\frac{3}{2}}} \tag{6-14}$$

By differentiating the denominator with respect to γ, the maximum and minimum values are determined. This yields the solution for the most stable geometry for the 6-6 platform.

$$\frac{\partial}{\partial\gamma}\left[\frac{1}{\gamma^2} - \frac{\sqrt{3}}{\gamma} + 1\right]^{\frac{3}{2}} = \frac{3}{2}\left[\frac{1}{\gamma^2} - \frac{\sqrt{3}}{\gamma} + 1\right]^{\frac{1}{2}}\left[\frac{-2}{\gamma^3} + \frac{\sqrt{3}}{\gamma^2}\right] = 0 \qquad (6\text{-}15)$$

The vanishing of the first bracket of the right side of the equation yields imaginary solution, whilst the second bracket yields

$$\gamma = \frac{2}{\sqrt{3}} = \frac{b}{a} \qquad (6\text{-}16)$$

$$h = \frac{a}{\sqrt{3}} \quad \text{and} \quad b = \frac{2a}{\sqrt{3}} \qquad (6\text{-}17)$$

<div align="center">Variable Screw Motion on the Z-Axis</div>

Duffy et al. [1998] presented a study of special motions for an octahedron using screw theory. The moving platform remains parallel to the base and moves on a screw of variable pitch (**p**). The screw axis is along the Z direction.

$$X_A = r\cos(\phi_z) \qquad (6\text{-}18)$$

$$Y_A = r\sin(\phi_z) \qquad (6\text{-}19)$$

$$X_B = r\cos(\phi_z + 60^o) = r(\frac{1}{2}\cos\phi_z - \frac{\sqrt{3}}{2}\sin\phi_z) \qquad (6\text{-}20)$$

$$Y_B = r\sin(\phi_z + 60^o) = r(\frac{1}{2}\sin\phi_z + \frac{\sqrt{3}}{2}\cos\phi_z) \qquad (6\text{-}21)$$

$$X_C = r\cos(\phi_z + 120^o) = -r(\frac{1}{2}\cos\phi_z + \frac{\sqrt{3}}{2}\sin\phi_z) \qquad (6\text{-}22)$$

$$Y_C = r\sin(\phi_z + 120^o) = -r(\frac{1}{2}\sin\phi_z - \frac{\sqrt{3}}{2}\cos\phi_z) \qquad (6\text{-}23)$$

$$X_D = r\cos(\phi_z + 180^o) = -r\cos\phi_z \tag{6-24}$$

$$Y_D = r\sin(\phi_z + 180^o) = -r\sin\phi_z \tag{6-25}$$

$$X_E = r\cos(\phi_z + 240^o) = -r(\frac{1}{2}\cos\phi_z - \frac{\sqrt{3}}{2}\sin\phi_z) \tag{6-26}$$

$$Y_E = r\sin(\phi_z + 240^o) = -r(\frac{1}{2}\sin\phi_z + \frac{\sqrt{3}}{2}\cos\phi_z) \tag{6-27}$$

$$X_F = r\cos(\phi_z + 300^o) = r(\frac{1}{2}\cos\phi_z + \frac{\sqrt{3}}{2}\sin\phi_z) \tag{6-28}$$

$$Y_F = r\cos(\phi_z + 300^o) = r(\frac{1}{2}\sin\phi_z - \frac{\sqrt{3}}{2}\cos\phi_z) \tag{6-29}$$

It is important to recognize that simply actuating the struts by giving each the same incremental increase or decrease in length can produce the motion. Continuity requires that the sum of the coordinates (about the circle defined) sums to zero.

$$X_A + X_B + X_C + X_D + X_E + X_F = 0 \qquad Y_A + Y_B + Y_C + Y_D + Y_E + Y_F = 0 \tag{6-30}$$

Similar to previous octahedron and square platform papers, the radius from the center of the structure to the platform coordinates is equal to the length of the platform side ($r = a$).

Using the base and platform coordinates previously defined, the Plücker line coordinates are calculated using the Grassmann principle by counting the 2 x 2 determinants of each of the 2 x 4 arrays.

$$S_1[G_A \quad A]: \begin{bmatrix} 1 & \frac{\sqrt{3}b}{2} & -\frac{b}{2} & 0 \\ 1 & X_A & Y_A & h \end{bmatrix} \qquad S_2[G_B \quad A]: \begin{bmatrix} 1 & \frac{\sqrt{3}b}{2} & \frac{b}{2} & 0 \\ 1 & X_A & Y_A & h \end{bmatrix} \tag{6-31}$$

$$S_3[G_B \quad B]: \begin{bmatrix} 1 & \dfrac{\sqrt{3}b}{2} & \dfrac{b}{2} & 0 \\ 1 & X_B & Y_B & h \end{bmatrix} \qquad S_4[G_C \quad B]: \begin{bmatrix} 1 & 0 & b & 0 \\ 1 & X_B & Y_B & h \end{bmatrix} \tag{6-32}$$

$$S_5[G_C \quad C]: \begin{bmatrix} 1 & 0 & b & 0 \\ 1 & X_C & Y_C & h \end{bmatrix} \qquad S_6[G_D \quad C]: \begin{bmatrix} 1 & -\dfrac{\sqrt{3}b}{2} & \dfrac{b}{2} & 0 \\ 1 & X_C & Y_C & h \end{bmatrix} \tag{6-33}$$

$$S_7[G_D \quad D]: \begin{bmatrix} 1 & -\dfrac{\sqrt{3}b}{2} & \dfrac{b}{2} & 0 \\ 1 & X_D & Y_D & h \end{bmatrix} \qquad S_8[G_E \quad D]: \begin{bmatrix} 1 & -\dfrac{\sqrt{3}b}{2} & -\dfrac{b}{2} & 0 \\ 1 & X_D & Y_D & h \end{bmatrix} \tag{6-34}$$

$$S_9[G_E \quad E]: \begin{bmatrix} 1 & -\dfrac{\sqrt{3}b}{2} & -\dfrac{b}{2} & 0 \\ 1 & X_E & Y_E & h \end{bmatrix} \qquad S_{10}[G_F \quad E]: \begin{bmatrix} 1 & 0 & -b & 0 \\ 1 & X_E & Y_E & h \end{bmatrix} \tag{6-35}$$

$$S_{11}[G_F \quad F]: \begin{bmatrix} 1 & 0 & -b & 0 \\ 1 & X_F & Y_F & h \end{bmatrix} \qquad S_{12}[G_A \quad F]: \begin{bmatrix} 1 & \dfrac{\sqrt{3}b}{2} & -\dfrac{b}{2} & 0 \\ 1 & X_F & Y_F & h \end{bmatrix} \tag{6-36}$$

The Plücker coordinates are defined by the 2x2 determinants of these 2x4 arrays.

$$\hat{S}_1^T = \left[\left(X_A - \frac{\sqrt{3}b}{2} \right) \quad \left(Y_A + \frac{b}{2} \right) \quad h; \quad -\frac{bh}{2} \quad -\frac{\sqrt{3}bh}{2} \quad \frac{b}{2}\left(\sqrt{3}Y_A + X_A \right) \right] \tag{6-37}$$

$$\hat{S}_2^T = \left[\left(X_A - \frac{\sqrt{3}b}{2} \right) \quad \left(Y_A - \frac{b}{2} \right) \quad h; \quad \frac{bh}{2} \quad -\frac{\sqrt{3}bh}{2} \quad \frac{b}{2}\left(\sqrt{3}Y_A - X_A \right) \right] \tag{6-38}$$

$$\hat{S}_3^T = \left[\left(X_B - \frac{\sqrt{3}b}{2} \right) \quad \left(Y_B - \frac{b}{2} \right) \quad h; \quad \frac{bh}{2} \quad -\frac{\sqrt{3}bh}{2} \quad \frac{b}{2}\left(\sqrt{3}Y_B - X_B \right) \right] \tag{6-39}$$

$$\hat{S}_4^T = \left[X_B \quad \left(Y_B - b \right) \quad h; \quad bh \quad 0 \quad -bX_B \right] \tag{6-40}$$

$$\hat{S}_5^T = \left[X_C \quad \left(Y_C - b \right) \quad h; \quad bh \quad 0 \quad -bX_C \right] \tag{6-41}$$

$$\hat{S}_6^T = \left[\left(X_C + \frac{\sqrt{3}b}{2} \right) \quad \left(Y_C - \frac{b}{2} \right) \quad h; \quad \frac{bh}{2} \quad \frac{\sqrt{3}bh}{2} \quad -\frac{b}{2}\left(\sqrt{3}Y_C + X_C\right) \right] \tag{6-42}$$

$$\hat{S}_7^T = \left[\left(X_D + \frac{\sqrt{3}b}{2} \right) \quad \left(Y_D - \frac{b}{2} \right) \quad h; \quad \frac{bh}{2} \quad \frac{\sqrt{3}bh}{2} \quad -\frac{b}{2}\left(\sqrt{3}Y_D + X_D\right) \right] \tag{6-43}$$

$$\hat{S}_8^T = \left[\left(X_D + \frac{\sqrt{3}b}{2} \right) \quad \left(Y_D + \frac{b}{2} \right) \quad h; \quad -\frac{bh}{2} \quad \frac{\sqrt{3}bh}{2} \quad -\frac{b}{2}\left(\sqrt{3}Y_D - X_D\right) \right] \tag{6-44}$$

$$\hat{S}_9^T = \left[\left(X_E + \frac{\sqrt{3}b}{2} \right) \quad \left(Y_E + \frac{b}{2} \right) \quad h; \quad -\frac{bh}{2} \quad \frac{\sqrt{3}bh}{2} \quad -\frac{b}{2}\left(\sqrt{3}Y_E - X_E\right) \right] \tag{6-45}$$

$$\hat{S}_{10}^T = \left[X_E \quad \left(Y_E + b \right) \quad h; \quad -bh \quad 0 \quad bX_E \right] \tag{6-46}$$

$$\hat{S}_{11}^T = \left[X_F \quad \left(Y_F + b \right) \quad h; \quad -bh \quad 0 \quad bX_F \right] \tag{6-47}$$

$$\hat{S}_{12}^T = \left[\left(X_F - \frac{\sqrt{3}b}{2} \right) \quad \left(Y_F + \frac{b}{2} \right) \quad h; \quad -\frac{bh}{2} \quad -\frac{\sqrt{3}bh}{2} \quad \frac{b}{2}\left(\sqrt{3}Y_F + X_F\right) \right] \tag{6-48}$$

This yields the transpose of the Jacobian matrix.

$$
J^T = \begin{bmatrix}
\left(X_A - \dfrac{\sqrt{3}b}{2}\right) & \left(Y_A + \dfrac{b}{2}\right) & h & -\dfrac{bh}{2} & -\dfrac{\sqrt{3}bh}{2} & \dfrac{b}{2}\left(\sqrt{3}Y_A + X_A\right) \\[2mm]
\left(X_A - \dfrac{\sqrt{3}b}{2}\right) & \left(Y_A - \dfrac{b}{2}\right) & h & \dfrac{bh}{2} & -\dfrac{\sqrt{3}bh}{2} & \dfrac{b}{2}\left(\sqrt{3}Y_A - X_A\right) \\[2mm]
\left(X_B - \dfrac{\sqrt{3}b}{2}\right) & \left(Y_B - \dfrac{b}{2}\right) & h & \dfrac{bh}{2} & -\dfrac{\sqrt{3}bh}{2} & \dfrac{b}{2}\left(\sqrt{3}Y_B - X_B\right) \\[2mm]
X_B & \left(Y_B - b\right) & h & bh & 0 & -bX_B \\[2mm]
X_C & \left(Y_C - b\right) & h & bh & 0 & -bX_C \\[2mm]
\left(X_C + \dfrac{\sqrt{3}b}{2}\right) & \left(Y_C - \dfrac{b}{2}\right) & h & \dfrac{bh}{2} & \dfrac{\sqrt{3}bh}{2} & -\dfrac{b}{2}\left(\sqrt{3}Y_C + X_C\right) \\[2mm]
\left(X_D + \dfrac{\sqrt{3}b}{2}\right) & \left(Y_D - \dfrac{b}{2}\right) & h & \dfrac{bh}{2} & \dfrac{\sqrt{3}bh}{2} & -\dfrac{b}{2}\left(\sqrt{3}Y_D + X_D\right) \\[2mm]
\left(X_D + \dfrac{\sqrt{3}b}{2}\right) & \left(Y_D + \dfrac{b}{2}\right) & h & -\dfrac{bh}{2} & \dfrac{\sqrt{3}bh}{2} & -\dfrac{b}{2}\left(\sqrt{3}Y_D - X_D\right) \\[2mm]
\left(X_E + \dfrac{\sqrt{3}b}{2}\right) & \left(Y_E + \dfrac{b}{2}\right) & h & -\dfrac{bh}{2} & \dfrac{\sqrt{3}bh}{2} & -\dfrac{b}{2}\left(\sqrt{3}Y_E - X_E\right) \\[2mm]
X_E & \left(Y_E + b\right) & h & -bh & 0 & bX_E \\[2mm]
X_F & \left(Y_F + b\right) & h & -bh & 0 & bX_F \\[2mm]
\left(X_F - \dfrac{\sqrt{3}b}{2}\right) & \left(Y_F + \dfrac{b}{2}\right) & h & -\dfrac{bh}{2} & -\dfrac{\sqrt{3}bh}{2} & \dfrac{b}{2}\left(\sqrt{3}Y_F + X_F\right)
\end{bmatrix}
\tag{6-49}
$$

The first three of the six Plücker coordinates define the length of the leg. The odd numbered legs for this structure are the same length.

$$
\begin{aligned}
\ell_o &= \left[L_o^2 + M_o^2 + N_o^2\right]^{\frac{1}{2}} \\[3mm]
&= \left[\left(X_A - \frac{\sqrt{3}b}{2}\right)^2 + \left(Y_A + \frac{b}{2}\right)^2 + h^2\right]^{\frac{1}{2}} \\[3mm]
&= \left[X_A^2 - \sqrt{3}bX_A + \frac{3b^2}{4} + Y_A^2 + bY_A + \frac{b^2}{4} + h^2\right]^{\frac{1}{2}}
\end{aligned}
\tag{6-50}
$$

$$= \left[r^2 \cos^2 \phi_z - \sqrt{3} br \cos \phi_z + \frac{3b^2}{4} + r^2 \sin^2 \phi_z + br \sin \phi_z + \frac{b^2}{4} + h^2 \right]^{\frac{1}{2}}$$

$$= \left[r^2 + br \left(\sin \phi_z - \sqrt{3} \cos \phi_z \right) + b^2 + h^2 \right]^{\frac{1}{2}}$$

$$= \left[a^2 + ab \left(\sin \phi_z - \sqrt{3} \cos \phi_z \right) + b^2 + h^2 \right]^{\frac{1}{2}} \tag{6-51}$$

Similarly, lengths of the even numbered legs are equal.

$$\ell_e \quad = \left[a^2 - ab \left(\sin \phi_z + \sqrt{3} \cos \phi_z \right) + b^2 + h^2 \right]^{\frac{1}{2}} \tag{6-52}$$

Lee et al. [1998] used the following notation to describe the screw motion.

$$\delta \ell = J^{*T} \delta \hat{D} \tag{6-53}$$

This notation describes an incremental change in leg length as a product of the

normalized line coordinates (J^{*T}) and the platform incremental change (Δx, $\Delta \theta$, etc.). To

normalize the leg coordinates, each value is divided by the instantaneous leg lengths.

$$\delta \ell_i = \hat{S}_i^{*T} \delta \hat{D} = \frac{\hat{S}_i^T}{\ell_i} \delta \hat{D} \tag{6-54}$$

Calculating the summation of the individual coordinates shows that all the values

are zero except for N and R.

$$L_1 + L_3 + L_5 + L_7 + L_9 + L_{11} = X_A - \frac{\sqrt{3}b}{2} + X_B - \frac{\sqrt{3}b}{2} + X_C + X_D + \frac{\sqrt{3}b}{2} + X_E + \frac{\sqrt{3}b}{2} + X_F$$

$$= r \cos \phi_z - \frac{\sqrt{3}b}{2} + r \left(\frac{1}{2} \cos \phi_z - \frac{\sqrt{3}}{2} \sin \phi_z \right) - \frac{\sqrt{3}b}{2} - r \left(\frac{1}{2} \cos \phi_z + \frac{\sqrt{3}}{2} \sin \phi_z \right) - r \cos \phi_z \tag{6-55}$$

$$+ \frac{\sqrt{3}b}{2} - r \left(\frac{1}{2} \cos \phi_z - \frac{\sqrt{3}}{2} \sin \phi_z \right) + \frac{\sqrt{3}b}{2} + r \left(\frac{1}{2} \cos \phi_z + \frac{\sqrt{3}}{2} \sin \phi_z \right) = 0$$

$$M_1 + M_3 + M_5 + M_7 + M_9 + M_{11} = Y_A + \frac{b}{2} + Y_B - \frac{b}{2} + Y_C - b + Y_D - \frac{b}{2} + Y_E + \frac{b}{2} + Y_F + b$$

$$= r\sin\phi_z + \frac{b}{2} + r\left(\frac{1}{2}\cos\phi_z + \frac{\sqrt{3}}{2}\sin\phi_z\right) - \frac{b}{2} - r\left(\frac{1}{2}\cos\phi_z - \frac{\sqrt{3}}{2}\sin\phi_z\right) - b - r\sin\phi_z \qquad (6\text{-}56)$$

$$-\frac{b}{2} - r\left(\frac{1}{2}\cos\phi_z + \frac{\sqrt{3}}{2}\sin\phi_z\right) + \frac{b}{2} + r\left(\frac{1}{2}\cos\phi_z - \frac{\sqrt{3}}{2}\sin\phi_z\right) + b = 0$$

$$N_1 + N_3 + N_5 + N_7 + N_9 + N_{11} = 6h \qquad (6\text{-}57)$$

$$P_1 + P_3 + P_5 + P_7 + P_9 + P_{11} = -\frac{bh}{2} + \frac{bh}{2} + bh + \frac{bh}{2} - \frac{bh}{2} + -bh = 0 \qquad (6\text{-}58)$$

$$Q_1 + Q_3 + Q_5 + Q_7 + Q_9 + Q_{11} = -\frac{\sqrt{3}bh}{2} - \frac{\sqrt{3}bh}{2} + 0 + \frac{\sqrt{3}bh}{2} + \frac{\sqrt{3}bh}{2} + 0 = 0 \qquad (6\text{-}59)$$

$$R_1 + R_3 + R_5 + R_7 + R_9 + R_{11} = \frac{b}{2}\left(\sqrt{3}Y_A + X_A\right) + \frac{b}{2}\left(\sqrt{3}Y_B - X_B\right) - bX_C - \frac{b}{2}\left(\sqrt{3}Y_D + X_D\right)$$

$$-\frac{b}{2}\left(\sqrt{3}Y_E - X_E\right) + bX_F$$

$$= \frac{br}{2}\left(\sqrt{3}\sin\phi_z + \cos\phi_z\right) + \frac{br}{2}\left[\left(\frac{\sqrt{3}}{2}\sin\phi_z + \frac{3}{2}\cos\phi_z\right) - \left(\frac{1}{2}\cos\phi_z - \frac{\sqrt{3}}{2}\sin\phi_z\right)\right]$$

$$+br\left(\frac{1}{2}\cos\phi_z + \frac{3}{2}\sin\phi_z\right) + \frac{br}{2}\left(\sqrt{3}\sin\phi_z + \cos\phi_z\right) \qquad (6\text{-}60)$$

$$\frac{br}{2}\left[\left(\frac{\sqrt{3}}{2}\sin\phi_z + \frac{3}{2}\cos\phi_z\right) - \left(\frac{1}{2}\cos\phi_z - \frac{\sqrt{3}}{2}\sin\phi_z\right)\right] + br\left(\frac{1}{2}\sin\phi_z + \frac{\sqrt{3}}{2}\cos\phi_z\right)$$

$$= 3br\left(\sqrt{3}\sin\phi_z + \cos\phi_z\right)$$

The second pair of legs sum similarly.

$$L_2 + L_4 + L_6 + L_8 + L_{10} + L_{12} = 0$$
$$M_2 + M_4 + M_6 + M_8 + M_{10} + M_{12} = 0$$
$$P_2 + P_4 + P_6 + P_8 + P_{10} + P_{12} = 0 \qquad (6\text{-}61)$$
$$Q_2 + Q_4 + Q_6 + Q_8 + Q_{10} + Q_{12} = 0$$

$$N_2 + N_4 + N_6 + N_8 + N_{10} + N_{12} = 6h$$
$$R_2 + R_4 + R_6 + R_8 + R_{10} + R_{12} = 3br\left(\sqrt{3}\sin\phi_z + \cos\phi_z\right) \qquad (6\text{-}62)$$

Adding the first, third, fifth, seventh, ninth, and eleventh rows of the matrix and substituting the expressions for the coordinates yields the necessary expression. Note that **z** replaces **h** in this calculation.

$$
\begin{aligned}
6l_0\delta l_0 \quad &= (N_1 + N_3 + N_5 + N_7 + N_9 + N_{11})\delta z + (R_1 + R_3 + R_5 + R_7 + R_9 + R_{11})\delta\phi_z \\
&= 6z\delta z + 3br\left(\sqrt{3}\sin\phi_z + \cos\phi_z\right)\delta\phi_z
\end{aligned}
\tag{6-63}
$$

$$
l_0\delta l_0 = z\delta z + \frac{br}{2}\left[\sqrt{3}\sin\phi_z + \cos\phi_z\right]\delta\phi_z
\tag{6-64}
$$

The even leg calculation yields a similar result.

$$
l_e\delta l_e = z\delta z + \frac{br}{2}\left[\sqrt{3}\sin\phi_z - \cos\phi_z\right]\delta\phi_z
\tag{6-65}
$$

Special Tensegrity Motions

Using the assumption that the even numbered legs are struts (2, 4, 6, 8, 10, and 12 have no longitudinal displacement) then the equation reduces to a function of rotation and translation.

$$
z\delta z = -\frac{br}{2}\left[\sqrt{3}\sin\phi_z + \cos\phi_z\right]\delta\phi_z
\tag{6-66}
$$

The pitch is defined by the ratio of linear **z** change to rotation about the **z**-axis.

$$
p = \frac{\delta z}{\delta\phi_z}
\tag{6-67}
$$

This yields the pitch equation.

$$
p = \frac{\delta z}{\delta\phi_z} = -\frac{br}{2z}\left[\sqrt{3}\sin\phi_z + \cos\phi_z\right]
\tag{6-68}
$$

The subsequent integration yields the z calculation. This proves that the odd numbered struts can be commanded to yield a pitch motion (**z** and **θz** motions are coupled).

$$\int_{z_0}^{z} z\delta z = -\frac{br}{2} \int_{0}^{\phi_z} \left[\sqrt{3}\sin\phi_z + \cos\phi_z\right]\delta\phi_z \tag{6-69}$$

$$z^2 = z_0^2 - br\left\{\sqrt{3}(\cos\phi_z + 1) - \sin\phi_z\right\} \tag{6-70}$$

Equation (6-70) can be modified (**a=r** and **z₀**=0) to define the square of the platform

height.

$$z^2 = ab\left\{\sin\phi_z - \sqrt{3}(\cos\phi_z + 1)\right\} \tag{6-71}$$

Therefore, the platform height (**z**) is the root of (6-71).

$$z = \sqrt{ab}\left\{\sin\phi_z - \sqrt{3}(\cos\phi_z + 1)\right\}^{\frac{1}{2}} \tag{6-72}$$

This result shows that for a given twist about the **z**-axis (ϕ_z), there is a corresponding

displacement along the **z**-axis, defined by a finite screw (**p=z/ϕ_z**), as shown.
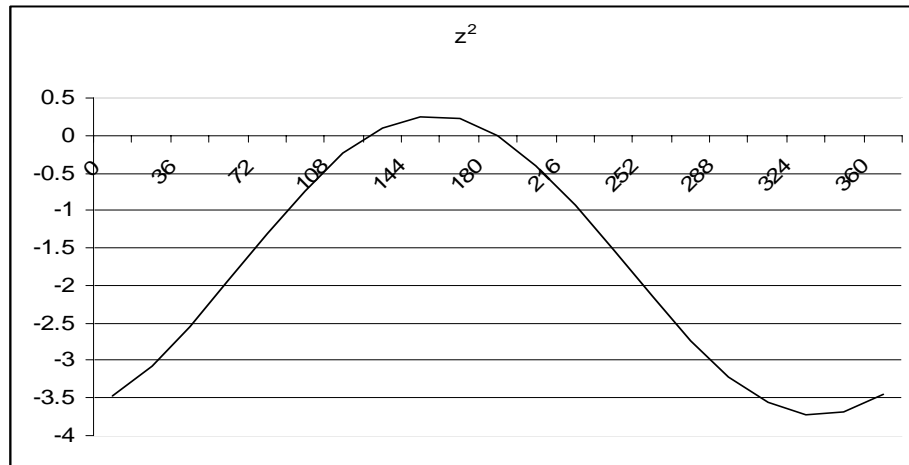
Figure 6-3. The Pitch Relationship

CHAPTER 7.
DEPLOYMENT AND MECHANICS

While this research addresses the theory for a new class of deployable antenna structures, there remains significant work in defining the mechanics of such a subsystem. There does appear to be a potential reduction in mechanical component count as compared to current systems. This chapter addresses a potential deployment scheme, the mechanics necessary to achieve the motion, and some potential mechanisms to support these motions.

Paramount to this design study is the combination of struts and ties. Waters and Waters [1987] suggested that there should be twelve (12) struts and twelve (12) ties for his hyperboloidal antenna model. This research suggests that there need only be six struts to define a six-degree of freedom structure.

First, the struts are defined, including various approaches to deployment. Second, the strut/tie length and stiffness ratios are addressed. Third, a useful approach to deploying a semi-precision, mesh reflector is presented.

<u>Strut Design</u>

In order to deploy the struts from a stowed position, the end points of the stowage-to-deployment plan must be defined. Figure 7-1 presents a nominal 15-meter (tip to tip) deployed surface with six struts. This first position is considered the starting position (α=0) according to Kenner (1976). The subsequent sketches show rotation to tensegrity (α=60$^\mathrm{o}$). The strut lengths are shown increasing for simplicity, but an actual design would

show the upper surface approaching the lower surface as the struts rotated to the

tensegrity position.
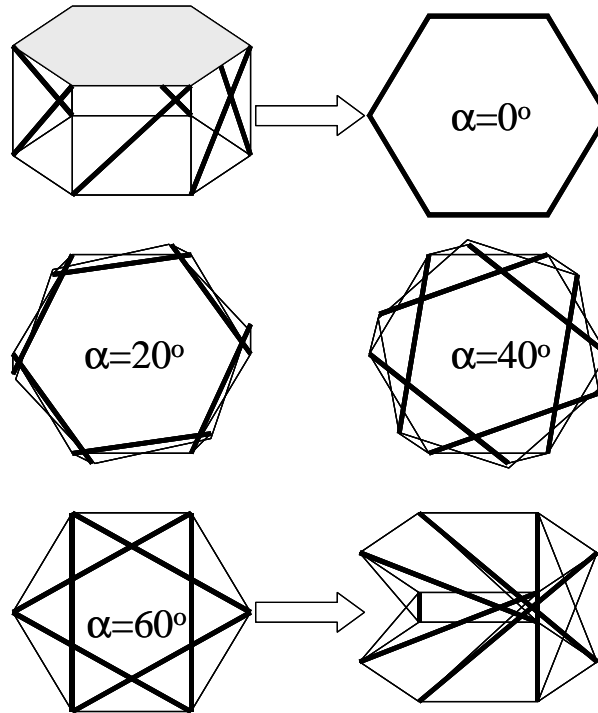
Figure 7-1. 6-6 Structure Rotated from $\alpha=0^{o}$ to $\alpha=60^{o}$ (Tensegrity)
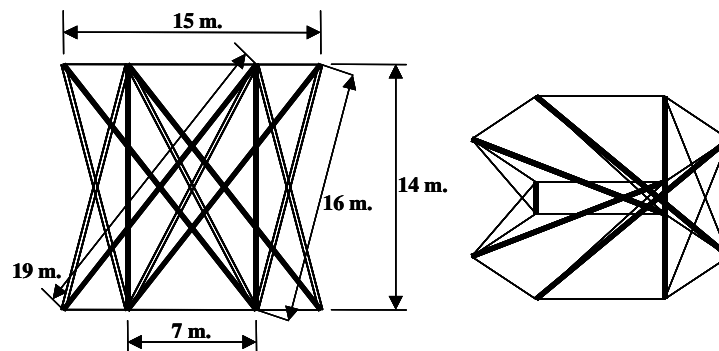
Figure 7-2. Dimensions for Model Tensegrity Antenna

Based on these design assumptions the structure (Figure 7-2) would have the values found in Table 7-1.

Table 7-1. Deployable Tensegrity Design Values

Design Parameter	NOMINAL VALUE
Tip to Tip Diameter	15 meters
Deployed Height	14 meters
Planar Ties (top and bottom)	7 meters
Tension Ties (upper to lower)	16 meters
Struts (upper to lower)	19 meters

Based on this model, it is clear that this structure would require a stowage space approximately 20 meters in length and an isosceles triangle three times the diameter of the struts. For a conventional 75 mm tube design, the total stowage volume would be a 20 m. long x 0.25 m. diameter. This is unacceptable for spacecraft design, as the trend in launch vehicle design is toward smaller systems, with correspondingly smaller fairings. In Figure 7-3, the nominal dimensions are presented for the Taurus and Delta launch vehicle. It is obvious from these sketches that a 20m x .25m antenna could not fit in even the 7.2m x 2.7m Extended Delta fairing. Design experience shows that the center of gravity for the spacecraft should be maintained at the centerline of the launch vehicle; therefore the usable height could be reduced to 5.3m x 2.7m. Clearly, a method for deploying the struts must be developed. The following examples are suggested for solving this design issue.
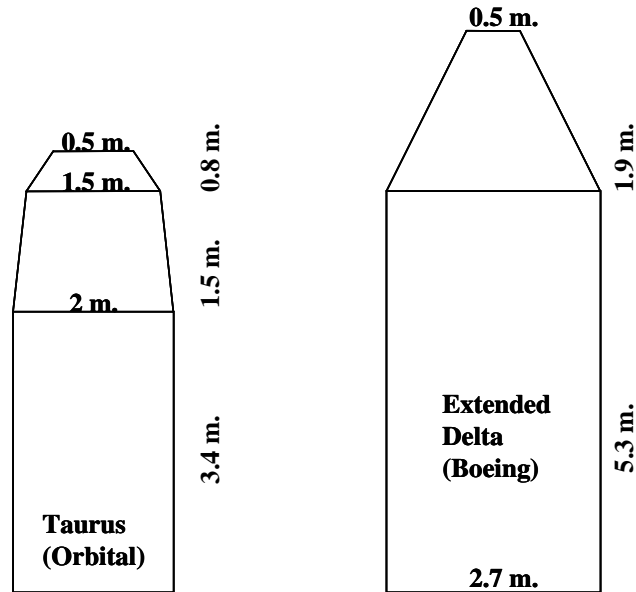
Figure 7-3. Taurus and Delta Launch Vehicle Fairings

- Folding Hinge Struts: Numerous antenna systems have been developed in the last 30 years that utilize folding struts. They usually require some drive motion to deploy, including a latching mechanism at the end of the deployment travel. Figure 7-4 shows a simple hinge design, which could have an over-center locking mechanism.

- Sliding Coupling Struts: Similar to the folding design, sliding struts could be used, with a locking mechanism at the end of travel. Typically there is less force necessary to latch these struts, as it would take significant force to return them to the sliding configuration. Figure 7-5 shows this configuration, with a large angle sliding surface to lock the surface into place. Springs could be used to hold the mechanism in position.

- Telescoping Struts: Due to excessive weight and drive force required telescoping struts have not been applied to deployable space applications. As motor cost and

efficiency increase, this could become a viable option. Figure 7-6 presents this configuration, which would encourage tapered diameter struts, which improve the specific stiffness of a complete system.

- Inflatable Struts: A very different approach, but one that has been gaining favor with the space structures design community, is inflatable spars. The leaders in the field are ILC Dover (DE), L'Garde (CA), and SPS (AL). This approach can minimize the stowed spar volume, but analysis has shown that the size and weight of the deployment system is comparable to the three mechanical deployment schemes. The deployment requires a charge of gas energy, which requires a space qualified pump and tubing. One patented approach uses a UV hardening polymer that creates a solid structure once the inflatable is deployed. Another uses humidity evacuation technology to harden the tube. In all cases, structural integrity on orbit cannot be maintained merely by gas pressure; a solid structure must be provided.
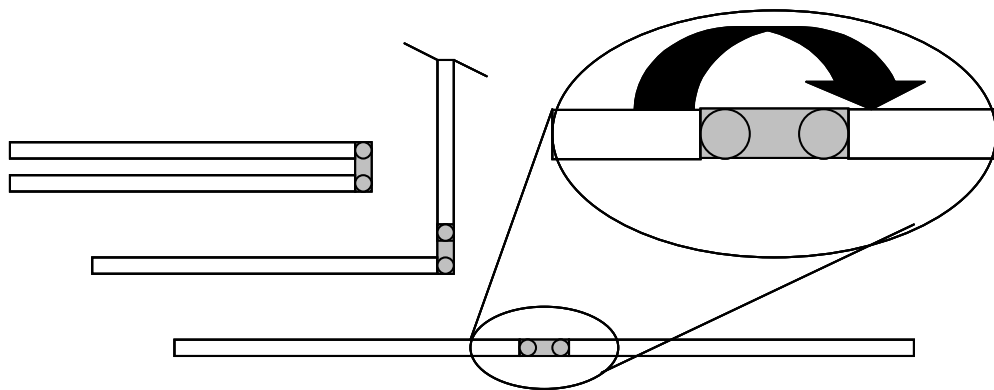
Figure 7-4. Folding Hinge Design
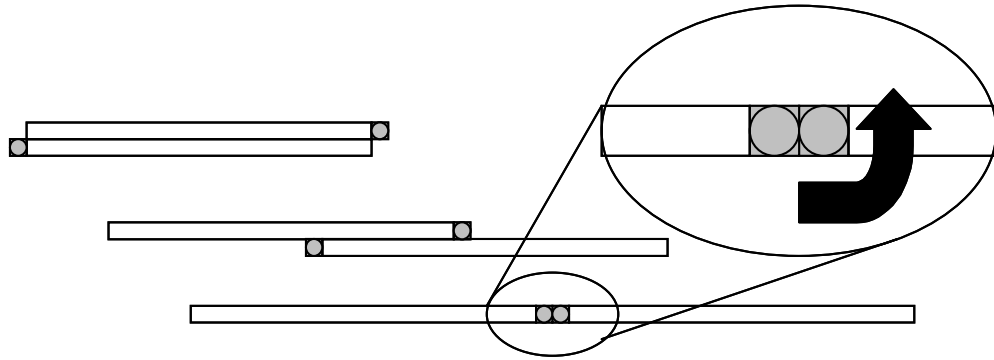
Figure 7-5. Sliding Coupling Design
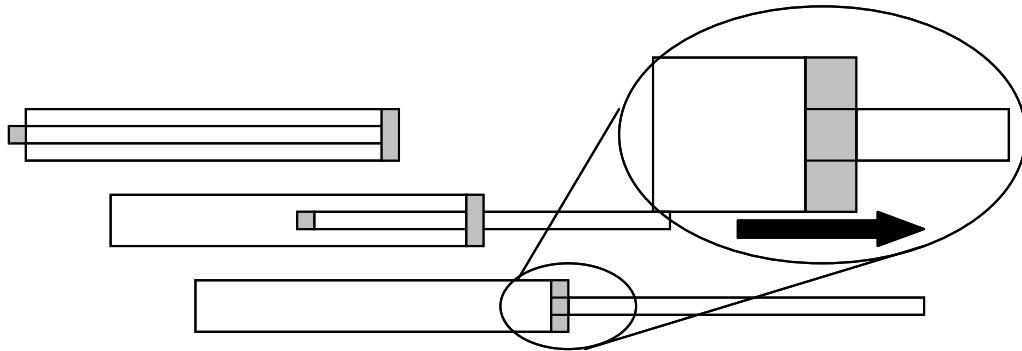
Figure 7-6. Telescoping Design

The greatest advantage to inflatables is that once the struts are deployed, they are almost uniform in cross sectional area and material properties. The mechanical approaches presented above introduce stiffness discontinuities at a minimum, and non-linear load responses as the worst case. A trade study of these approaches is presented below.

Table 7-2. Strut Deployment Trade Study

Strut Deployment Design	Advantages	Disadvantages
Folding	• Design history • Design relevance to other industries • Moderate deployment forces	• Potential stiffness non-linearities • Potential hinge surface galling • Locking hardware required
Sliding	• Minimal deployment forces • Positive locking position	• Potential bending stiffness non-linearities • Limited design history • Potential contact surfaces galling
Telescoping	• Compact packaging • Minimal stiffness non-linearities	• Requires interference fittings at deployment • Potential contact surface galling • Large deployment forces
Inflatables	• Very compact packaging • Near homogeneous deployed structure • Advanced materials application	• Requires deployment pump and tubing • Weight savings limited • Expensive

Strut/Tie Interaction

The key to maintaining control over the surface once the antenna is deployed, as well as modifying the surface direction and accuracy, is the strut/tie interaction. Two approaches have been studied to manage the ties during deployment.

- Stowed Ties: By simply folding the ties along the struts (Figure 7-7), they can be released by force restraints, which are highly sensitive and as the loads reach a predetermined value, will release the ties. Elastic ties would save the need for a reel to take up the slack, but the disadvantage is extreme loads in the tension ties prior to deployment. This could be required for months.
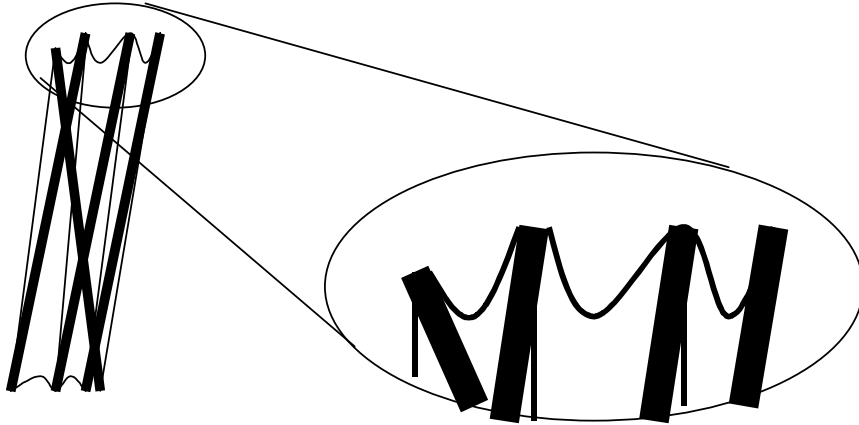
Figure 7-7. Stowed Ties

- Reel Ties: Whether or not the ties are elastic, a reel could be used to take up the slack, changing the forces in the structure (Figure 7-8). This added hardware (potentially one motor per strut) increases complexity, weight, and therefore cost.
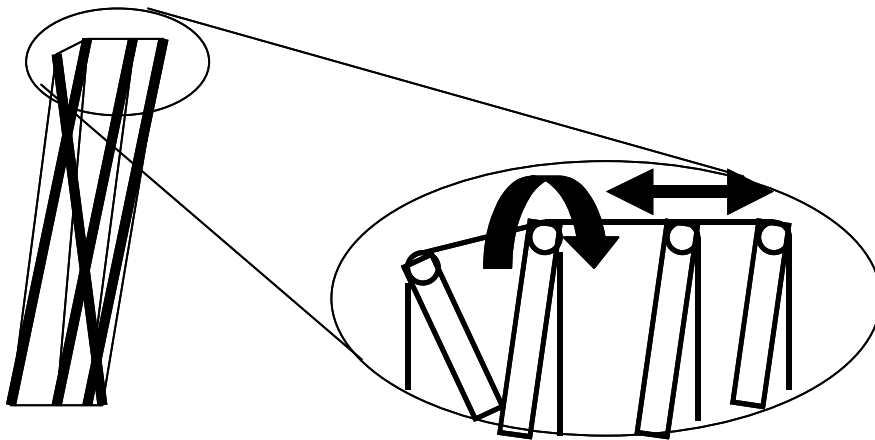
Figure 7-8. Reel Ties

A trade study for these approaches is presented below.

Table 7-3. Strut/Tie Trade Study

Strut/Tie Interaction Design	Advantages	Disadvantages
Stowed Ties (cord)	• High stiffness • Minimal Creep	• Can only be used for planar ties due to elasticity needs
Stowed Ties (elastic)	• Ease of stowage	HIGH STOWAGE LOADS
Reel Ties (cord)	• Clean, snag-free design	REQUIRES ADDITIONAL HARDWARE
Reel Ties (elastic)	• Stiffness constant adjustments	COMPLEX DESIGN AND POTENTIAL STIFFNESS CREEP

One design issue, which is critical to the mission success of this type of subsystem, is snag prevention. Since these antennas are deployed remotely, any potential snag could degrade or destroy the reflector surface. By using elastic ties, which are under prestress, they are less likely to catch on deploying struts. Similarly, the cord-ties must be stowed to ensure deployment success. This issue will be addressed further in Chapter 8.

Deployment Scheme

Figure 7-9 presents a potential deployment scheme. The requirements for this operation are primarily low shock load and continuous motion. Despite the inherent self-deploying nature of tensegrity structures, they cannot be allowed to "spring" into position for fear of introducing high shock and vibration loading into the system. Once the system has deployed, changing tension in the ties, and therefore position of the struts, can alter surface accuracy.

Extension → Separation → Release

Deployment and Surface Adjustment
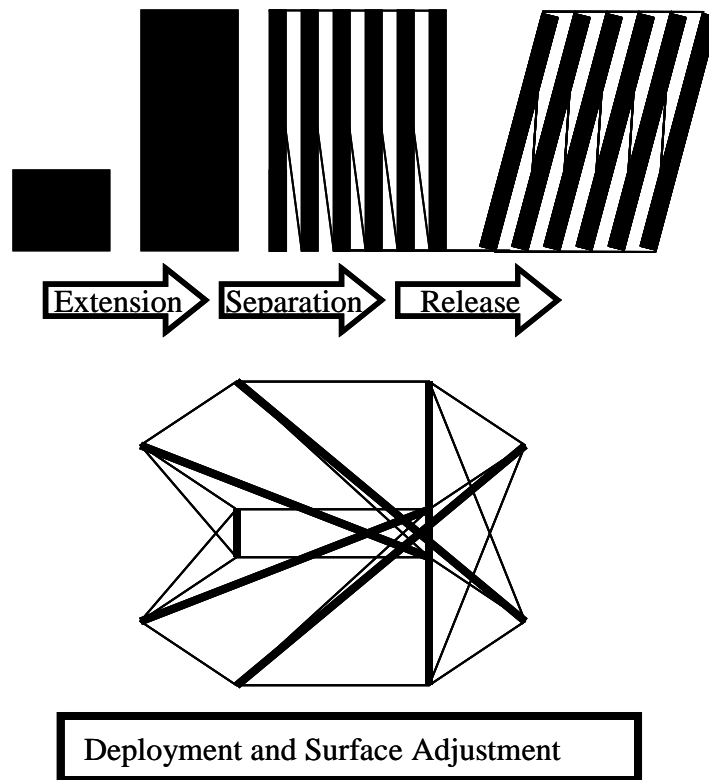
Figure 7-9. Deployment Scheme

Previous Related Work

During the 1990s, tensegrity structures became increasingly applicable to space

structure design, including space frames, precision mechanisms, and deployables. The

leading names in this new field have been Motro (France), Wang (China), Pellegrino

(England), and Skelton (United States). Motro [1992] edited a special edition of the

International Journal of Space Structures, which was dedicated to tensegrity. Kenneth

Snelson wrote an introductory letter for this edition describing his invention, Fuller's

contribution to its development, and the synergy between art and engineering.

Motro's work [1996] has predominantly focused on the stability of tensegrity

structures, including force density, non-linear analysis and morphology. Despite his clear

focus on the engineering aspects of tensegrity, he has an excellent grasp of the artistic applications for this work. There is a clear development of stable, strut/tie structures from rectilinear (one dimensional), planar (two dimensional), through to spatial (three dimensional). The 3-3, octahedron tensegrity is an excellent example of a spatial structure. He has developed multiple tensegrity structure designs, which solve some of the toughest curved-surface problems for space structures. This class of structure requires extremely lightweight with excellent geometric stability and deployability.

Wang [1998 a & b] has performed some of the best work on cable-strut systems as an extension of tensegrity. Reciprocal prisms (RP) and crystal-cell pyramidal (CP) grids, which technically exclude tensegrity systems, are the basis for his space frame applications. He developed a hierarchy of feasible cable-strut systems that include his new discoveries and tensegrity. Starting with triangular RP and CP simplexes, square, pentagonal, and hexagonal systems are developed to build cable domes, ring beams [Wang, 1998c], and double-layer tensegrity grids [Wang and Liu, 1996]. His work in the feasibility of these new applications is very important to space structure development.

Dr. S. Pellegrino's staff at the University of Cambridge has focused on the application of tensegrity to deployable space structures. Precision is of great concern with these kinematic systems, and recent system developments have required even higher precision from much lighter structures. By developing the mathematics for cable-constrained nodes, You [1997] has been able to very accurately model the position of mesh antenna surfaces, including proven experimental results. Studies in the analysis of mechanisms [Calladine and Pellegrino, 1991], folding concepts for flexible but solid surface reflectors [Tibbalds et al. 1998], and shape control based on stress analysis

[Kawaguchi et al. 1996] have all greatly contributed to the state of the art. Infinitesimal mechanism analysis has led to prestressing conditions, which are critical to understanding deployable tensegrity structures. Their work with semi-solid antenna reflectors has solved some of the fundamental problems associated with deploying these delicate systems. Launch capacity (size and weight) has continually reduced in recent years, requiring multiple folding systems to provide larger and larger structures. Obviously, once these structures are deployed and in operation, the surface must be maintained to meet performance requirements. Pellegrino has led the community in predictive models for using stress profiles (and node position control) to ensure reflector surface positioning is maintained.

Skelton and Sultan [1997] has seen the control of tensegrity structures as a new class of smart structures. This work has been applied to deployable telescope design [Sultan et al. (1999a)], where precision is orders of magnitude tougher than deployable antennas. He has also been instrumental in the development of integrated design [Sultan and Skelton, 1997] and reduction of prestress [Sultan et al. (1999b)], which are critical to solving position correction and dynamic control issues.

<u>Alabama Deployment Study</u>

The University of Alabama provided a deployment study for Harris Aerospace that suggested some alternative approaches to deployment. One such approach, gas-filled shock absorbers, would allow a self-deploying system like this tensegrity structure, to maintain a controlled deployment sequence. This study found that, based on the current design practices deployable space structures, the highest scoring actuator was the motor and lead screw combination. This is the most common scheme employed today. Alabama

also suggested that other forms of deployment control should be considered due to the high cost of space qualification for these subsystems. The viable options presented included: spiral springs, pneumatic cylinders, and compression springs. Since the tensegrity design provides the spring energy, a pneumatic design might be of use. The proportional velocity law governed this passive type design (damper). The energy equation is first order from stowage to deployment [Equation (1)], suggesting that a controlled sequence could be determined to ensure safe, low transient force deployment.

$$C\dot{x} + Kx = 0$$

(7-1)

Deployment Stability Issues

The calculations for the 3-3 design, which were presented in Chapter 3 (Parallel Platform Results), suggest that there is a singularity at the tensegrity position. Figure 7-10 presents a sequence from the *Central Position*, through the *Aligned Position* and the *Tensegrity Position* to the *Crossover Position*, where the struts intersect. The angle ϕ is equal to 0 at the *Central* Position and increases as the platform rotates counterclockwise. The angle α is equal to 0 in the aligned position. The former value is consistent with the CIMAR calculations. The later value is consistent with Kenner's works.

For the tensegrity design, the *Central and Aligned Positions* are not stable, as the ties are in compression. The *Tensegrity Position* is a stable critical point. This suggests that the design has *instantaneous mobility*, and any minor perturbation to the structure, while not necessarily causing instability, would provide sufficient energy to oscillate the antenna enough to degrade antenna performance.
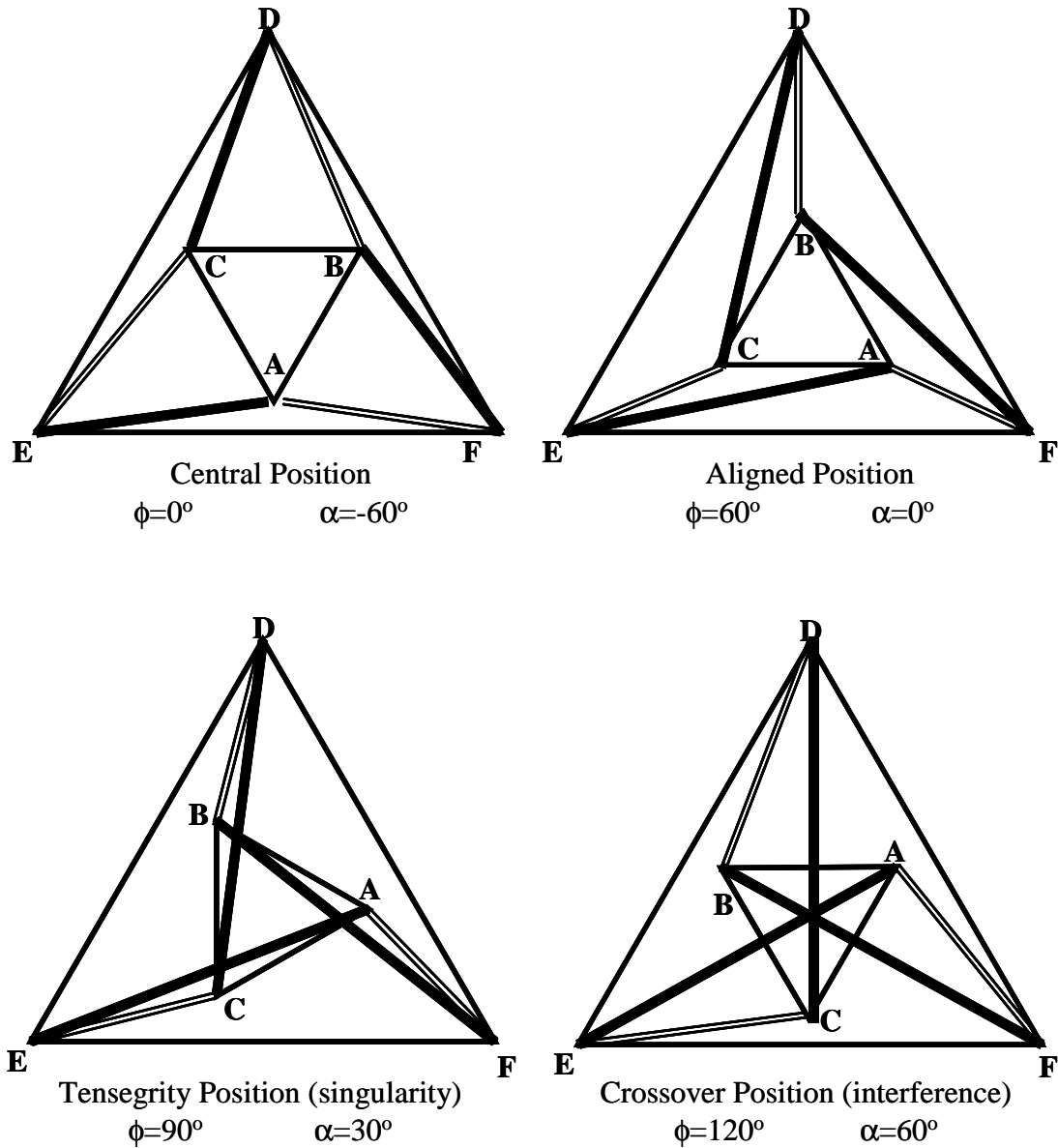
Figure 7-10. Octahedron Configurations

To improve the design and stability of the tensegrity structure, while not affecting the self-deployability, another set of ties is added between the vertex of the base and the opposite vertex of the platform (Figure 7-11).
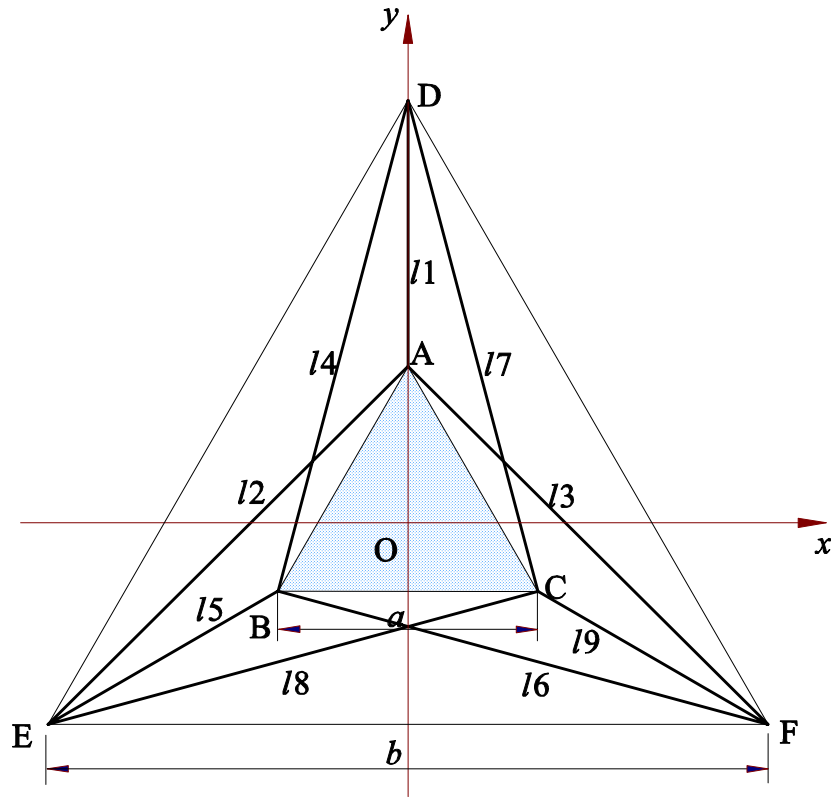
Figure 7-11. Redundant 3-3 Structure

This results in four ties at the end of each strut, versus the three in the original design.

Again, the angles ϕ and α represent the works of CIMAR and Kenner, respectively.

Figure 7-12 presents the rotations from the *Central Position*, through the *Aligned and Tensegrity Positions*, to the *Crossover Position*, where the struts intersect.

Central Position
$\phi=0^o$ $\alpha=-60^o$

Aligned Position
$\phi=60^o$ $\alpha=0^o$

Tensegrity Position (singularity)
$\phi=90^o$ $\alpha=30^o$

Crossover Position (interference)
$\phi=120^o$ $\alpha=60^o$
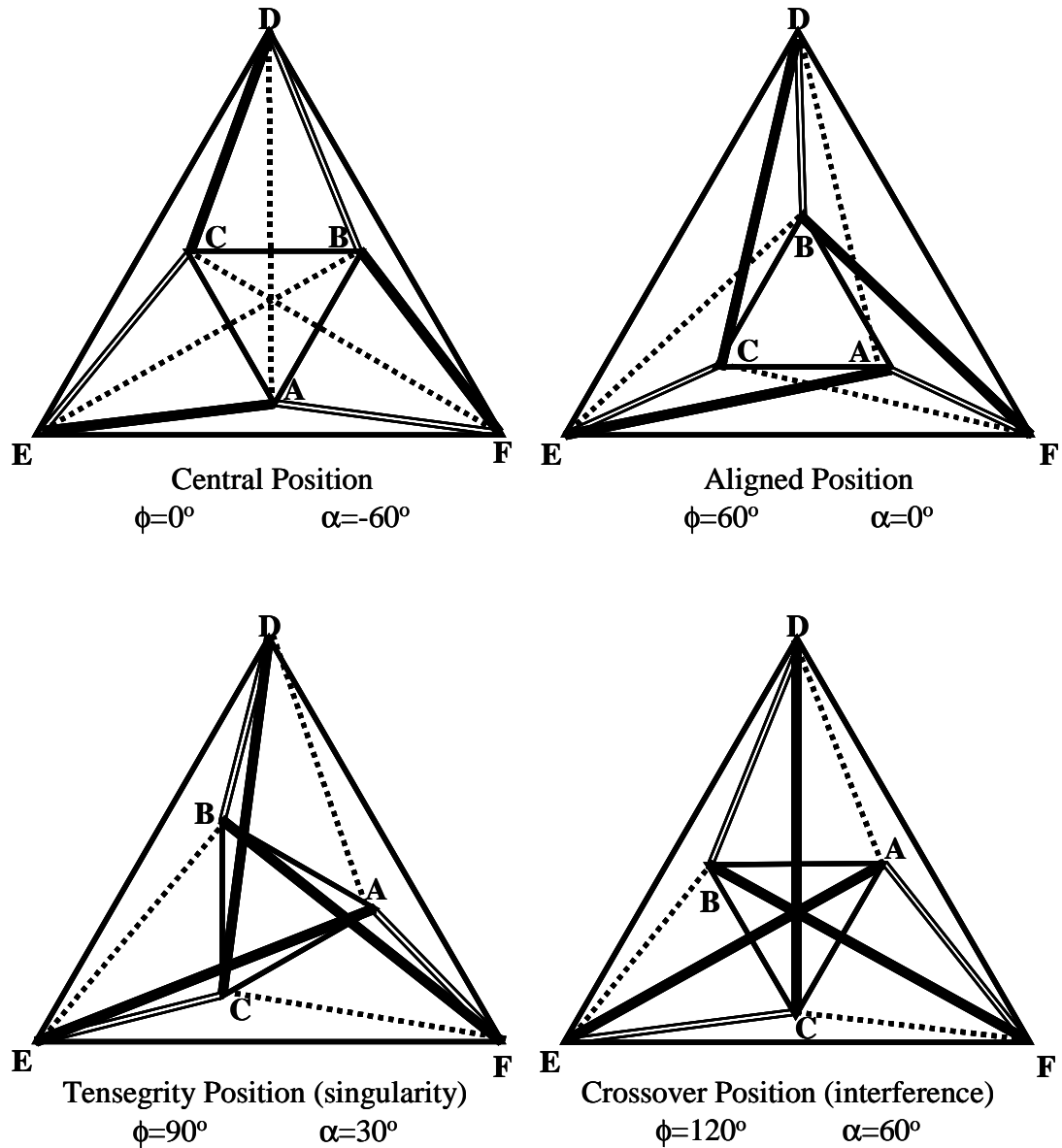
Figure 7-12. Redundant Octahedron Configurations

The mathematics to calculate this "3-3+" structure is similar that for the 4-4 and 6-6 structures, in that the Cauchy-Binet theorem is employed. Because there are now nine (9) connections between the platform and the base, the resultant **J** is a 6x9 matrix.

$$J = \begin{bmatrix} \vec{S}_1 & \vec{S}_2 & \vec{S}_3 & \vec{S}_4 & \vec{S}_5 & \vec{S}_6 & \vec{S}_7 & \vec{S}_8 & \vec{S}_9 \end{bmatrix} \qquad (7\text{-}2)$$

Therefore, $\mathbf{J}^T$ is a 9x6 matrix.

$$\mathbf{J}^T = \begin{bmatrix} \vec{S}_1 \\ \vec{S}_2 \\ \vec{S}_3 \\ \vec{S}_4 \\ \vec{S}_5 \\ \vec{S}_6 \\ \vec{S}_7 \\ \vec{S}_8 \\ \vec{S}_9 \end{bmatrix} \qquad (7\text{-}3)$$

As shown in Chapter 5, the quality index is calculated using the determinant of the combined matrices ($\mathbf{det\ JJ^T}$). The ratios for $\mathbf{a}$, $\mathbf{b}$, and $\mathbf{h}$, which represent the maximum quality index ratios, were also calculated. The significance of this design change is shown in the Figure 7-13. The quality index remains relatively constant as the platform rotates through 120°, varying a total of 25%, from a minimum of .75, to a maximum of 1.0. This amount of variation is negligible, as compared to the standard 3-3 design, and suggests that the fourth tie creates redundancy, avoiding the singularity at tensegrity. The structure is stable and practical. Note that for the standard 3-3 design, $\lambda=0$ at $\alpha=30^o$, as predicted by the calculations in Chapter 5.

Further, there is a suggestion here that the articulation of a single strut could provide necessary antenna surface motions. Since the reflector surface for a deployable antenna is couple to the ends and midpoints of the struts, extension of these structural members could alter the surface of the antenna, thereby performing various or simultaneous mission tasks. If this were true, the same antenna reflector could be used to communicate with more than one location.
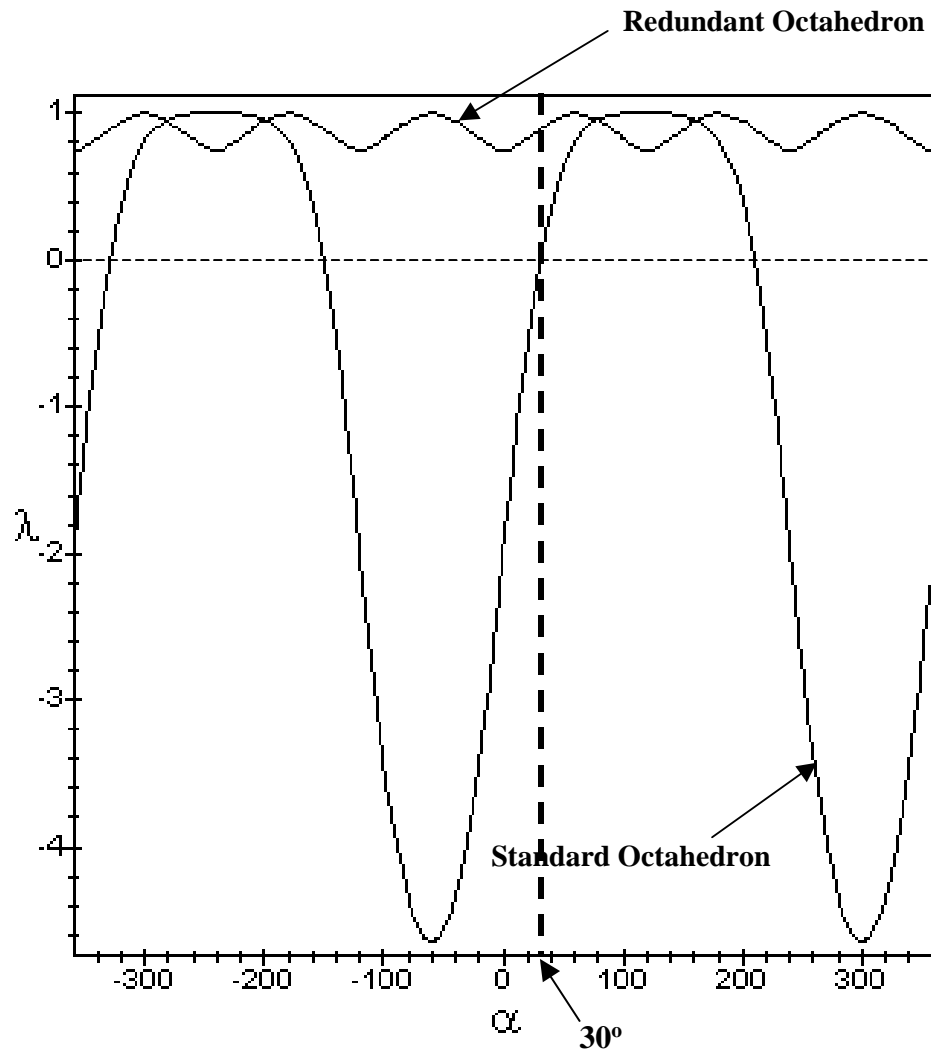
Figure 7-13. Quality Index vs. Rotation About the Vertical Axis

CHAPTER 8.
STOWAGE DESIGN

An efficient (minimized) stowage volume is an equally important requirement to the

deployment and antenna functions previously presented. Typically, antennas are designed

with extra folds along the length of the struts to reduce the launch vehicle shroud height

requirement. For a standard "hub and spoke" design deployable antenna, an extra fold

can be included at the midpoint of the spar (see section view in Figure 8-1). With this

method, a 15-meter diameter antenna would have a stowed package volume of

approximately 4-meter height and 4-meter diameter. This extra fold along the spar length

greatly increases the material content, complexity of the structure, and touch labor to

assemble the system.
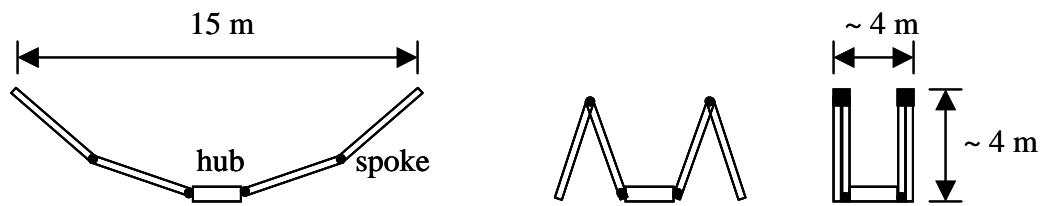
Figure 8-1. Current Deployable Antenna Design

This chapter addresses the final goal for this research: a study of the tensegrity

structure parameters. This approach will increase the efficiency of the stowed package,

by maximizing the use of the spars for the antenna, and not just the structure. In Chapter

6, at the maximum 6-6 quality index (Central Position), the height **h** was equal to

approximately 0.6 times **a**. The base dimension **b** was equal to approximately 1.2 times **a**.

Modifying the **a/b** and **a/h** ratios would reduce the length of the spars. This would

improve the efficiency of the structure by maximizing the deployed structure (tip to tip)

diameter for a minimized strut length.

<div align="center">Minimized Strut Length</div>

As presented in Chapter 7, the typical launch vehicle (Extended Delta Class) shroud

could not accommodate the baseline, 15-meter diameter deployed tensegrity antenna,

wherein the strut length is 19 meters. The following is a mathematical trade analysis

between the size of the base (**b**) as defined in Chapter 5 (6-6 Design), the diameter of the

deployed surface (**2a** for the 6-6 design), and the strut length (**l**). The purpose of this

analysis is to design a stable structure while minimizing the strut length for the 15-meter

antenna. The 6-6 design is the basis for the deployable design. Table 8-1 presents the

geometric relationships for the three candidate structures (3-3, 4-4, and 6-6).

<div align="center">Table 8-1. The Three Tensegrity Structure Designs Considered</div>

Design	# of Struts	# of Ties (total)	Tip-to-Tip Diameter
3-3	3	9	a
4-4	4	12	$\sqrt{2}a$
6-6	6	18	2a

<div align="center">3-3 Optimization</div>

The tensegrity position for the 3-3 structure, as defined in Chapter 7, is at $\phi=90^o$ and

$\alpha=30^o$. Despite any changes in the **a**, **b**, or **h** values, tensegrity structures maintain the

same rotation angle relative to the Central Position (Chapter 7). This characteristic of

tensegrity, related to the static force balance in each strut. This position is uniquely in a singularity at this equilibrium position. Unfortunately, the quality index approaches zero at the tensegrity position. This is known as a "stable critical point", which means that the structure has instantaneous mobility (i.e. small forces can produce motion), but because the energy is at a minimum in this position, the structure is stable. The quality index is zero because the determinant (**det J**) becomes zero. To determine this mathematic trade, the Central Position will be analyzed and the results hypothesized for the tensegrity structures.

For the 3-3 structure, the Central Position is defined as $\phi=0^\circ$ or $\alpha=-60^\circ$. As presented in Chapter 5, the determinant of the **J** matrix and the determinant of the maximum of this

matrix (**J$_m$**) are $|J| = \dfrac{3\sqrt{3}a^3b^3h^3}{4\left(\dfrac{a^2-ab+b^2}{3}+h^2\right)^3}$ and $|J_m| = \dfrac{27a^3b^3}{32\left(a^2-ab+b^2\right)^{\frac{3}{2}}}$, respectively.

J$_m$ is a simplification of the **J** matrix with a substitution of the maximum height (**h$_m$**) values. This geometry corresponds to the maximized quality index. The value is

$h_m = \sqrt{\dfrac{1}{3}\left(a^2-ab+b^2\right)}$, found by taking the partial derivative $\dfrac{\partial}{\partial h}$ and setting it equal to

zero (a calculus inflection point). Calculating the quality index, $\lambda = \dfrac{|J|}{|J_m|}$, yields:

$$\lambda = \frac{8\sqrt{3}h^3\left(a^2-ab+b^2\right)^{\frac{3}{2}}}{9\left(\dfrac{a^2-ab+b^2}{3}+h^2\right)^3} \tag{8-1}$$

As the $\lim\limits_{b \Rightarrow 0} (\lambda)$, which means that the base reduces to a point, the Equation 1 reduces to

$$\lambda = \frac{8\sqrt{3}}{9\left(\dfrac{a}{3h} + \dfrac{h}{a}\right)^3} \tag{8-2}$$

Rooney et al. [1999] refers to this design as the "tensegrity pyramid".

As a first-design, the ratio **a/h=1** is chosen. This further reduces the equation to

$$\lambda = \frac{8\sqrt{3}}{9\left(\dfrac{1}{3} + 1\right)^3} = \frac{8\sqrt{3}}{9\left(\dfrac{4}{3}\right)^3} = 0.65 \tag{8-3}$$

which is an acceptable quality index (optimum is λ=1.0). But to define a class of

structures with acceptable Quality Indices, a new value γ is introduced. This value, $\gamma = \dfrac{h}{a}$

or $\mathbf{h = \gamma a}$, represents the ratio of the side of the platform relative to the height of the

structure. This changes the equation to

$$\lambda = \frac{8\sqrt{3}}{9\left(\dfrac{1}{3\gamma} + \gamma\right)^3} \tag{8-4}$$

and taking the derivative $\dfrac{\partial}{\partial \gamma}$ of the denominator, the maximum values for the quality

index (the denominator equals zero) is found at $\gamma = \dfrac{1}{\sqrt{3}} \approx 0.58$. Figure 8-2 presents the

plot of the quality index (λ) vs. the ratio values ($\gamma = \dfrac{h}{a}$). At this value of γ, the quality

index has a relative value of 1.0.
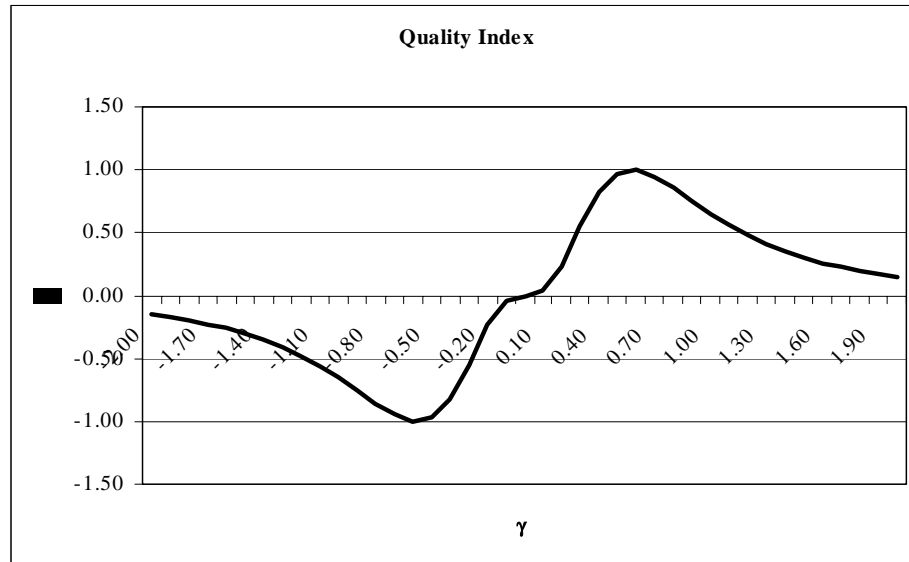
Figure 8-2. λ vs. $\gamma\left(\dfrac{a}{h}=1\right)$

Although there appears to be a mathematic benefit to designing a deployable

platform, such as a tensegrity structure, with a base width of zero (hence a point) there

are practical engineering limitations. The most obvious one is that the lines of the ties and

the struts approach each other. This reduces the structure's stability to zero. As the ties

that define the base approach zero length (**b**=0), the ties that define the platform cease to

be in tension. This is due to the connecting ties becoming collinear with the struts, and

therefore ceasing to create an off-axis moment (see Figure 8-3). Additionally, it is

impractical to connect an antenna structure at a point, as moment loads would approach

infinity.
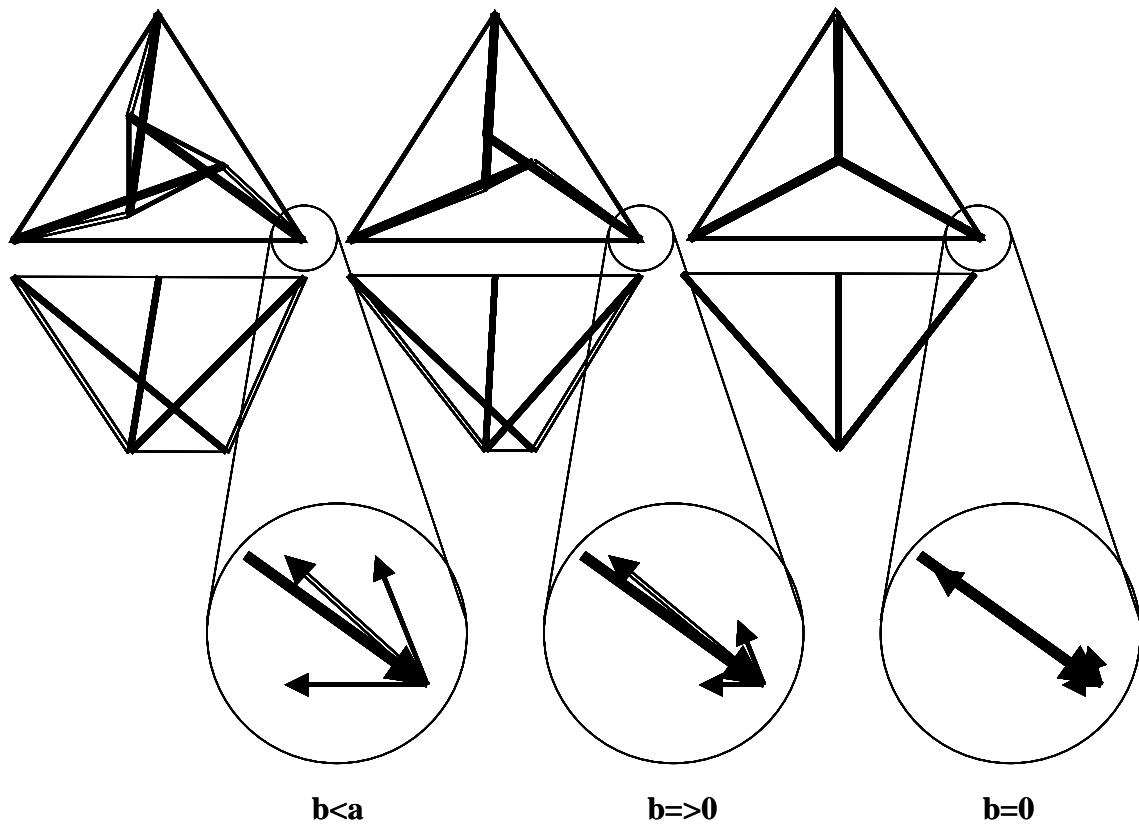
Figure 8-3. Reduction of the Base to Zero

Based on these observations, a compromised geometry is necessary. To this end, the

base should be minimized, and the $\gamma = \dfrac{h}{a}$ ratio chosen for the maximized quality index.

Table 8-2 presents the results of three choices of Base Planar Tie length (**b**) with

maximized quality index. Figures 8-4, 8-5, and 8-6 present the curves for the b=$\dfrac{a}{2}$, $\dfrac{a}{4}$,

and $\dfrac{a}{8}$ cases, respectively.

Table 8-2. Quality Index for $b=\dfrac{a}{2}$, $\dfrac{a}{4}$, and $\dfrac{a}{8}$ Cases

b	$|J|$	h_m	$|J_m|$	λ	γ at λ_{max}
$\dfrac{a}{2}$	$\dfrac{3\sqrt{3}}{32\left(\dfrac{1}{4h}+\dfrac{h}{a^2}\right)^3}$	$\dfrac{a}{2}=0.5a$	$\dfrac{3\sqrt{3}a^3}{32}\approx 0.2a^3$	$\dfrac{1}{\left(\dfrac{1}{4\gamma}+\gamma\right)^3}$	0.50
$\dfrac{a}{4}$	$\dfrac{3\sqrt{3}}{256\left(\dfrac{13}{48h}+\dfrac{h}{a^2}\right)^3}$	$\dfrac{\sqrt{13}}{4\sqrt{3}}a\approx 0.52a$	$\dfrac{27a^3}{416\sqrt{13}}\approx 0.02a^3$	$\dfrac{13\sqrt{39}}{72\left(\dfrac{13}{48\gamma}+\gamma\right)^3}$	0.52
$\dfrac{a}{8}$	$\dfrac{3\sqrt{3}}{2048\left(\dfrac{57}{192h}+\dfrac{h}{a^2}\right)^3}$	$\dfrac{\sqrt{19}a}{8}\approx 0.55a$	$\dfrac{3\sqrt{3}a^3}{608\sqrt{19}}\approx 0.002a^3$	$\dfrac{19\sqrt{19}}{64\left(\dfrac{57}{192\gamma}+\gamma\right)^3}$	0.54
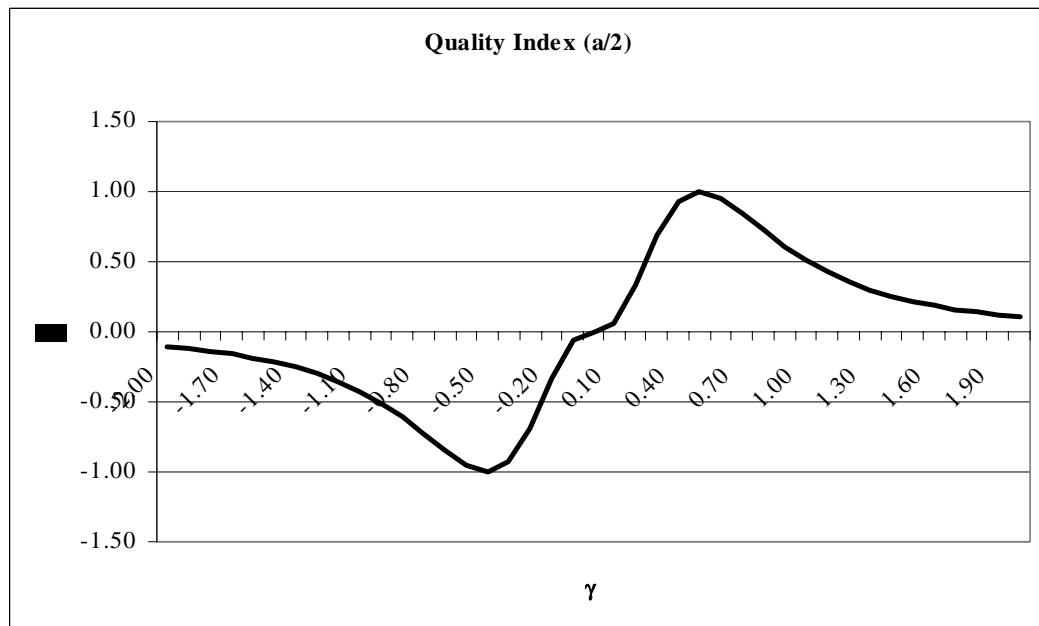
Figure 8-4. λ vs. $\gamma\left(b=\dfrac{a}{2}\right)$
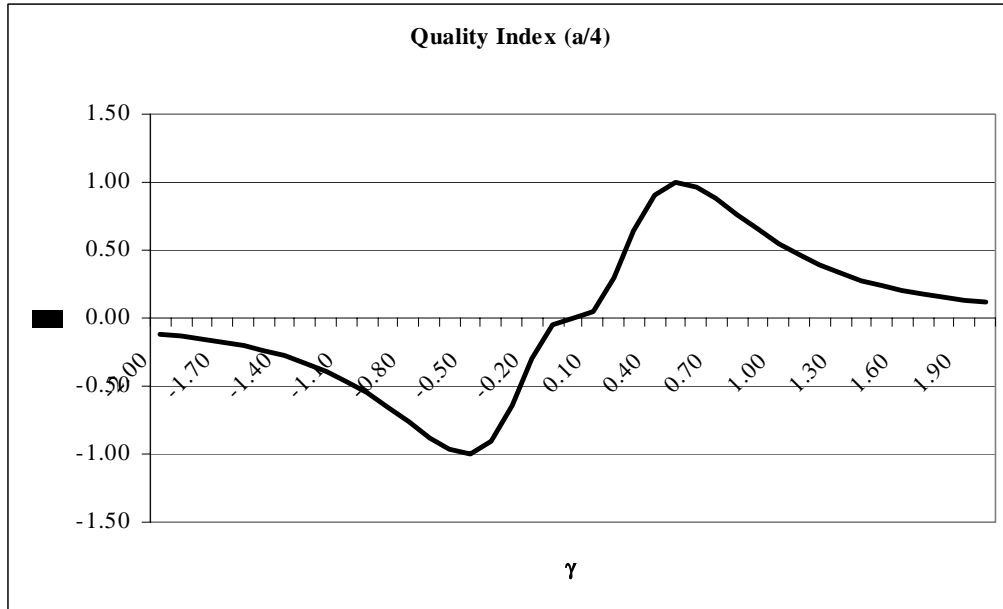
Figure 8-5. λ vs. $\gamma \left(b = \dfrac{a}{4} \right)$
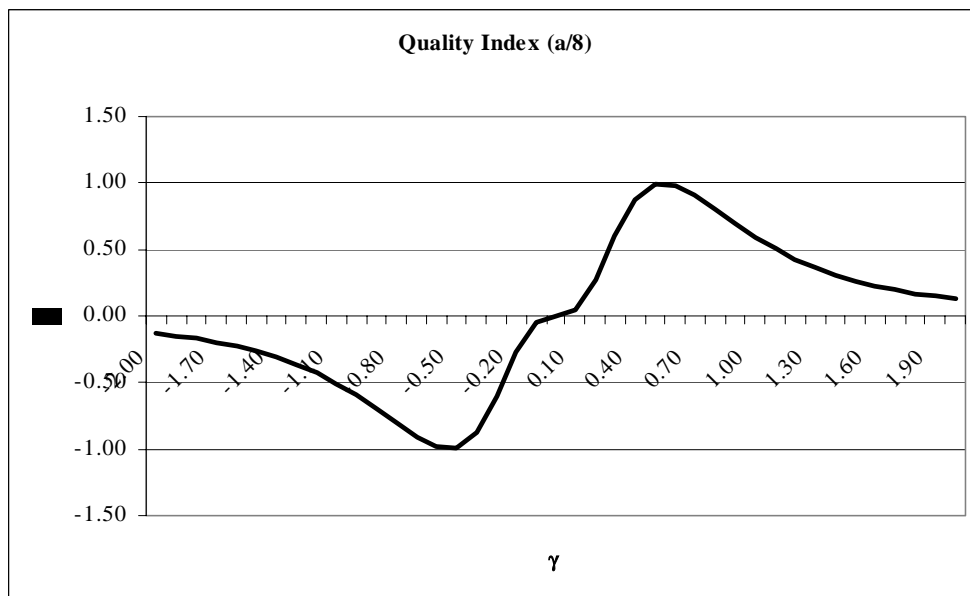
Figure 8-6. λ vs. $\gamma \left(b = \dfrac{a}{8} \right)$

The conclusion drawn by this analysis of the base size is that there is no appreciable improvement by making the base larger or smaller. That is, by using just the stability of the structure (quality index) as the decision criterion. Stern [1999] developed a series of equations to describe the forces in the ties as the platform (**a**) and base (**b**) dimensions are varied. Simply put, the ratio of **a/b** changes linearly with the force in the ties. In other words, if the base dimension is reduced by 50%, the force in the base ties increases by 50%. Based on this research, it would be impractical to reduce the base dimension to **a/8**, as the forces would increase an order of magnitude. Therefore, the ratio **a/4** was chosen because it reduces the strut lengths, provides a sufficient base dimension to attach the antenna, and still does not increase the tie forces too greatly.

As presented in Chapter 7, additional ties can be included in the 3-3 design, thereby improving the quality index. For the 4-4 and 6-6 structures, the index approaches 1.0 for virtually any position. Figure 8-7 presents the design for the 3-3 structure. In this case, the λ varies only 25% from 0.75 to 1.0 (as shown in Figure 7-13).

(a)   (b)   (c)
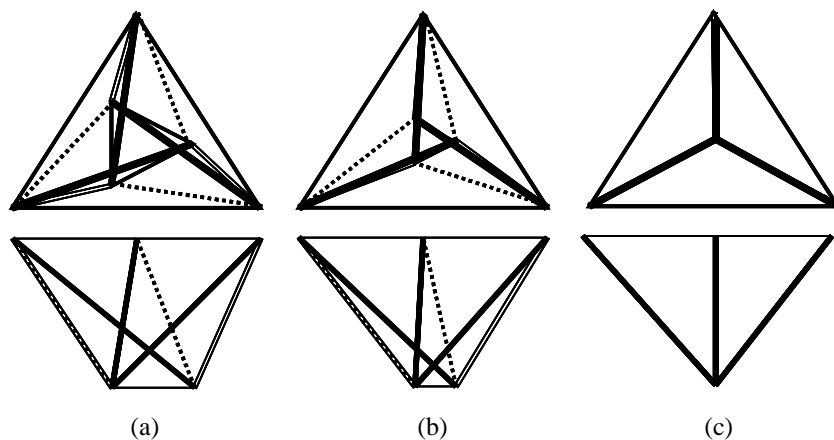
Figure 8-7. Reduction of the Base to Zero (Redundant Octahedron)
a) b<a; b) b=>0; c) b=0

4-4 Optimization

As presented in Chapter 4, the Jacobian (**J**) for the 4-4 structure is a 6x8 matrix, and

an understanding of the Cauchy-Binet Theorem aids in obtaining the quality index. As

previously presented, the numerator for the quality index (λ) reduces to

$$\sqrt{\det JJ^T} = \frac{32\sqrt{2}\, a^3 b^3 h^3}{\left(a^2 - \sqrt{2}\, ab + b^2 + 2h^2\right)^3}$$. The denominator represents the maximum

possible vale for the numerator was found by using **h=0**. This value is

$$\sqrt{\det J_m J_m^T} = \frac{2\, a^3 b^3}{\left(a^2 - \sqrt{2}\, ab + b^2\right)^{3/2}}$$. The height (**h**), which is used to find the

denominator, is $h_m = \sqrt{\frac{1}{2}\left(a^2 - \sqrt{2}\, ab + b^2\right)}$. Again, following the work in Chapter 4, the

quality index is therefore,

$$\lambda = \frac{16\sqrt{2} h^3 \left(a^2 - \sqrt{2}\, ab + b^2\right)^{\frac{3}{2}}}{\left(a^2 - \sqrt{2}\, ab + b^2 + 2h^2\right)^3} \tag{8-5}$$

As the $\lim_{b \Rightarrow 0} (\lambda)$ this reduces to

$$\lambda = \frac{16\sqrt{2}\, a^3 h^3}{\left(a^2 + 2h^2\right)^3} \tag{8-6}$$

By using $\gamma = \dfrac{h}{a}$, the equation reduces further to

$$\lambda = \frac{16\sqrt{2}\, h^3}{\left(a + 2\dfrac{h^2}{a}\right)^3} = \frac{16\sqrt{2}}{\left(\dfrac{a}{h} + 2\dfrac{h}{a}\right)^3} = \frac{16\sqrt{2}}{\left(2\gamma + \dfrac{1}{\gamma}\right)^3} \tag{8-7}$$

with a maximum λ at $\gamma = \dfrac{1}{\sqrt{2}} \approx \mathbf{0.71}$. Figure 8-8 plots λ vs. γ.
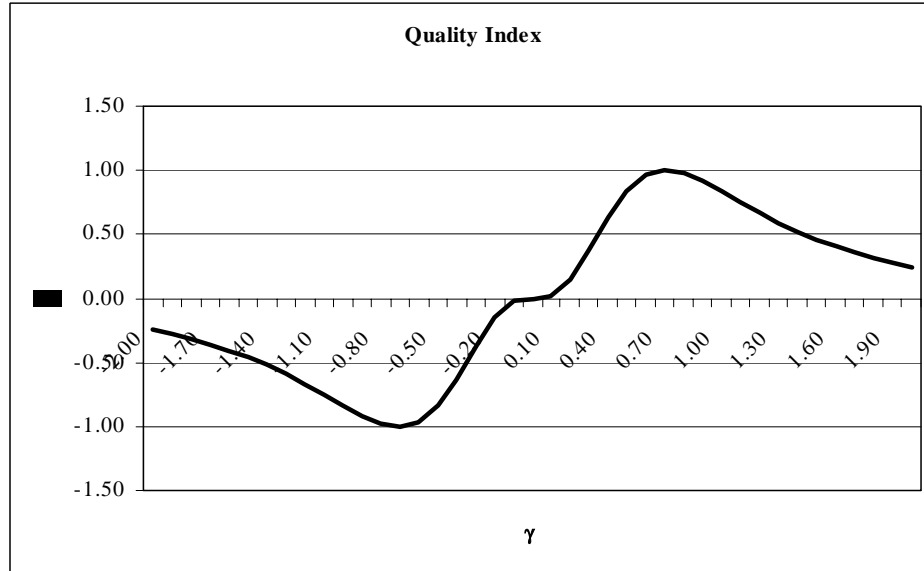
Figure 8-8. λ vs. $\gamma \left(\gamma = \dfrac{h}{a} \right)$ for the Square Anti-prism
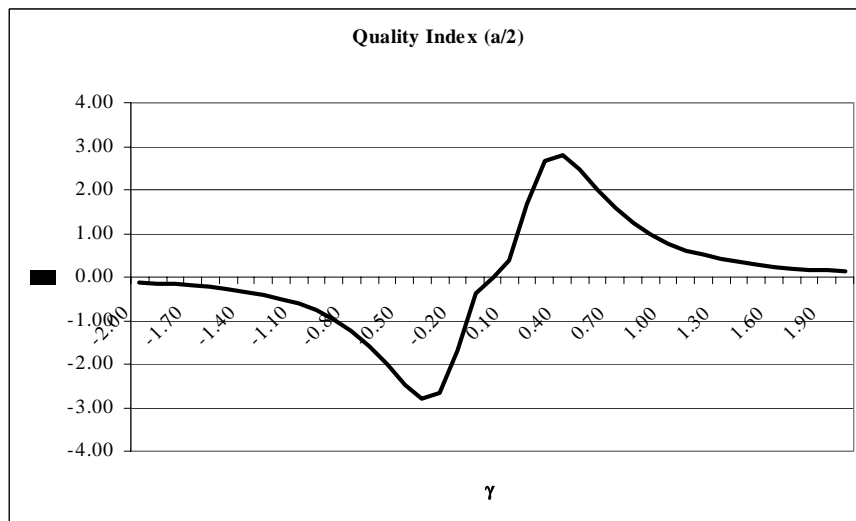
Figure 8-9. λ vs. $\gamma \left(b = \dfrac{a}{2} \right)$ for the Square Anti-prism

Similarly, the equations for **b** equals $\dfrac{\mathbf{a}}{\mathbf{2}}$, $\dfrac{\mathbf{a}}{\mathbf{4}}$, and $\dfrac{\mathbf{a}}{\mathbf{8}}$ are presented in Table 8-3. Figure

8-9 presents the first λ vs. γ plot. The second and third cases are similar, but it is obvious

that the γ value at $\lambda_{\mathbf{max}}$ changes significantly between **a/2** and **a/8**.

Table 8-3. γ at b=$\dfrac{\mathbf{a}}{\mathbf{2}}$, $\dfrac{\mathbf{a}}{\mathbf{4}}$, and $\dfrac{\mathbf{a}}{\mathbf{8}}$

b	λ (γ=h/a)	γ at λ_{max}
$\dfrac{a}{2}$	$\dfrac{16\sqrt{2}\left(\dfrac{5}{4}-\dfrac{1}{\sqrt{2}}\right)^{3/2}}{\left(2\gamma+\dfrac{1}{\gamma}\left(\dfrac{5}{4}-\dfrac{1}{\sqrt{2}}\right)\right)^{3}}$	$\left(\dfrac{\left(\dfrac{5}{4}-\dfrac{1}{\sqrt{2}}\right)}{2}\right)^{1/2} \approx 0.52$
$\dfrac{a}{4}$	$\dfrac{16\sqrt{2}\left(\dfrac{17}{16}-\dfrac{1}{2\sqrt{2}}\right)^{3/2}}{\left(2\gamma+\dfrac{1}{\gamma}\left(\dfrac{17}{16}-\dfrac{1}{2\sqrt{2}}\right)\right)^{3}}$	$\left(\dfrac{\dfrac{17}{16}-\dfrac{1}{2\sqrt{2}}}{2}\right)^{1/2} \approx 0.60$
$\dfrac{a}{8}$	$\dfrac{16\sqrt{2}\left(\dfrac{65}{64}-\dfrac{1}{4\sqrt{2}}\right)^{3/2}}{\left(2\gamma+\dfrac{1}{\gamma}\left(\dfrac{65}{64}-\dfrac{1}{4\sqrt{2}}\right)\right)^{3}}$	$\left(\dfrac{\dfrac{65}{64}-\dfrac{1}{4\sqrt{2}}}{2}\right)^{1/2} \approx 0.65$

6-6 Optimization

The 6-6 tensegrity design is the basis for this new class of deployable antenna

structures. The calculations are similar to those for the 4-4 to solve the 6x12 **J** matrix.

The numerator for λ, taken from Chapter 4, is $\sqrt{\det \mathbf{J}\mathbf{J}^{T}} = \dfrac{54\,a^{3}b^{3}h^{3}}{\left(a^{2}-\sqrt{3}\,ab+b^{2}+h^{2}\right)^{3}}$. The

denominator, which is found by using **h** equals zero is

$$\sqrt{\det J_m J_m^T} = \frac{54 a^3 b^3}{8\left(a^2 - \sqrt{3}\,ab + b^2\right)^{3/2}}$$. This **h** value is $h_m = \sqrt{\left(a^2 - \sqrt{3}\,ab + b^2\right)}$. The

quality index is therefore,

$$\lambda = \frac{8h^3\left(a^2 - \sqrt{3}\,ab + b^2\right)^{3/2}}{\left(a^2 - \sqrt{3}\,ab + b^2 + h^2\right)^3} \tag{8-8}$$

As the $\lim_{b \Rightarrow 0} (\lambda)$ this reduces to

$$\lambda = \frac{8\,a^3 h^3}{\left(a^2 + h^2\right)^3} \tag{8-9}$$

By using $\gamma = \dfrac{h}{a}$, the equation reduces further to

$$\lambda = \frac{8h^3}{\left(a + \dfrac{h^2}{a}\right)^3} = \frac{8}{\left(\dfrac{a}{h} + \dfrac{h}{a}\right)^3} = \frac{8}{\left(\gamma + \dfrac{1}{\gamma}\right)^3} \tag{8-10}$$

with a maximum λ at $\gamma = 1$. Figure 8-10 plots λ vs. γ.

Similarly, the equations for **b** equals $\dfrac{\mathbf{a}}{\mathbf{2}}$, $\dfrac{\mathbf{a}}{\mathbf{4}}$, and $\dfrac{\mathbf{a}}{\mathbf{8}}$ are presented in Table 8-4. Figure

8-11 presents the λ vs. γ plot for the $\dfrac{\mathbf{a}}{\mathbf{2}}$ case. The second and third cases are similar.

Again, the γ at λ_{max} values vary greatly as **b** is reduced from **a/2** to **a/8**. Keeping the work

of Stern [1999] in mind to minimize the tie forces, **b=a/4** is chosen as a compromise.

Using this chosen ratio, **h/a=0.79**, **b/a=0.25**, and therefore, **b/h=0.32**.

Quality Index
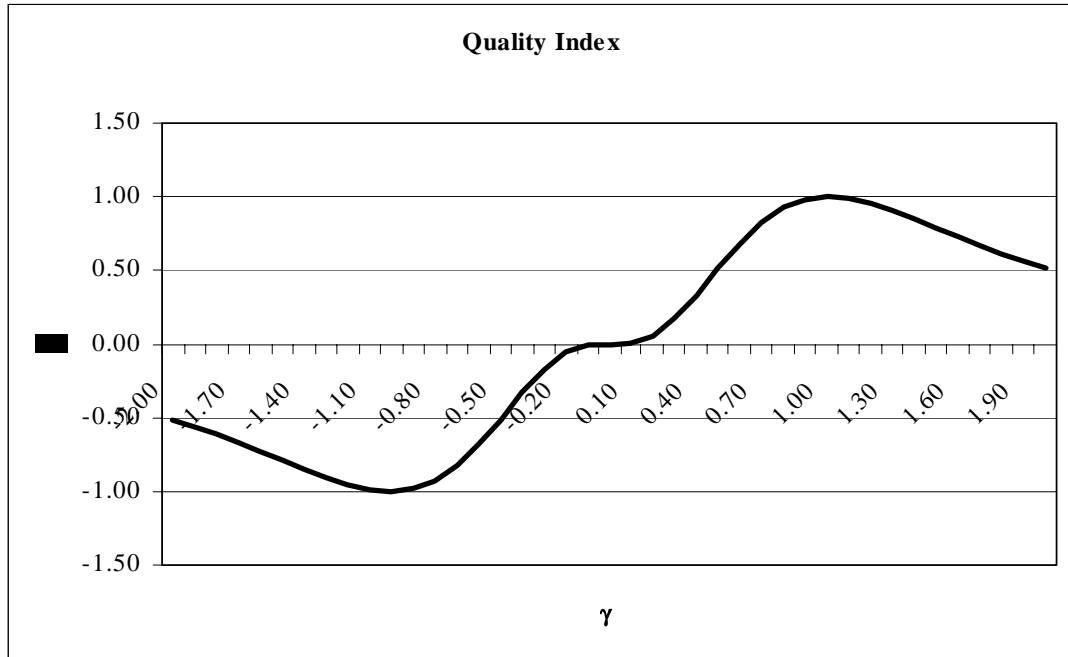
Figure 8-10. λ vs. $\gamma \left(\gamma = \dfrac{h}{a} \right)$ for the Hexagonal Anti-prism

Quality Index (a/2)
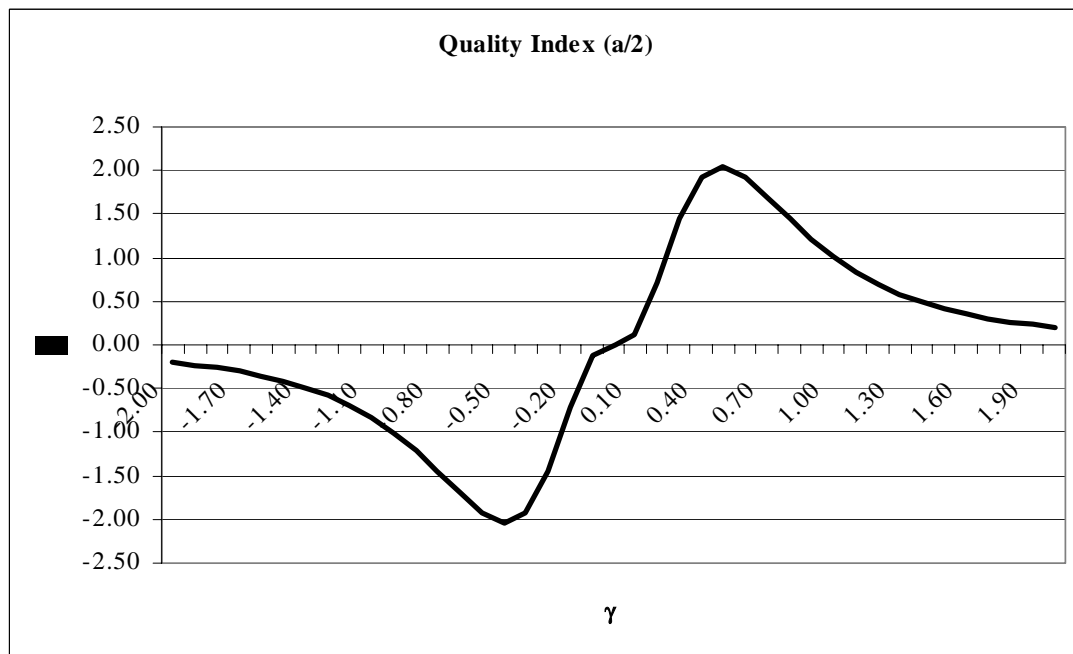
Figure 8-11. λ vs. $\gamma \left(b = \dfrac{a}{2} \right)$ for the Hexagonal Anti-prism

Table 8-4. λ and γ for $b = \dfrac{a}{2}$, $\dfrac{a}{4}$, and $\dfrac{a}{8}$

b	λ $(\gamma = h/a)$	γ at λ_{max}
$\dfrac{a}{2}$	$\dfrac{8\left(\dfrac{5}{4} - \dfrac{\sqrt{3}}{2}\right)^{3/2}}{\left(\gamma + \dfrac{1}{\gamma}\left(\dfrac{5}{4} - \dfrac{\sqrt{3}}{2}\right)\right)^{3}}$	$\left(\dfrac{5}{4} - \dfrac{\sqrt{3}}{2}\right)^{1/2} \approx 0.62$
$\dfrac{a}{4}$	$\dfrac{8\left(\dfrac{17}{16} - \dfrac{\sqrt{3}}{4}\right)^{3/2}}{\left(\gamma + \dfrac{1}{\gamma}\left(\dfrac{17}{16} - \dfrac{\sqrt{3}}{4}\right)\right)^{3}}$	$\left(\dfrac{17}{16} - \dfrac{\sqrt{3}}{4}\right)^{1/2} \approx 0.79$
$\dfrac{a}{8}$	$\dfrac{8\left(\dfrac{65}{64} - \dfrac{\sqrt{3}}{8}\right)^{3/2}}{\left(\gamma + \dfrac{1}{\gamma}\left(\dfrac{65}{64} - \dfrac{\sqrt{3}}{8}\right)\right)^{3}}$	$\left(\dfrac{65}{64} - \dfrac{\sqrt{3}}{8}\right)^{1/2} \approx 0.89$

CHAPTER 9.
CONCLUSIONS

The requirements process introduced in Chapter 1 comes from a history defined by predictive engineering and unfortunate system failures. The participating hardware development companies have been greatly aided over the years by the work of analyst such as James R. Wertz. This process is based on problem definition and end vision, with a activity definition to reach the end goals. Space structures in general, and precision subsystems such as deployable antennas in particular, have become mired in this predictive process. The critical need for these subsystems has driven the development process to be extremely conservative, building larger, heavier, and stronger structures than are necessary to meet the mission requirements.

This work has applied the theories of some of the greatest minds in mathematics (Ball, Plücker, etc.) and engineering (Kenner, Hunt, etc.) to the simple and elegant architectural designs of Snelson and Fuller. The premise for embarking on this work was that architecture, by definition, leans more toward art than engineering, but combines form with function. Pearce (1990) accurately presented the theory whereby nature abhors inefficiency, requiring everything from dragonfly wings to cracked mud to find a minimal potential energy. It is this confidence in the efficiency of nature and its obvious tie with architecture which defines this work.

In Chapter 3, a geometrical stability criterion measured by the quality index was introduced as defining an acceptable design. Within this stability, the structure should

deploy (preferably self deploy) and stow to allow placement in the space environment. After development of the 3-3, 4-4, and 6-6 parallel structures, this theory was applied to the tensegrity position. It is most interesting to note that this position happens to occur when the quality index is zero. This is known as a "stable critical point" in Chaos Theory. In this position, the structure has instantaneous mobility, whereby small perturbations can create small deflections of the antenna. Adding extra connecting ties between the "platform" and the "base" nullifies the instant mobility and provides a very stable structure. Further analysis proved that the antenna surface of this class of structures can be commanded to move on a screw whose axis is perpendicular to the surface. This happens to be a useful function for antenna surfaces, allowing them to address various feed centers (located at the focal points of the parabola).

<div align="center">Applying Tensegrity Design Principles</div>

The idea for applying tensegrity design to deployable antennas has been suggested numerous times over the last two decades, but this work has addressed the mathematics necessary to prove its stability and therefore its applicability. The 6-6 structure has been chosen to provide enough radial spars on which to "hang" the reflective surface of the antenna. Again, possible advantages and disadvantages of the instantaneous mobility issue at the tensegrity position warrant further investigation.

An improvement was presented for these designs with additional ties above the basic tensegrity design (two ties from each base vertex). A mathematic analysis of the quality index for these augmented 3-3 and 4-4 structures showed a marked improvement in the indices. For the 6-6 design, the basic tensegrity design with 12 platform/base connections

(Figure 9-1a) is augmented to a total of 18 (Figure 9-1b), 24 (Figure 9-2a), 30 (Figure 9-2b), and 36 (Figure 9-3).

(a)   (b)
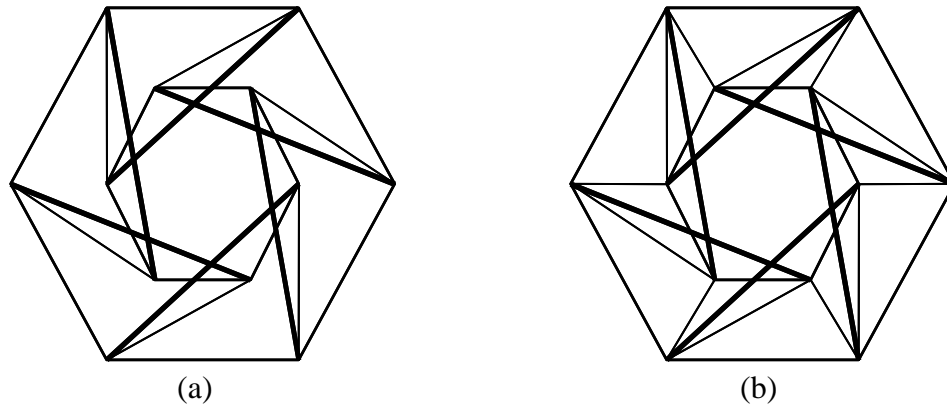
Figure 9-1. Hexagonal Anti-prism Designs
(a) Basic Tensegrity Design (12 platform/base connections); (b) Augmented Tensegrity
Design (18)

(a)   (b)
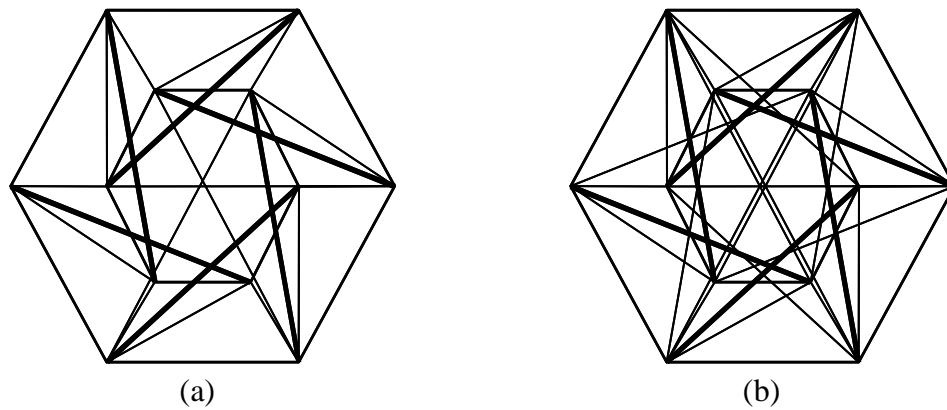
Figure 9-2. Augmented 6-6 Hexagonal Anti-prism Designs
(a) Augmented Tensegrity Design (24); (b) Augmented Tensegrity Design (30)
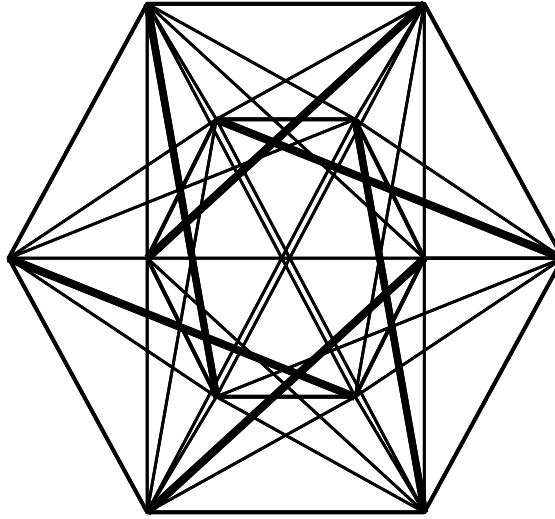
Figure 9-3. Augmented 6-6 Hexagonal Anti-prism Design with the Maximum (36)
Number of Platform/Base Connections

As presented in Chapter 7, the augmented 3-3 index (λ_9) only varies between .75 and

1.0 (Figure 9-4), with three minimum potential energy position located symmetrically

about the Central Position (basic platform design position). Note that only one additional

tie per vertex is required, increasing the number of platform/base connections from 6 to 9.

The quality index (λ_{16}) for the 4-4 with four ties between each base vertex and the

corresponding platform vertices, the value varies less than 5% between the maximum and

minimum. Again, the number of minimum potential energy nodes is equal to the number

of sides in the geometry, and these nodes are symmetrically placed about the Central

Position. The point design will use one set of additional ties between the "base" and the

"platform, as shown in Figure 9-1(b). This will simplify the calculations, but still improve

the stability of the structure above that of for the basic tensegrity design.
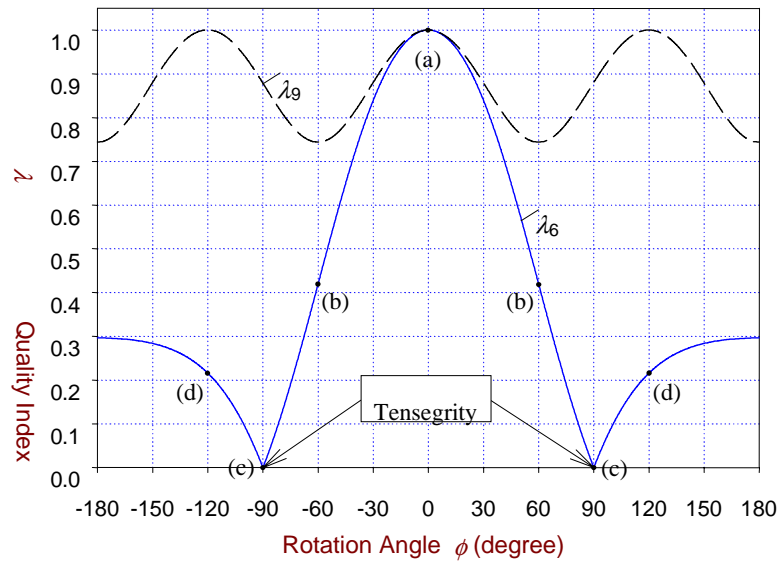
Figure 9-4. A Comparison of the λ vs. φ Curves for the Basic (λ_6) and Augmented (λ_9) Tensegrity Designs for the Octahedron
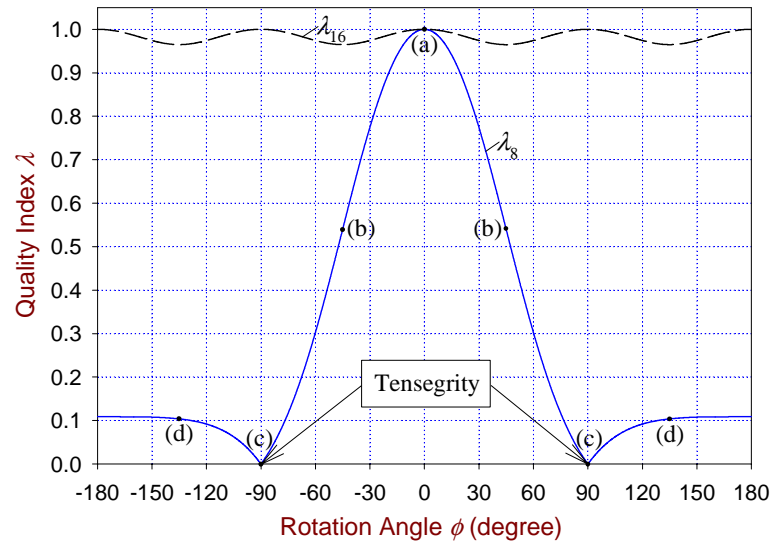
Figure 9-5. A Comparison of the λ vs. φ Curves for the Basic (λ_8) and Augmented (λ_{16}) Tensegrity Designs for the Square Anti-Prism

Antenna Point Design

As presented in Chapter 7, a 15-meter, tip-to-tip design meets the needs of current

systems. For this research, this dimension is increased to 16-meters, providing sufficient

structure to suspend a 15-meter diameter parabolic surface within. Chapter 8 has shown

that the ratios between **a**, **b**, and **h** can be varied to improve the efficiency and utility of

the spars while ensuring the stability (quality index) is sufficient to form a usable

structure. The design that can meet the requirements of the space community, while

improving the subsystem efficiency is presented in Figure 9-6. To simplify the design,

these parameter ratios were altered slightly to **h/a=0.50**, **b/a=0.25**, and **b/h=0.50**. This

design maintains the necessary **b/a** ratio, while only altering the **h** value slightly to flatten

the "cup" of the antenna. This applies to the **f/d** ratio to be addressed later.

This chosen design is only one of a family of choices which include various

numbers of extra ties, **a/b** and **h/a** ratios. The assumption is, to avoid the instantaneous

mobility issue for tensegrity-class structures; an additional set of ties would be included.

Nominally this would be one set, connecting each base vertex with its corresponding

platform vertex above.

Figure 9-7 presents the baseline design. Note that the reflector surface, suspended

within the strut framework could accommodate a focus to diameter (**f/d**) ratio of

approximately 0.3. This value is typical for deployable antennas in service today. As

noted in the figure, the distance from the parabola vertex to the edge of the antenna

structure is nominally 2-meters. For a15-meter diameter parabolic reflector surface, the

focal point (for an **f/d**=0.3) would be a total of 3.75-meters above the parabola vertex.

Therefore, the focal point is located at 1.75-meters above the edge of the structure. This is

significant because additional structure may be needed to place the feed electronics for

this antenna. What changes a hexagonal anti-prism to the truncated structure on which the

6-6 tensegrity structure is based in a "hat" structure above and below the platform and

base. This "extra" structure, above what is being considered the edge of the antenna

structure, could be used for this feed support structure.
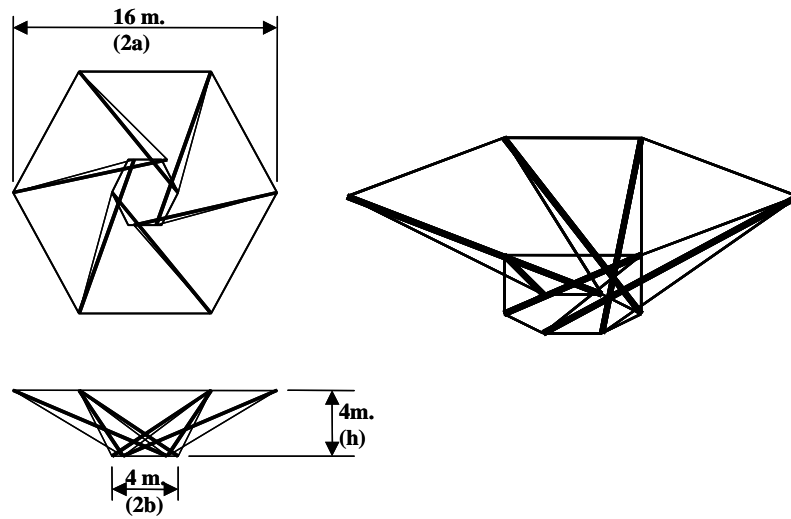
Figure 9-6. The Proposed 6-6, Hexagonal Anti-prism, Deployable Tensegrity Antenna
Design
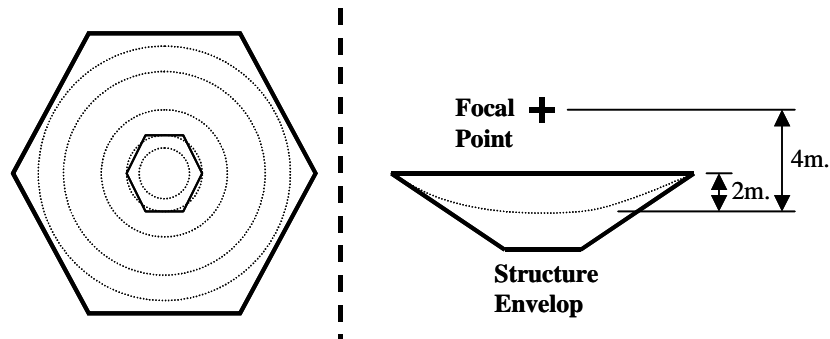
Figure 9-7. The Relationship Between the Antenna Structure Envelope and the Focal
Point Location

Patent Disclosure

Harris Corporation, Melbourne, Florida, in conjunction with the University of Florida, Gainesville, Florida, has filed a patent disclosure on the application of tensegrity structures to self-deploying space antennas. The concept of using tensegrity of structures, even space structures, has been suggested in technical literature over the last two decades. The specifics for applying tensegrity, the concept of self-deployment, and the mathematics, which proves its value to the design community, is the basis for this patent. This new approach has the potential to radically change the deployable structures market place, reducing cost, weight, and complexity, therefore improving the subsystem efficiency.

Future Work

Although current deployable antenna design approaches meet most of the goals necessary for space flight, the cost and development time are still much too great. This research, which addresses the application of tensegrity structures to these subsystems, has proven both stability and possible special motions (screw theory based), which would meet the mission needs. Future work in this area would address these special motions, particularly as they affect the reflector surface, which is suspended between the struts. Additionally, a trade between strut deployment schemes relative to subsystem stiffness should be performed to benefit from the advances over the last decade in inflatable structures. Of all the subsystems necessary for space missions, deployable antennas are potentially the least package-efficient.

REFERENCES

Ball, R.S. (1998), "A Treatise on the Theory of Screws," Cambridge University Press, London.

Bottema, O., Roth, B., (1979), "Theoretical Kinematics," Dover Press, New York.

Calladine, C., Pellegrino, S., (1991), "First-Order Infinitesimal Mechanisms," International Journal of Solid Structures, Vol. 27, No. 4, pp. 505-515.

Connelly, R., and Black, A., (1998), "Mathematics and Tensegrity," American Scientist, Vol. 86, pp. 142-151.

Duffy, J., Knight, B., Crane, C., Rooney, J., (1998), "An Investigation of Some Special Motions of an Octahedron Manipulator Using Screw Theory," Proceedings of the 1998 Florida Conference on Recent Advances in Robotics.

Duffy, J., Rooney, J., Knight, B., Crane, C., (June 1998), "An Analysis of the Deployment of Tensegrity Structures Using Screw Theory," Proceedings of Sixth International Symposium on Advances in Robot Kinematics: Analysis and Control, Strobl, Austria, Kluwer Academic Publishers.

Fuller, R.B., (1960), "Tensegrity," Portfolio and Art News Annual, No. 4, the Art Foundation Press, Inc., New York.

Fuller, R.B., (1975), "Synergetics: Explorations in the Geometry of Thinking," Macmillan Publishing, New York.

Gabriel, J.F., (1977), "Beyond the Cube: the Architecture of Space," John Wiley and Sons, Inc., New York.

Hamlin, G. J., Sanderson, A. C., (1998), "TETROBOT, A Modular Approach to Reconfigurable Parallel Robotics, Kluwer Academic Publishers.

Hunt, K. H., (1990), "Kinematic Geometry of Mechanisms," Oxford Engineering Sciences Series-7, Oxford University Press, New York.

Jessop, C.M., (1969) "A Treatise on the Line Complex," Chelsea Publishing Company, New York, NY, (1st publication in Cambridge, UK, 1903).

Kaplan, R., Schultz, J. L., (October 23, 1975), "Deployable Reflector Structure," Grumman Aerospace Corporation, United States Patent Number: 4030102.

Kawaguchi, K., Hangai, Y., Pellegrino, S., Furuya, H., (December 1996), "Shape and Stress Control Analysis of Prestressed Truss Structures," Journal of Reinforced Plastics and Composites, Vol. 15, pp. 1226-1236.

Kenner, H., (January 1976) "Geodesic Math and How to Use It," University of California Press, Berkeley, Los Angeles.

Kitamura, T., Yamashiro, K., (August 31, 1990), "Extendable Mast", Japan Aircraft Mfg. Co., Ltd., United States Patent Number: 5085018.

Knight, B., (June 1998), "An Analysis of Special Redundant Motions for a Square Platform," CIMAR Paper.

Krishnapillai, A., (1988), "Deployable Structures," United States Patent Number: 5167100.

Larson, W. J. and Wertz, J. R., (1992), "Space Mission Analysis and Design," Microcosm, Inc., Los Angeles

Lee, J., Duffy, J., and Hunt K.H., (1998), "A Practical Quality Index based on the Octahedral Manipulator," The International Journal of Robotics Research, Vol. 17, No. 10, pp. 1081-90.

Marcus, M., and Minc, H, (1965), "Introduction to Linear Algreba," The Cauchy-Binet Theorem, The Macmillan Company, New York.

Meserve, B., (1983), "Fundamental Concepts of Geometry," Dover Press, New York.

Motro, R., Editor, (1992), "Special Issue of the International Journal of Space Structures: Tensegrity Systems," Multi-Science Publishing Co., Ltd., Vol. 7, No. 2.

Motro, R., (1996), "Structural Morphology of Tensegrity Systems," International Journal of Space Structures, Multi-Science Publishing Co., Ltd., Vol. 11, Nos.1 & 2, pp. 233-240.

Natori, M., (1985), "Jointed Extendible Truss Beam," Japan Aircraft Mfg. Co., Ltd., United States Patent Number: 4655022.

Nelson, R.A., (1983), "Biaxial Scissors Fold, Post Tensioned Structure," LTV Aerospace and Defense Co., United States Patent Number: 4539786.

Newman, D. D., (1998), "Classification and Optimization of Actuators for Space Deployment Mechanisms," M.S.M.E. Thesis, University of Alabama–Tuscaloosa.

Onoda, J., (May 3, 1985), "Deployable Truss Structure," Japan Aircraft Mfg. Co., Ltd., United States Patent Number: 4745725.

Onoda, J., (July 11, 1986), "Collapsible Truss Unit, and Frameworks Constructed by Combinations of Such Units," Fuji Jukogyo Kabushiki Kaisha, United States Patent Number: 4667451

Onoda, J., (February 24, 1987a), "Deployable Truss," Hitachi, Ltd., United States Patent Number: 4819399.

Onoda, J., (March 12, 1987b), "Collapsible Truss Unit for Use in Combination with Other Like Units for the Construction of Frameworks," Fuji Jukogyo Kabushiki Kaisha, United States Patent Number: 4771585.

Onoda, J., (March 27, 1990), "Collapsible Truss Structures," Fuji Jukogyo Kabushiki Kaisha, United States Patent Number: 5040349.

Onoda, J., Fu, D. Y., Minesugi, K., (May-June 1996), "Two-Dimensional Deployable Hexapod Truss," Journal of Spacecraft and Rockets, Vol. 33, No. 3, pp. 416-21.

Pearce, P., (1990) "Structure in Nature Is a Strategy for Design," MIT Press, Cambridge, MA.

Pugh, A., (1976), "An Introduction to Tensegrity," University of California Press, Berkeley, CA.

Rhodes, M. D., Hedgepeth, J. M., (August 22, 1986), "Synchronously Deployable Double Fold Beam and Planar Truss Structure," NASA, United States Patent Number: 5016418.

Rooney, J., Duffy, J., Lee, J., (June 1999), "Tensegrity and Compegrity Configurations in Anti-prism Manipulator Platforms," Paper ID: 760, Tenth World Congress on the Theory of Machines and Mechanisms (IFToMM), Oulu, Finland.

Skelton, R.E., (October 31, 1995), "Deployable Tendon-Controlled Structure," Dynamic Systems Research, Inc., United States Patent Number: 5642590.

Skelton, R., Sultan, C., (1997), "Controllable Tensegrity, a New Class of Smart Structures," SPIE, Vol. 3039, 0277-786X/97, pp. 166-177.

Snelson, K., (1996), "Snelson on the Tensegrity Invention," International Journal of Space Structures, Vol. 11, No. 1-2, Multi-Science Publishing Co., Ltd., pp. 43-48.

Snyder, V., and Sisam, C.H., (1914), "Analytic Geometry of Space," Chapter VI; Henry Holt and Co., New York.

Stern, I., (1999), "Development of Design Equations for Self-Deployable N-Strut Tensegrity Systems," University of Florida, MSME Thesis.

Stewart D., (1965), "A Platform with Six Degrees of Freedom," Proceedings of the Institution of Mechanical Engineers, Vol. 180, No. 15, pp. 371-386.

Sultan, C., Corless, M., Skelton, R., (1999a), "Peak to Peak Control of an Adaptive Tensegrity Space Telescope," SPIE Conference on Mathematics and Control in Smart Strutures, Vol. 3667, March, pp. 190-210.

Sultan, C., Corless, M., Skelton, R., (1999b), "Reduced Prestressability Conditions for Tensegrity Strutures," American Institute of Aeronautics and Astronautics, AIAA-99-1478, pp. 2300-2308.

Sultan, C., Skelton, R., (1997), "Integrated Design of Controllable Tensegrity Strutures," Adaptive Structures and Material Systems, ASME, pp. 27-35.

Tibbalds, B., Guest, S., Pellegrino, S., (1998), "Folding Concept for Flexible Surface Reflectors," American Institute of Aeronautics and Astronautics, Publication: AIAA-98-1836.

Tidwell, P. H., Reinholtz, C. F., Robertshaw, H. H., Horner, C. G., (November 13-15, 1990), "Kinematic Analysis of Generalized Adaptive Trusses," First Joint U.S./Japan Conference on Adaptive Structures, Technomic Publishing Co., pp. 772-791.

Tobie, S.T., (1967), "A Report on an Inquiry into the Existence, Formation and Representation of Tensile Structures," Master of Industrial Design, Pratt Institute.

Wada, B. K., Fanson, J. L., Chen, G. S., (November-December 1991), "Using Adaptive Structures to Enable Future Missions by Relaxing Ground Test Requirements," Journal of Spacecraft, Vol. 28, No. 6, pp. 663-669.

Wang, B., (March 1998a), "Cable-Strut Systems: Part I–Tensegrity," Journal of Construction Steel Research, Elsevier Science Ltd., Vol. 45, No. 3, pp. 281-289.

Wang, B., (March 1998b), "Cable-Strut Systems: Part II–Tensegrity," Journal of Construction Steel Research, Elsevier Science Ltd., Vol. 45, No. 3, pp. 291-299.

Wang, B., (1998c), "Definitions and Feasibility Studies of Tensegrity Systems," International Journal of Space Structures, Multi-Science Publishing Co. Ltd., Vol. 13, No. 1, pp. 41-47.

Wang, B., Liu, X., (1996), "Integral-Tension Research in Double-Layer Tensegrity Grids," International Journal of Space Structures, Multi-Science Publishing Co., Ltd., Vol. 11, No. 4, pp. 349-355.

Warnaar, D.B., (1992), "Evaluation Criteria for Conceptual of Deployable-Foldable Truss Structures," ASME Design Engineering: Mechanical Design and Synthesis, Vol. 46, pp. 167-173.

Warnaar, D.B. and Chew M., (September 1990a), "Conceptual Design of Deployable-Foldable Truss Structures Using Graph Theory–Part 1: Graph Generation," ASME 1990 Mechanisms Conference, pp. 107-113.

Warnaar, D.B. and Chew M., (September 1990b), "Conceptual Design of Deployable-Foldable Truss Structures Using Graph Theory–Part 2: Generation of Deployable Truss Module Design Concepts," ASME 1990 Mechanisms Conference, pp. 115-125.

Waters, T. J., Waters, M. T., (January 27, 1987), "Hyperboloidal Deployable Space Antenna," United States Patent Number: 4825225.

WTEC Panel Report, "Global Satellite Communications Technology and Systems," (November 11, 1998), Executive Summary, http://www.itri.loyala.edu/satcom2/.

Wu, K.C. and Lake, M.S., (May-June 1996), "Multicriterion Preliminary Design of a Tetrahedral Truss Platform," Journal of Spacecraft and Rockets, Vol. 33, No. 3, pp. 410-415.

You, Z., (March 15, 1997), "Displacement Control of Prestressed Structures," Computational Methods in Applied Mechanics and Engineering, Volume 144, pp. 51-59.

BIOGRAPHICAL SKETCH

During his 18-year career, Mr. Knight has worked for Harris (Melbourne, FL, 1982-85; 1990-present), Unisys (Reston, VA, 1986-88), and Lockheed (Kennedy Space Center, FL, 1985-86), developing electro-mechanical systems. In 1998 he had the great honor of serving as a Technology Fellow to the National Reconnaissance Office, managing a communications dissemination project. This achievement-focused organization contributed greatly to this research, guiding the requirements and designs necessary to meet the space mission needs for future space systems. Currently, Mr. Knight is leading an R&D effort to study the applicability of tensegrity structures to space antenna systems.

Mr. Knight's post-secondary education began with math and physics undergraduate work at Florida State University, which led to a Bachelor of Science in Mechanical Engineering (1982) from the University of Michigan (Ann Arbor). He was a Research Assistant to Dr. George S. Springer, a national authority in composite structures. He returned to earn a Master of Science in Mechanical Engineering (1990) from North Carolina State University (Raleigh). This research, under Dr. Thomas A. Dow, focused on precision manufacturing design and control, including assembly of the country's first nanometer-accurate testbed.

I certify that I have read this study and that in my opinion it conforms to acceptable standards of scholarly presentation and is fully adequate, in scope and quality, as a dissertation for the degree of Doctor of Philosophy.

_____

Joseph Duffy, Chairman
Graduate Research Professor of
    Mechanical Engineering

I certify that I have read this study and that in my opinion it conforms to acceptable standards of scholarly presentation and is fully adequate, in scope and quality, as a dissertation for the degree of Doctor of Philosophy.

_____

Carl D. Crane III
Professor of Mechanical Engineering

I certify that I have read this study and that in my opinion it conforms to acceptable standards of scholarly presentation and is fully adequate, in scope and quality, as a dissertation for the degree of Doctor of Philosophy.

_____

Ali A. H. Seireg
Ebaugh Professor of Mechanical
    Engineering

I certify that I have read this study and that in my opinion it conforms to acceptable standards of scholarly presentation and is fully adequate, in scope and quality, as a dissertation for the degree of Doctor of Philosophy.

_____

Ralph Selfridge
Professor of Computer and Information
    Science and Engineering

I certify that I have read this study and that in my opinion it conforms to acceptable standards of scholarly presentation and is fully adequate, in scope and quality, as a dissertation for the degree of Doctor of Philosophy.

_____
Gloria Jean Wiens
Associate Professor of Mechanical
   Engineering

This dissertation was submitted to the Graduate Faculty of the College of Engineering and to the Graduate School and was accepted as partial fulfillment of the requirements for the degree of Doctor of Philosophy.

May 2000

_____
M. J. Ohanian
Dean, College of Engineering

_____
Winfred M. Phillips
Dean, Graduate School